VUB FACULTY OF ENGINEERING

Department of
Fundamental Electricity
and Instrumentation (ELEC)

Thesis submitted in fulfillment of the requirements for the degree of
Doctor in Engineering (Doctor in de Ingenieurswetenschappen) by

ir. Gustavo Quintana Carapia

Statistical analysis and experimental validation of data-driven dynamic measurement methods

PROMOTERS

prof. dr. ir. Ivan Markovsky
Vrije Universiteit Brussel, Belgium

prof. dr. ir. Rik Pintelon
ELEC Department, Vrije Universiteit Brussel, Belgium.

MEMBERS OF THE JURY

prof. dr. ir. Patrick Guillaume (President)
MECH Department, Vrije Universiteit Brussel, Belgium.

prof. dr. ir. Roger Vounckx (Vice-President)
ETRO Department, Vrije Universiteit Brussel, Belgium.

dr. ir. Philippe Dreesen (Secretary)
ELEC Department, Vrije Universiteit Brussel, Belgium.

dr. ir. Nikolaos Deligiannis
ETRO Department, Vrije Universiteit Brussel, Belgium.

prof. dr. ir. Lyudmila Mihaylova
ACSE Department, University of Sheffield, United Kingdom.

prof. dr. ir. Stephane Chretien
ERIC Laboratory, University Lyon 2, France.

prof. dr. ir. Guillaume Mercère
LIAS Laboratory, Université de Poitiers, France.

Acknowledgements

I could not have done this without your support.

Text.

Here comes your acknowledgement.

Contents

List of Abbreviations

CRLB   Cramér-Rao Lower Bound

EIV   Errors in Variables
EWRLS   Exponentially Weighted Recursive Least Squares

FRF   Frequency Response Function

LS   Least Squares
LTI   Linear Time Invariant
LTV   Linear Time Varying

MC   Monte Carlo
ML   Maximum Likelihhod
MSE   Mean Squared Error

pdf   probability density function
PSD   Power Spectral Density

RLS   Recursive Least Squares
RMS   Root Mean Square
RMSE   Root Mean Square Error

SISO   Single-Input Single-Output
SNR   Signal-to-Noise Ratio

TV   Time Varying

1. Summary

Sensors are dynamical systems and the physical quantity is the input excitation. To have fast measurements, the input must be estimated during the sensor transient state. Otherwise, users have to wait for the sensor steady state when the response is proportional to the input through the sensor static gain. One approach to get fast input estimation is filtering the sensor transient response with another dynamical system aiming to reconstruct the input and to compensate the estimation time. Another approach is processing the transient response on a digital signal processor (DSP). Compensators are model based and DSPs allow model free methods that can reduce the estimation time.

There exists a model-free method that directly estimates the step input level from the sensor step response. This method was formulated as a Hankel structured errors-in-variables (EIV) problem where the regression matrix and the regressor are correlated. The structured EIV problem is solved with recursive least-squares to allow real-time implementation. The range of application of this step input estimation method is wide because it is independent from sensor models.

The stochastic properties of the step input estimation method are unknown and are not straightforwardly evident. To validate the method for metrology applications, we studied the estimate uncertainty by doing a statistical analysis of the step input estimation. The estimate uncertainty can be defined in terms of the estimate bias and variance. The statistical analysis of the estimation method yields expressions that predict the estimate first and second moments.

We computed the Cramér-Rao bound of the structured EIV problem to determine the minimum theoretical variance of the estimate. This bound was compared to the estimate mean squared error (MSE) in simulations and in experiments with temperature and weighing sensors. It was found that the input estimation is biased but with small variance, and that the estimate MSE is less than one order of magnitude larger than the Cramér-Rao bound. In the practice, the step input estimation method was found to be robust when the Gaussian and white measurement noise assumption was not satisfied.

2. Introduction

A measurement is a dynamical process and a sensor is a dynamical system. The physical quantities of interest are the inputs of the system, and the outputs are the electrical signals collected from the sensor. The inputs interact with the sensor, and there are energy transferences between them that modify the sensor state. The sensor output response depends on the applied inputs, and on the sensor initial conditions.

There is a trade-off between speed and accuracy in a measurement with a linear time invariant sensor. The input excitation drives the sensor into a transient state, that is followed by a steady state. During the sensor transient state, the response does not represent directly the input, but in steady state, the sensor response is proportional to the input. The input can be estimated accurately from the sensor steady state response using the sensor static gain. However, waiting for the steady state is not advisable for practical applications that need fast measurements. In these practical applications, the input must be estimated during the sensor transient state.

One approach to get a fast input estimation is filtering the sensor transient response with another dynamical system that inverts the dynamics of the sensor. The filter output is an input estimate that compensates the measurement time. The transient duration of the compensation filter is smaller than that of the sensor. The compensator is designed to deconvolve the sensor response and is based on a sensor model.

Another approach relies in the use of digital signal processors (DSP) to estimate the input value from the sensor transient response. DSPs offer an extra versatility level since they allow the implementation of methods that do not necessarily recreate dynamic systems, such as digital filters. A suitable data-driven method in a DSP can provide faster input estimations than with the model-based compensators.

An example of a data-driven method devised for a DSP is the direct step input level estimation from the sensor step response [Markovsky, 2015a]. This method formulates a Hankel structured errors-in-variables (EIV) problem with correlation. The regression matrix has a block-Hankel structure. The correlation exists because both the regression matrix and the regressor are constructed from the transient response perturbed by measurement noise. The measurement noise is assumed to have zero mean and given variance. The method is implemented in real-time using a recursive least-squares (RLS) solution of the structured EIV problem.

The main advantage of the data-driven input estimation method is that it does not identify the sensor model but instead it directly estimates the input. This differs from the classic two-stage methodology where the sensor model is first identified before the input is estimated. In this method, the output-error (OE) problem is converted into an EIV problem that is harder to solve, but the RLS solution is easy to compute. The range of application of the data-driven input estimation method is wide because it is independent of the sensor model. The main disadvantage of the data-driven input estimation method is that its stochastic properties are not straightforwardly evident. It is more complex to find the stochastic properties of EIV problems when they have structure and correlation.

The estimate uncertainty must be assessed to validate the estimation methods for metrology applications. The uncertainty of the data-driven step input estimation method [Markovsky, 2015b] is unknown. The uncertainty can be defined in terms of the estimate bias and variance [Pintelon and Schoukens, 2012], and these can be obtained by conducting an elementwise statistical analysis. The validation of the step input estimation method requires also to demonstrate its effectiveness on real-life measurements. In real-life experiments, the experimens were conducted with sensors of temperature and mass. One challenge of using real-life data is that the noise may not fulfill the whiteness assumptions considered in the estimation problem formulation and in the statistical analysis. The simulation and experimental results permit to compare the performance of the step input estimation method.

The ideas behind the step input estimation method raise the curiosity towards the design of estimation methods for other input models. One of this input models is the ramp. The ramp input estimation method is, in addition, motivated by the dynamic weighing that is performed in conveyor systems. The dynamic weighing estimates the mass of materials or products during their transportation. Ideally, when the conveyor belt transports the materials at a constant speed, i.e., the weighing sensor is excited with a ramp profile. The ramp is an affine input model that consists of two parameters, the slope and the interception. The slope depends on the applied mass and can be used to estimate it from the transient response.

An adaptation of the step input estimation method can estimate the parameters of affine inputs.

This thesis describes three works iniciated after the data-driven step input estimation method. The first work is a statistical analysis to elucidate the bias and the covariance of the estimate that this method provides. With these statistical moments, the estimate uncertainty is built and we can assess the effectiveness of the method.

2.1. State of the art

Recent studies in metrology deal with the dynamic process effects that exist in measurements. Processing the response of linear time invariant sensors to get fast and accurate input estimations motivates the need to estimate inherent dynamical errors [?] and to develop methods for dynamic correction in time domain [Hessling, 2008]. The industrial requeriments impose new challenges by increasing the number of sensors distributed in the production lines that provide feedback for quick decision taking to control autonomous activation [Esward et al., 2009].

To implement the input estimation methods in the practice, the compensation filters based on deconvolution [Eichstädt et al., 2010] are the preferred methodology to develop analog filters [Jafaripanah et al., 2005], adaptive digital filters [Shu, 1993], lattice adaptive filters [Hernandez, 2006], compensators for simultaneous responses of different sensors [Boschetti et al., 2013], regularized deconvolution compensators [Dienstfrey and P.D., 2014], and a multiple choice set of filters [Huang et al., 2016]. All these methods have in common the use of the measurement system model to build the compensator, for instance, after the model parameters.

A list of measurement methods based on digital signal processors (DSP) include a study of the data-driven dynamic error correction and its impact on the measured temperature [Saggin et al., 2001], a modulation quality measurement of microwave access systems [Angrisani and Napolitano, 2010], a real-time rotational speed estimation using correlation [Wang et al., 2014], a development of an biology-inspired electronic nose [Jing et al., 2016], and impedance measurements for material damage estimation using cross-correlation [de Castro et al., 2019]. The data-driven step input estimation method [Markovsky, 2015a] is added to this list, highlighting the fact that can be implemented for the measurement of different physical magnitudes bacause is model independent.

In metrology, each measurement is an estimation that can be modeled as a random variable. Every measurement is inherently perturbed by noise and, therefore, the input estimation is commonly expressed with its two first statistical moments [Ferrero and Salicone, 2006]. In an effort to standardize the uncertainty assessment of the input estimation, a guideline [BIPM et al., 2008]has been prepared and has a overall acceptance in the metrolgy community. A review of measurement uncertainty analysis of common use is presented in [Hack and ten Caten, 2012]. The Monte Carlo method has been shown to be an effective uncertainty evaluation tool in [Cox and Siebert, 2006], and supports the usefulness of simulation for quantifying measurement uncertainties by software [Esward, 2016]. Another example of the Monte Carlo method is the dynamic measurement uncertainty evaluation of clinical thermometers described in [Ogorevc et al., 2016].

Nevertheless, researchers still pinpoint the need to study more the uncertainty assessment methods [Esward et al., 2009; Hessling, 2010]. It is recommended to consider the uncertainties of all the measurement chain components [Diniz et al., 2017], and to avoid the direct uncertainty propagation from the calibration towards the to-be-measured quantity. Methods for evaluating the uncertainty associated with the output of compensation filters have been investigated, such as for a discrete-time infinite-response filter in [Link and Elster, 2009], a discrete-time finite-response filter in [Elster et al., 2007; Elster and Link, 2008], and the Kalman filter in [Eichstädt et al., 2016]. All these works propagate the uncertainty through the filter but it is also necessary to upward the propagation up to the sensor model to include all systematic error contributions [Hessling, 2011].

2.2. Original contributions

This thesis describes research work iniciated after the data-driven step input estimation method. This method was proposed for metrology applications but it lacked of an uncertainty assessment, and, therefore, its appropriateness was questionable. The first research work conducted is a statistical analysis to elucidate the bias and the covariance of the estimate that the data-driven step input estimation method provides. After obtaining these statistical moments, the estimate uncertainty is built, and the effectiveness of the method is evaluated. The second research work conducted is a series of experiments that aims to validate the data-driven step input estimation method in real-life applications. The experiments were realizations of the step input excitation using temperature and mass sensors. The step input estimation method showed robustness when the measurement noise is not Gaussian and white as it was assumed in the theoretical analyses. The third

research work conducted is the estimation of affine input parameters following the data-driven approach. The data-driven method is proposed for real-time applications, and uses exponential weighing in the recursive least squares solution of a structured errors-in-variables problem, to give preference to recent samples over the older samples. The data-driven affine input estimation method methodology and performance is compared those of a maximum likelihood method based.

2.2.1. Statistical analysis

The data-driven step input estimation method formulates a structured errors-in-variables (EIV) problem. In linear estimation EIV problems, the regression matrix and the regressor are perturbed by measurement noise [Van Huffel and Vandewalle, 1991], [Markovsky and Van Huffel, 2007]. The regression matrix, in structured EIV problems, has a structure that depends on the problem formulation. The Hankel and Toeplitz matrices appear in problems of metrology [Markovsky, 2015a], system identification [Söderström, 2007], image restoration [Feiz and Rezghi, 2017], nuclear magnetic resonance spectroscopy [Cai et al., 2016], direction-of-arrival estimation [Pan et al., 2018], and time-of-arrival estimation [Jia et al., 2018].

The data-driven step input estimation method directly estimates the input from the sensor transient response. The perturbations in the EIV problem of interest come from the sensor output, that is the only observed signal [Markovsky, 2015a], and is used to construct both the regression matrix and the regressor. The structure in this regression matrix is block-Hankel. The direct estimation is a data-driven methodology that reduces the input estimation time of the classical two-stage approach where a sensor model is first identified, and later the input is estimated using the sensor model [Azam et al., 2015; Niedźwiecki et al., 2016].

Instead of using a total least-squares (TLS) solution of the structured EIV problem, the recursive least squares solution (RLS) is proposed to get the step input estimate. The TLS solution of unstructured EIV problems is consistent when the perturbations have zero mean with a given positive definite covariance, and the TLS solution is equivalent to the maximum likelihood (ML) solution when the perturbations of the EIV problems are i.i.d. normally distributed [Markovsky and Van Huffel, 2007]. However, regarding structured EIV problems, the TLS estimator does not give general results since each structure requires a specific treatment [Van Huffel et al., 2007], and the ML estimator leads to non-convex optimization problems where the global optimum is not guaranteed [Rhode et al., 2014]. Moreover, the computational complexity of TLS and ML inhibits their

real-time implementation. The least-squares (LS) estimator is a suboptimal but simple solution to structured EIV problems that admits a recursive form (RLS) suitable for real-time implementation.

The previously published works that propose LS estimators to solve structured EIV problems do not study the required statistical moments to know the uncertainty of the data-driven step input estimation method. In the literature we find the design of a fast algorithm for matrices with small displacement rank [Mastronardi and O'Leary, 2007], the study of the LS estimator consistency [Palanthandalam-Madapusi et al., 2010], the determination of the bias, and the mean squared error of the parameter estimates in the identification of AR models [Kiviet and Phillips, 2012], [Kiviet and Phillips, 2014], and a discussion of the causes of bias and inconsistency in homogeneous estimators [Yeredor and De Moor, 2004]. The literature does not address the uncertainty of the reported LS estimators for structured EIV problems.

The uncertainty of an estimation method is expressed using the bias and covariance of the estimate [Pintelon and Schoukens, 2012]. To know the uncertainty of the data-driven step input estimation method, I quantified the bias and the covariance of the LS solution of EIV problems, for unstructured and structured cases. This quantification extends the perturbation analysis of the LS estimator of unstructured and uncorrelated problems that was investigated in [Stewart, 1990] and in [Vaccaro, 1994]. The analysis of the unstructured EIV case provides an insight of the impact that the structure of the regression matrix and the correlation between the regression matrix and the regressor perturbations have on the uncertainty of the LS estimate. The study presented in this thesis illustrates a methodology to conduct statistical analysis for any structured EIV problem.

I derived expresions that quantify the bias and covariance by obtaining the mathematical expectation of the LS estimate approximated by the second-order Taylor series expansion. Using Monte Carlo simulations, I validated the accuracy of the bias and covariance expressions. These expressions estimate the bias and covariance that the data-driven step input estimation method will exhibit for given sample size and perturbation level. I compared the mean squared error of the LS estimate to the minimum variance specified by the Cramér-Rao lower bound of the structured EIV problem, to determine the conditions in which the data-driven step input estimation method is appropriate for practical applications.

2.2.2. Experimental validation

The validation of the data-driven step input estimation method in a practical application was necessary to demonstrate the usefulness of the method. The method performance was illustrated by simulations and temperature experiments on a digital signal processor (DSP) of low cost [Markovsky, 2015a]. The method estimates the unknown level of step inputs by processing the sensor step response, and avoiding the sensor modeling stage. The formulation of the estimation method is a correlated errors-in-variables (EIV) problem with block-Hankel structure.

Other methods for input estimation mainly compensate the sensor transient response, for example, by recursive estimation of the compensator parameters [Shu, 1993], finite impulse response (FIR) filtering [Elster et al., 2007], [Niedźwiecki and Pietrzak, 2016] filters and infinite impulse response (IIR) filtering [Pintelon et al., 1990], [Elster and Link, 2008]. The uncertainty propagation for these model-based compensators is based on the transfer function or state space representations of the LTI sensor and filter systems [Link and Elster, 2009], [Hale et al., 2009]. Another way to assess the measurement uncertainty is by observing the results of multiple practical measurements as it is described in [Pietrzak et al., 2014] for mass and in [Ogorevc et al., 2016] for temperature sensors.

To validate the data-driven step input estimation method I built a weighing system setup based on a load cell sensor. The weighing setup was constructed to ensure repeatability and reproducibility along different experimental realizations. Load cell sensors are versatil devices that are found in heart and breathing physiological signal monitoring [Lee et al., 2016], clinical analysis of sleep quality [Zahradka et al., 2018], automobile safety studies [Ballo et al., 2016], wind turbine design [Rossander et al., 2015], civil engineering [Olmi, 2016], and sport bicycle design [Casas et al., 2016], to name a few.

The signal from the load cell sensor in the weighing system is conditioned using operational amplifiers. The signal conditioning amplifier has a low-pass filter to prevent aliasing noise. The observed measurement noise has non-white noise properties, mainly due to the characteristics of the load cell sensor. One of the assumptions of the step input estimation method formulation is that the measurement noise is Gaussian white. Nevertheless, the estimation results show that the method is still able to provide useful input estimations.

The empirical bias an covariance obtained after repeating the weighing experiment was compared to the bias and covariance estimations obtained in the previous research work [Quintana-Carapia et al., 2019], and to the minimal variance given by the Cramér-Rao lower bound (CRLB) of the structured EIV problem. I found

that the mean squared error (MSE) of the step input estimate is near the CRLB, and the distance between the MSE and the CRLB provides a confidence interval for the input estimate with respect to the level of the measurement noise.

2.2.3. Affine input estimation

A dynamic measurement is present when the fluctuations of the measurand impact on the input estimation, such as when a low-bandwidth sensor is excited with a fast changing input. The detection of input characteristics is of interest in several scientific and industrial applications for temperature [Saggin et al., 2001], pressure [Matthews et al., 2014], acceleration [Link et al., 2007], force [Vlajic and Chijioke, 2016], [Hessling, 2008], and mass [Shu, 1993], [Boschetti et al., 2013].

I worked on a method to estimate the parameters of inputs that vary at a constant rate, influenced by the data-driven signal processing method that estimates the step level value using subspace techniques [Markovsky, 2015a], [Markovsky, 2015b]. An input varies at a constant rate in applications where the magnitude of interest activates the sensor gradually. An example of this affine activation is the measurement of mass while the to-be-weighted object is transported by a conveyor belt, and the profile of the input is a saturated ramp. Current solutions to the weighing in motion are low pass filters that estimate the mass using the saturated part of the input [Tasaki et al., 2007; Pietrzak et al., 2014]. The signal processing affine input estimation methods are motivated by the need to obtain the mass of the object from the ramp before it reaches saturation.

The proposed data-driven method for the estimation of the affine input parameters. The affine input is parameterized as a straight line model where the slope and the interception are the parameters of interest. The data-driven affine input estimation method formulates a structured errors-invariables (EIV) problem, similar to the one fourmulated for the step input estimation. An exponential weight is added to the recursive least squares. This is a forgetting factor that considers that the newer samples are more relevant for the input parameters estimation. The data-driven affine input estimation method is a recursive algorithm that can be implemented in real-time since it has low computational cost.

The performance of the proposed method is compared to that of a maximum-likelihood (ML) estimation method based on local-optimization and a time-varying compensation filter. The ML method simulates the response of a sensor model to an affine input, and minimizes a cost function that is the sum of the squared differences between the actual and the simulated sensor responses. The ML method resembles the model predictive control approach in the sense that a cost

function is minimized iteratively to optimize the parameters of a sensor model using the observed sensor response in a receding time horizon [Mayne, 2014]. The difference is that the ML method aims to estimate the unknown value of the affine input parameters instead of identifying a model and controlling the dynamic system.

After observing the simulation results, the data-driven affine input estimation method is suitable for real-time applications since it requires low computational resources. The ML method is more appropriate for off-line processing of the sensor transient response, but it can estimate also the parameters of a sensor model, and the initial conditions of the sensor. The main drawback of the ML method is the need of high computational resources.

3. Preliminaries

3.1. Preliminaries

In metrology, we use the concepts of linear systems theory to estimate the value of an unknown quantity. A sensor is considered to be a causal linear time-invariant (LTI) system. The unknown quantity is the input $\mathbf{u}$ of the sensor, and the consequences of this excitation are a change in the sensor state $\mathbf{x}$, from the initial conditions $\mathbf{x}_{\text{ini}}$, and a transient response in the sensor output $\mathbf{y}$, see Figure 3.1. A measurement estimates the input value using the sensor response.
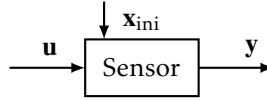
Figure 3.1.: Block diagram of an LTI sensor. The input $\mathbf{u}$ excites the sensor and generates the sensor response $\mathbf{y}$. To estimate the input value it is necessary to process the response.

The discrete-time state-space representation of an LTI system is

$$\begin{aligned}
\mathbf{x}(k+1) &= \mathbf{A}\mathbf{x}(k) + \mathbf{B}\mathbf{u}(k), \quad \text{with} \quad \mathbf{x}_{\text{ini}} = \mathbf{x}(0) \\
\mathbf{y}(k) &= \mathbf{C}\mathbf{x}(k) + \mathbf{D}\mathbf{u}(k) + v(k),
\end{aligned} \tag{3.1}$$

where $\mathbf{A} \in \mathbb{R}^{n \times n}$, $\mathbf{B} \in \mathbb{R}^{n \times m}$, $\mathbf{C} \in \mathbb{R}^{p \times n}$, and $\mathbf{D} \in \mathbb{R}^{p \times m}$, are the model matrices, v is the measurement noise, n is the system order, m is the number of inputs, and p is the number of outputs. Although we may think that most sensors are single-input single output (SISO) like temperature sensors, there are sensors with single input and multiple outputs such as gas sensors [Munther et al., 2019], and sensors with multiple inputs and multiple outputs like the three-axis accelerometers [D'Emilia

et al., 2016], the radio-frequency intruder-detection sensors [Ushiki et al., 2013], and the radar sensor [Kueppers et al., 2017].

The discrete-time state-space representation suggests that when the model, and the initial conditions are known, and in absence of measurement noise, it is sufficient to solve the system of equations

$$
\underbrace{\begin{bmatrix} y(0) \\ y(1) \\ y(2) \\ \vdots \\ y(T) \end{bmatrix}}_{\mathbf{y}} = \underbrace{\begin{bmatrix} \mathbf{C} \\ \mathbf{CA} \\ \mathbf{CA}^2 \\ \vdots \\ \mathbf{CA}^T \end{bmatrix}}_{O} \mathbf{x}(0) + \underbrace{\begin{bmatrix} \mathbf{D} & & & & \\ \mathbf{CB} & \mathbf{D} & & & \\ \mathbf{CAB} & \mathbf{CB} & \mathbf{D} & & \\ \vdots & \ddots & & & \\ \mathbf{CA}^{T-1}\mathbf{B} & \cdots & \mathbf{CAB} & \mathbf{CB} & \mathbf{D} \end{bmatrix}}_{T} \underbrace{\begin{bmatrix} u(0) \\ u(1) \\ u(2) \\ \vdots \\ u(T) \end{bmatrix}}_{\mathbf{u}},
\tag{3.2}
$$

to find the input. This system of equations is constructed from the recursions of (3.1), where O is the observability matrix of the system, and T is a Toeplitz matrix of the Markov parameters of the system.   formulated as the input estimation problem from the response of a system.

The input estimation problem is more complex when one or more of these assumptions are not fulfilled. If the initial conditions and the measurement noise are unknown, the typical approach is to feed the output $\mathbf{y}$ to an additional system. This additional system is modeled to invert the dynamics of the sensor by doing an operation that is equivalent to deconvolution, aiming to estimate the input $\mathbf{u}$ with the output $\widehat{\mathbf{u}}$ of the additional system. This system is called compensator because the transient time of the estimated input $\widehat{\mathbf{u}}$ is smaller than the transient time of $\mathbf{y}$, see Figure 3.2.
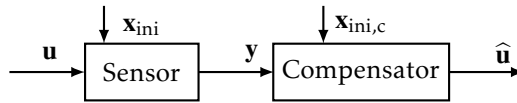
Figure 3.2.: Input estimation using a compensator that processes the sensor response $\mathbf{y}$. The compensator is an additional system that reverts the dynamics of the sensor.

If a model of the sensor is not available, the first idea may be to identify a model using the inputs and outputs, and later to estimate the input using the identified model. However, the input is unknown and the model must be identified using only the sensor output. Modeling the input as a multiple of the unit step function allows an analytical treatment of the input estimation problem. This chapter describes step input estimation methods derived from linear systems theory. The

description starts with the case in which the model is known, continues with the unknown sensor model case that performs model identification, and ends with a direct estimation of the input without model identification. The suitability of data-driven methods on-line implementation is higher because there is no need for high computational power to identify the system.

Step input estimation with system model

With a step input $\mathbf{u} = \bar{\mathbf{u}}s$, where $s(t) = 1$, for $t \geq 0$, and $s(t) = 0$, for $t < 0$, the discrete-time state space representation of the LTI sensor is equivalent to an augmented autonomous system

$$\mathbf{x}_a(k+1) = \underbrace{\begin{bmatrix} \mathbf{A} & \mathbf{B} \\ 0 & 1 \end{bmatrix}}_{\mathbf{A}_a} \mathbf{x}_a(k), \quad , \quad \text{where} \quad \mathbf{x}_a(k) = \begin{bmatrix} \mathbf{x}(k) \\ \mathbf{u}(k) \end{bmatrix}, \quad \mathbf{x}_{\text{ini}} = \mathbf{x}(0)$$

$$\mathbf{y}(k) = \underbrace{\begin{bmatrix} \mathbf{C} & \mathbf{D} \end{bmatrix}}_{\mathbf{C}_a} \mathbf{x}_a(k).$$

(3.3)

The eigenvalues λ of the augmented autonomous system are found using

$$|\lambda \mathbf{I} - \mathbf{A}_a| = \left| \lambda \mathbf{I} - \begin{bmatrix} \mathbf{A} & \mathbf{B} \\ 0 & 1 \end{bmatrix} \right| = |\lambda \mathbf{I} - \mathbf{A}| (\lambda - 1) = 0.$$

Therefore, the eigenvalues, poles, of the augmented autonomous system (3.3) are the eigenvalues, poles, of the LTI system, with the additional eigenvalue $\lambda = 1$, pole at $(1,0)$.

Since the input $\mathbf{u}(t+1) = \mathbf{u}(t)$, for $t \geq 0$, is an augmented state of the autonomous system, and the system is known, a state estimator is sufficient to estimate the input. In these conditions, the Kalman filter estimates recursively the input value.

Step input estimation without system model

Reduction to autonomous equivalent model

A first method, when the model of the LTI sensor is unknown and we have exact data, identifies a model of the sensor from the step response, and the estimates the input using the identified sensor model. The model identification consists in the estimation of the matrices $\widehat{\mathbf{A}}_a$ and $\widehat{\mathbf{C}}_a$, and the initial conditions $\widehat{\mathbf{x}}(0)$. To do this, consider that a Hankel matrix $H(\mathbf{y}) \in \mathbb{R}^{n \times n}$, constructed from any linearly independent n autonomous responses from the sensor initial conditions, is full

column rank. Thus, we can express

$$\underbrace{\begin{bmatrix} y(1) & y(2) & \cdots & y(n) \\ y(2) & y(3) & \cdots & y(n+1) \\ \ddots & \ddots & \ddots & \\ y(n) & y(n+1) & \cdots & y(2n-1) \end{bmatrix}}_{H(\mathbf{y})} = \underbrace{\begin{bmatrix} \widehat{\mathbf{C}}_a \\ \widehat{\mathbf{C}}_a \widehat{\mathbf{A}}_a \\ \vdots \\ \widehat{\mathbf{C}}_a \widehat{\mathbf{A}}_a^n \end{bmatrix}}_{O_a} \underbrace{\begin{bmatrix} \mathbf{x}_a(0) & \mathbf{x}_a(1) & \cdots & \mathbf{x}_a(n) \end{bmatrix}}_{\mathbf{X}_{ini}},$$

where $\mathbf{X}_{ini}$ is a matrix with the initial conditions of the n free responses. A singular value decomposition of $H(\mathbf{y})$

$$\mathbf{U}\mathbf{\Sigma}\mathbf{V} = H(\mathbf{y}),$$

permits the estimation of the observability matrix O_a and the initial conditions $\mathbf{X}_{ini}$, for example, by choosing

$$\widehat{O}_a = \mathbf{U}\sqrt{\mathbf{\Sigma}}, \quad \text{and} \quad \widehat{\mathbf{X}}_{ini} = \sqrt{\mathbf{\Sigma}}\mathbf{V}.$$

The matrices $\widehat{\mathbf{A}}_a$ and $\widehat{\mathbf{C}}_a$ can be estimated, from $\widehat{O}_a$, by solving a system of equations. In order to estimate the input, it is necessary to find a minimal representation of the autonomous system, by doing a linear transformation that removes the pole at $(1,0)$, and recovers the matrices $\widehat{\mathbf{A}}, \widehat{\mathbf{B}}, \widehat{\mathbf{C}}$, and $\widehat{\mathbf{D}}$.

Identification of the model followed by input estimation

A second method is proposed to estimate the step input when the model of the LTI system is unknown but its steady-state gain $\mathbf{G}$ is known. Using the steady-state gain $\mathbf{G}$, we can express $\bar{\mathbf{y}} = \mathbf{G}\bar{\mathbf{u}}$, where $\bar{\mathbf{u}}$ is the input exact value and $\bar{\mathbf{y}}$ is the sensor steady state response. The total response of the system is the sum of the transient and the steady-state responses. Thus, considering the augmented autonomous model, we can write

$$\mathbf{y} = \mathbf{G}\,\bar{\mathbf{u}} + O_a\,\mathbf{x}(0),$$

that in matrix form is

$$\underbrace{\begin{bmatrix} y(0) \\ y(1) \\ \vdots \\ y(T) \end{bmatrix}}_{\mathbf{y}} = \underbrace{\begin{bmatrix} \mathbf{G} & \mathbf{C}_a \\ \mathbf{G} & \mathbf{C}_a\mathbf{A}_a \\ \vdots & \vdots \\ \mathbf{G} & \mathbf{C}_a\mathbf{A}_a^T \end{bmatrix}}_{\mathbf{K}} \begin{bmatrix} \bar{\mathbf{u}} \\ \mathbf{x}(0) \end{bmatrix}.$$

It is necessary to estimate the observability matrix of the augmented system, followed by the estimation of the input $\mathbf{u}$, and the initial conditions $\mathbf{x}_{ini}$, using least squares

$$\begin{bmatrix} \widehat{\mathbf{u}} \\ \widehat{\mathbf{x}}_{ini} \end{bmatrix} = \left(\mathbf{K}^\top \mathbf{K} \right)^{-1} \mathbf{K}^\top \mathbf{y}.$$

Data-driven estimation of an unknown step input given system response

A third method directly estimates the input value from the step response, without an identification of the sensor model. Applying the first difference operator, $\Delta = \sigma - 1$, to the system state space representation (3.1), we have

$$\Delta\mathbf{x}(k+1) = \mathbf{A}\Delta\mathbf{x}(k), \quad \Delta\mathbf{y}(k) = \mathbf{C}\Delta\mathbf{x}(k), \quad \text{with} \quad \Delta\mathbf{x}_{\text{ini}} = \Delta\mathbf{x}(0), \qquad (3.4)$$

where σ is the shift operator, defined as $(\sigma^\tau y)(t) = y(t + \tau)$, and $\Delta\mathbf{u}(k) = \mathbf{0}$, for $k \geq 0$, because we have a step input, and $\Delta\mathbf{x}(0) = (\mathbf{A} - \mathbf{I})\mathbf{x}(0) + \mathbf{B}\bar{\mathbf{u}}$. The resulting system (3.4) is autonomous. When the response $\Delta\mathbf{y}$ is persistingly exciting of order L, i.e., when the rank of the Hankel matrix $H_{L+1}(\Delta\mathbf{y})$ of $L + 1$ block rows constructed from $\Delta\mathbf{y}$ satisfies

$$\text{rank}\,(H_{L+1}\,(\Delta\mathbf{y})) \leq L,$$

the Hankel matrix $H_{L+1}(\Delta\mathbf{y})$ provides a linear map to the free responses of the augmented autonomous system (3.3). In this case, the total response of the system is given by

$$\mathbf{y} = \mathbf{G}\,\bar{\mathbf{u}} + H(\Delta\mathbf{y})\,\boldsymbol{\ell}$$

that is equivalent to

$$
\underbrace{\begin{bmatrix} y(n+1) \\ \vdots \\ y(T) \end{bmatrix}}_{\mathbf{y}} = \underbrace{\begin{bmatrix} \mathbf{G} & \Delta y(1) & \Delta y(2) & \cdots & \Delta y(n) \\ \mathbf{G} & \Delta y(2) & \Delta y(3) & \cdots & \Delta y(n+1) \\ \vdots & \ddots & \ddots & \ddots & \\ \mathbf{G} & \Delta y(T-n) & \Delta y(T-n+1) & \cdots & \Delta y(T-1) \end{bmatrix}}_{K} \begin{bmatrix} \bar{\mathbf{u}} \\ \boldsymbol{\ell} \end{bmatrix}.
$$

The step response observations $y(t) \in \mathbb{R}$ for $t = 1, \ldots, T$, where T is the number of samples, is perturbed by normally distributed measurement noise ε with zero mean and given variance σ_ε^2. We have

$$y = \bar{y} + \varepsilon, \quad \text{and} \quad K = \bar{K} + E, \qquad (3.5)$$

where $\bar{y}$ is the exact system response and E is the matrix that whose elements are the corresponding noise perturbations to the exact data elements in $\bar{K}$, and the vector ℓ is a linear transformation of the system initial conditions. The observed response of the system is a step-invariant discretization of the continuous-time response.

The system of equations $y = Kx$ is an errors-in-variables (EIV) minimization problem with block Hankel structure. The perturbation noise present in K is correlated to the perturbation of the elements in y. This EIV problem admits a least-squares

(LS) solution and the recursive LS enables the online implementation for real-time step input estimation applications. The step input estimation method was described in [Markovsky, 2015a].

The uncertainty assessment is compulsory in metrology

Pending Rik comments :noexport:

** 20190701 *** Introduction - Data-driven methodology: Moreover, the online uncertainty assessment may not be feasible and we have to rely on confidence bounds.

Consequently, avoiding the explicit model identification from input-output data and estimating directly the input from the transient response reduces the input estimation time and makes data-driven input estimation methods suitable for real-time metrology applications, where confidence bounds describe the estimation uncertainty. **** Rik: Obained in a calibration step? Please clarify *** Original contributions - Statistical analysis of structured EIV problems It was observed that the input estimation is biased but with small variance, and that the difference between theoretical minimum and the empirical variance is not large.

**** Rik: order of magnitude of RMSE for SNRs larger than XXX — (smaller than XXX for SNRs larger than YYY)

*** Original contributions - Experimental validation of the step input estimation method The results of the estimation method with respect to different sensor model order assumptions were compared and we concluded that increasing the order does not necessarily benefits the input estimation uncertainty.

**** Rik: On the contrary: the important conclusion here is that using an order that is larger than the true model order results in a smaller mean squared error.

*** Estimation of a step input y in $R^p u$ in R^m **** $Rik : Relationship between "m" and "p"? For sensors p = m is the generic situation. Do you know sensors where p <> m? If so, discuss these cases.$

*** Estimation of a step input - Step input estimation without system model - Data-driven estimation of an unknown step input given system response

The data-driven method is motivated by the persistency of excitation lemma of linear systems theory. Persistency of excitation of the input is a necessary identifiability condition in exact system identification.

**** Rik: persistence of excitations stems from identification theory, not system theory

4. Statistical Analysis

The results of this chapter ...

4.1. Introduction

The linear estimation problems with perturbation in both the regression matrix and the regressor are errors-in-variables (EIV) problems. To evaluate the properties of the solution to an EIV problem it is often required to calculate the statistical moments of the estimate. The calculation of the estimate statistical moments demands a larger effort when the regression matrix of a EIV problem is structured, and when is correlated to the regressor.

Structured total least squares and structured total maximum likelihood are two examples of methods that solve structured EIV problems, but that require large computational resources. For online applications where a real-time solution of the structured EIV problem is desired, the recursive least-squares (RLS) method is a suboptimal but computationally cheaper estimator.

To obtain the statistical moments of the RLS estimation for a structured and correlated EIV problem, and to assess the estimate uncertainty, that have not been obtained before, a statistical analysis was conducted.

This chapter describes the methodology and the results of the statistical analysis. The mathematical expectation of the RLS estimate, approximated by a second-order Taylor series expansion, allows a quantification of the first and second-order moments of the LS estimate. The results of the statistical analysis provide an insight of the impact that the structure of the regression matrix and the correlation between the regression matrix and the regressor perturbations have on the uncertainty of the RLS estimate.

4.2. Statistical analysis

For an overdetermined system of linear equations, the least-squares (LS) solution is given by

$$\widehat{\mathbf{x}} = \widetilde{\mathbf{K}}^{\dagger}\widetilde{\mathbf{y}} = (\widetilde{\mathbf{K}}^{\top}\widetilde{\mathbf{K}})^{-1}\widetilde{\mathbf{K}}^{\top}\widetilde{\mathbf{y}}, \tag{4.1}$$

where $\widetilde{\mathbf{K}}^{\dagger}$ is the pseudo-inverse of $\widetilde{\mathbf{K}}$. The objective of the statistical analysis is to obtain the bias and the covariance of the solution $\widehat{\mathbf{x}}$. The bias and the covariance are computed using the mathematical expectation operator $\mathbb{E}\{\cdot\}$. First we substitute (3.5) and (**??**) in (4.1) obtaining

$$\widehat{\mathbf{x}} = \left((\mathbf{K}+\mathbf{E})^{\top}(\mathbf{K}+\mathbf{E})\right)^{-1}(\mathbf{K}+\mathbf{E})^{\top}(\mathbf{y}+\boldsymbol{\epsilon}),$$

which is equivalent to

$$\widehat{\mathbf{x}} = (\mathbf{I}+\mathbf{M})^{-1}\mathbf{Q}^{-1}(\mathbf{K}+\mathbf{E})^{\top}(\mathbf{y}+\boldsymbol{\epsilon}), \tag{4.2}$$

where

$$\mathbf{Q} = \mathbf{K}^{\top}\mathbf{K}, \quad \text{and} \quad \mathbf{M} = \mathbf{Q}^{-1}(\mathbf{K}^{\top}\mathbf{E}+\mathbf{E}^{\top}\mathbf{K}+\mathbf{E}^{\top}\mathbf{E}). \tag{4.3}$$

Applying a second-order Taylor expansion of the inverse matrix

$$(\mathbf{I}+\mathbf{M})^{-1} \approx \mathbf{I}-\mathbf{M}+\mathbf{M}^{2}, \tag{4.4}$$

that is valid when the SNR is sufficiently high, and therefore $\mathbf{E}$ and $\mathbf{M}$ are small, satisfying the constraint on the spectral radius $\|\mathbf{M}\| < 1$. The neglected term in the Taylor series expansion is of the order $O(\|M\|^{3})$. We can express the estimate as

$$\widehat{\mathbf{x}} \approx \left(\mathbf{I}-\mathbf{M}+\mathbf{M}^{2}\right)\mathbf{Q}^{-1}(\mathbf{K}+\mathbf{E})^{\top}(\mathbf{y}+\boldsymbol{\epsilon}). \tag{4.5}$$

Now that the perturbation variables $\boldsymbol{\epsilon}$ and $\mathbf{E}$ are no longer inside an inverse matrix, we can compute the mathematical expectation of expressions derived from the Taylor series approximation (4.5) of $\widehat{\mathbf{x}}$. The bias of the estimate $\widehat{\mathbf{x}}$ is obtained from

$$\mathbf{b}\left(\widehat{\mathbf{x}}\right) = \boldsymbol{\mu}\left(\widehat{\mathbf{x}}\right) - \mathbf{x}, \tag{4.6}$$

where $\boldsymbol{\mu}\left(\widehat{\mathbf{x}}\right) = \mathbb{E}\{\widehat{\mathbf{x}}\}$, and $\mathbf{x} = \mathbf{K}^{\dagger}\mathbf{y} = \mathbf{Q}^{-1}\mathbf{K}^{\top}\mathbf{y}$ is the true value. The covariance of the estimate $\widehat{\mathbf{x}}$ is obtained from

$$\mathbf{C}\left(\widehat{\mathbf{x}}\right) = \mathbb{E}\left\{\left(\widehat{\mathbf{x}}-\boldsymbol{\mu}\right)\left(\widehat{\mathbf{x}}-\boldsymbol{\mu}\right)^{\top}\right\}. \tag{4.7}$$

The terms derived from (4.5) that do not contribute to the bias and to the covariance are filtered out by the mathematical expectation operator considering the following general rules that are valid regardless of the existence of structure in the regression problem:

- the expected values $\mathbb{E}\{\mathbf{E}\} = \mathbf{0}$, and $\mathbb{E}\{\boldsymbol{\epsilon}\} = \mathbf{0}$, since $\mathbf{E}$ and $\boldsymbol{\epsilon}$ are zero-mean random variables, and

- the expected values of odd order moments, such as $\mathbb{E}\{\mathbf{E}^\top \mathbf{E} \mathbf{E}^\top\}$, are zero.

Moreover, the second-order approximation disregards moments of order four and higher.

After removing the terms with negligible expected value, we have expressions that are approximations of the LS estimation bias and covariance. These expressions are different depending on the type of EIV problem considered. Subsections 3.1 and 3.2 describe the resulting expressions for the unstructured and structured EIV problems, respectively. The perturbations in the considered unstructured EIV problem are independent. Comparing the expressions that result from the statistical analysis, we get an insight of what is the impact that the structure and the correlation have on the LS solution of the structured EIV problem.

4.2.1. Bias and covariance of the LS estimator for an unstructured EIV problem with uncorrelated noise

First, the statistics of the least squares estimator (4.1) of an unstructured EIV problem is discussed, provided that the perturbations of the regression matrix and the regressor are i.i.d. normally distributed with zero mean, and variances $\sigma_{\mathbf{E}}^2$ and σ_{ϵ}^2, respectively. Therefore, the terms in the Taylor series expansion (4.5) that contain products of $\mathbf{E}$ and $\boldsymbol{\epsilon}$ have zero expected value. After removing the terms without contribution to the bias, and to the covariance, with the mathematical expectation operator, the analytic approximation of the bias (4.6) is given by

$$\mathbf{b}_\mathrm{p}\left(\widehat{\mathbf{x}}\right) \approx \sigma_{\mathbf{E}}^2 \left(2 + 2n - T\right) \mathbf{Q}^{-1}\mathbf{x}, \tag{4.8}$$

and the covariance (4.7) is approximated by

$$\mathbf{C}_\mathrm{p}\left(\widehat{\mathbf{x}}\right) \approx \sigma_{\epsilon}^2\, \mathbf{Q}^{-1} + \sigma_{\mathbf{E}}^2 \, \mathrm{trace}\left(\mathbf{x}\mathbf{x}^\top\right) \mathbf{Q}^{-1} - \sigma_{\mathbf{E}}^4 \left(2 + 2n - T\right)^2 \, \mathbf{Q}^{-1}\mathbf{x}\mathbf{x}^\top\mathbf{Q}^{-1}, \tag{4.9}$$

where the subscript p stands for prediction of the bias and covariance. The derivation of equations (4.8) and (4.9) is described in Appendix 1. We use the results described in [Vaccaro, 1994] §3 and [Stewart, 1990] §2.1 for the expected values of products of unstructured matrices with perturbations. Equations (4.8) and (4.9) depend on the unobservable true values $\mathbf{x}$, $\mathbf{K}$, and on the variance of the perturbations. The observed variables are $\widetilde{\mathbf{y}}$, $\widetilde{\mathbf{K}}$, and from them we compute $\widehat{\mathbf{x}}$. It is proposed to directly substitute the observed variables in the analytic expressions.

The substitution gives an approximation of the estimate bias and covariance using the observed data. We have then

$$\widetilde{\mathbf{b}}_{\mathrm{p}}\left(\widehat{\mathbf{x}}\right) \approx \sigma_{\widetilde{\mathbf{E}}}^2 \left(2 + 2n - T\right) \widetilde{\mathbf{Q}}^{-1} \widehat{\mathbf{x}}, \tag{4.10}$$

$$\widetilde{\mathbf{C}}_{\mathrm{p}}\left(\widehat{\mathbf{x}}\right) \approx \sigma_{\widetilde{\varepsilon}}^2 \, \widetilde{\mathbf{Q}}^{-1} + \sigma_{\widetilde{\mathbf{E}}}^2 \, \mathrm{trace}\left(\widehat{\mathbf{x}}\widehat{\mathbf{x}}^\top\right) \widetilde{\mathbf{Q}}^{-1} - \sigma_{\widetilde{\mathbf{E}}}^4 \left(2 + 2n - T\right)^2 \widetilde{\mathbf{Q}}^{-1} \widehat{\mathbf{x}}\widehat{\mathbf{x}}^\top \widetilde{\mathbf{Q}}^{-1}. \tag{4.11}$$

In order to have a prediction of the estimate bias and covariance, the variances $\sigma_{\widetilde{\mathbf{E}}}^2$ and $\sigma_{\widetilde{\varepsilon}}^2$ and the observed variables $\widetilde{\mathbf{y}}$, $\widetilde{\mathbf{K}}$, and $\widehat{\mathbf{x}}$ are needed.

4.2.2. Bias and covariance of the LS estimator for a structured EIV problem with noise correlation

This subsection describes the statistics of a structured EIV problem with correlation between the perturbations of the regression matrix and the regressor. The structured EIV problem is given by the step input estimation method (**??**). The correlation is a consequence of the construction of the block-Hankel matrix in the regression matrix $\widetilde{\mathbf{K}}$ with the first difference of the elements in the regressor $\widetilde{\mathbf{y}}$.

The mathematical expectation operator is applied to the Taylor series expansion of the LS estimate (4.5). After removing the terms with negligible expected value, and considering the structure of matrix $\mathbf{K}$, the estimation bias (4.6) is approximated by

$$\mathbf{b}_{\mathrm{p}}\left(\widehat{\mathbf{x}}\right) \approx \mathbf{Q}^{-1}\left(\left(\mathbf{K}^\top \mathbf{B}_1 - \mathbf{B}_2\right)x - \left(\mathbf{K}^\top \mathbf{B}_3 - \mathbf{B}_4\right)\right), \tag{4.12}$$

whereas, the estimation covariance (4.7) is approximated by

$$\mathbf{C}_{\mathrm{p}}\left(\widehat{\mathbf{x}}\right) \approx \mathbf{K}^\dagger \left(\sigma_\epsilon^2 \mathbf{I}_{T-n} + \mathbf{C}_1 - \mathbf{C}_2 - \mathbf{C}_2^\top\right) \mathbf{K}^{\dagger\top} - \mathbf{b}_{\mathrm{p}}\left(\widehat{\mathbf{x}}\right)\mathbf{b}_{\mathrm{p}}^\top\left(\widehat{\mathbf{x}}\right), \tag{4.13}$$

where $\mathbf{B}_1 = \mathbb{E}\left\{\mathbf{E}\mathbf{K}^\dagger\mathbf{E}\right\}$, $\mathbf{B}_2 = \mathbb{E}\left\{\mathbf{E}^\top\mathbf{P}_\perp\mathbf{E}\right\}$, $\mathbf{B}_3 = \mathbb{E}\left\{\mathbf{E}\mathbf{K}^\dagger\epsilon\right\}$, $\mathbf{B}_4 = \mathbb{E}\left\{\mathbf{E}^\top\mathbf{P}_\perp\epsilon\right\}$, $\mathbf{C}_1 = \mathbb{E}\left\{\mathbf{E}\mathbf{x}\mathbf{x}^\top\mathbf{E}^\top\right\}$, $\mathbf{C}_2 = \mathbb{E}\left\{\mathbf{E}\mathbf{x}\epsilon^\top\right\}$, $\mathbf{P} = \mathbf{K}\mathbf{K}^\dagger$, and $\mathbf{P}_\perp = \mathbf{I} - \mathbf{P}$. The derivation of equations (4.12) and (4.13) is described in Appendix 1. The expected values $\mathbf{B}_1$, $\mathbf{B}_2$, $\mathbf{B}_3$, $\mathbf{B}_4$, $\mathbf{C}_1$ and $\mathbf{C}_2$ are obtained using the results of Lemma 1.

Lemma 1. *Let $\mathbf{E} \in \mathbb{R}^{(T-n)\times(n+1)}$ be the partitioned matrix*

$$\mathbf{E} = \begin{bmatrix} \mathbf{0}_{T-n\times 1} & \mathscr{H}(\epsilon)\mathbf{D}_{n+1\times n}^{1,0} \end{bmatrix},$$

where $\mathscr{H}(\epsilon) \in \mathbb{R}^{(T-n)\times(n+1)}$ is the block-Hankel matrix of $T - n$ rows and n columns

$$\mathscr{H}(\epsilon) = \begin{bmatrix} \varepsilon(0) & \varepsilon(1) & \cdots & \varepsilon(n) \\ \varepsilon(1) & \varepsilon(2) & \cdots & \varepsilon(n+1) \\ \vdots & \vdots & & \vdots \\ \varepsilon(T-n-1) & \varepsilon(T-n) & \cdots & \varepsilon(T-1) \end{bmatrix},$$

constructed from samples of the i.i.d. normally distributed random variable $\epsilon \sim \mathcal{N}(0, \sigma_\epsilon^2)$. Let $\mathbf{D}_{r \times c}^{1,k}$ and $\mathbf{D}_{r \times c}^{2,k}$ be the first and second-order finite differences matricial operators of dimensions $r \times c$ starting from the subdiagonal k, for example,

$$\mathbf{D}_{4 \times 3}^{1,-1} = \begin{bmatrix} 0 & 0 & 0 \\ -1 & 0 & 0 \\ 1 & -1 & 0 \\ 0 & 1 & -1 \end{bmatrix}, \quad \mathbf{D}_{4 \times 3}^{2,0} = \begin{bmatrix} -1 & 0 & 0 \\ 2 & -1 & 0 \\ -1 & 2 & -1 \\ 0 & -1 & 2 \end{bmatrix}.$$

For a compatible deterministic matrix $\mathbf{A}$, or vector $\mathbf{a}$, the following expected values hold.

$\mathbb{E}\{\mathbf{EAE}\} = \mathbf{Z}$, *where* $\mathbf{z}_{i1} = \mathbf{0}$, *and* $z_{ij} = \sigma_\epsilon^2 \operatorname{Tr}\left(\mathbf{A} \begin{bmatrix} \mathbf{0}_{T-n} & \mathbf{D}_{T-n \times n}^{2,j-i} \end{bmatrix}\right)$,

   for $i = 1, \cdots, T-n$, *and* $j = 2, \cdots, n+1$.

$\mathbb{E}\left\{\mathbf{E}^\top \mathbf{AE}\right\} = \mathbf{Z}$, *where* $\mathbf{z}_{1j} = \mathbf{0}$, $\mathbf{z}_{i1} = \mathbf{0}$, *and* $z_{ij} = \sigma_\epsilon^2 \operatorname{Tr}\left(\mathbf{A} \mathbf{D}_{T-n \times T-n}^{2,j-i+1}\right)$,

   for $i = 2, \cdots, n+1$, *and* $j = 2, \cdots, n+1$.

$\mathbb{E}\left\{\mathbf{EAE}^\top\right\} = \mathbf{Z}$, *where* $z_{ij} = \sigma_\epsilon^2 \operatorname{Tr}\left(\mathbf{A} \begin{bmatrix} 0 & \mathbf{0}_n^\top \\ \mathbf{0}_n & \mathbf{D}_{n \times n}^{2,j-i+1} \end{bmatrix}\right)$,

   for $i = 1, \cdots, T-n$, *and* $j = 1, \cdots, T-n$.

$\mathbb{E}\{\mathbf{EA}\epsilon\} = \mathbf{z}$, *where* $z_i = \sigma_\epsilon^2 \operatorname{Tr}\left(\mathbf{A} \begin{bmatrix} \mathbf{0}_{T-n} & \mathbf{D}_{T-n \times n}^{1,n+1-i} \end{bmatrix}\right)$,

   for $i = 1, \cdots, T-n$.

$\mathbb{E}\left\{\mathbf{E}^\top \mathbf{A}\epsilon\right\} = \mathbf{z}$, *where* $z_1 = 0$, *and* $z_i = \sigma_\epsilon^2 \operatorname{Tr}\left(\mathbf{A} \mathbf{D}_{T-n \times T-n}^{1,n+2-i}\right)$,

   for $i = 2, \cdots, n+1$.

$\mathbb{E}\left\{\mathbf{Ea}\epsilon^\top\right\} = \mathbf{Z}$, *where each column* $\mathbf{Z}_j = -\sigma_\epsilon^2 \mathbf{D}_{T-n \times n+1}^{1,-j} \mathbf{R}_{n+1} \mathbf{a}$,

   for $j = 1, \cdots, T-n$, *with* $\mathbf{R}_{n+1} = \begin{bmatrix} \mathbf{R}_n \\ \mathbf{0} \end{bmatrix}$,

   where $\mathbf{R}_n$ *is a reversal matrix.*

The proof of the lemma is given in Appendix A.2.

The matrices $\mathbf{B}_1$, $\mathbf{B}_2$, $\mathbf{B}_3$, $\mathbf{B}_4$, $\mathbf{C}_1$ and $\mathbf{C}_2$ are considered in the different cases of Lemma 1. Each expected value in the lemma is a matrix, or a vector, whose elements are found following the indicated operations. These operations mainly compute the trace of a product of the corresponding deterministic matrix $\mathbf{A}$, and a matrix constructed from the finite differences matricial operator, which can be of first order $\mathbf{D}^1$ or of second order $\mathbf{D}^2$. The total number of operations in the computation of the bias and the covariance is $O\left(T^3 + n^2\right)$, but this order can be reduced since the $\mathbf{D}$ matrices are sparse.

The formulas for the bias and covariance (4.12) and (4.13) depend on the perturbation variance and on the unobservable variables $\mathbf{x}$ and $\mathbf{K}$. The substitution of the observed variables in the expression gives an approximation of the estimate bias and covariance based on the observed system response. We have then

$$\mathbf{b}_{\widetilde{p}}(\widehat{\mathbf{x}}) \approx \widetilde{\mathbf{Q}}^{-1} \left(\left(\widetilde{\mathbf{K}}^{\top} \widetilde{\mathbf{B}}_1 - \widetilde{\mathbf{B}}_2 \right) \widehat{\mathbf{x}} - \left(\widetilde{\mathbf{K}}^{\top} \widetilde{\mathbf{B}}_3 - \widetilde{\mathbf{B}}_4 \right) \right), \tag{4.14}$$

and

$$\mathbf{C}_{\widetilde{p}}(\widehat{\mathbf{x}}) \approx \widetilde{\mathbf{K}}^{\dagger} \left(\sigma_{\epsilon}^2 \mathbf{I}_{T-n} + \widetilde{\mathbf{C}}_1 - \widetilde{\mathbf{C}}_2 - \widetilde{\mathbf{C}}_2^{\top} \right) \widetilde{\mathbf{K}}^{\dagger \top} - \mathbf{b}_{\widetilde{p}}(\widehat{\mathbf{x}}) \mathbf{b}_{\widetilde{p}}^{\top}(\widehat{\mathbf{x}}), \tag{4.15}$$

where $\widetilde{\mathbf{B}}_1 = \mathbb{E}\left\{ \mathbf{E}\widetilde{\mathbf{K}}^{\dagger}\mathbf{E} \right\}$, $\widetilde{\mathbf{B}}_2 = \mathbb{E}\left\{ \mathbf{E}^{\top} \widetilde{\mathbf{P}}_{\perp} \mathbf{E} \right\}$, $\widetilde{\mathbf{B}}_3 = \mathbb{E}\left\{ \mathbf{E}\widetilde{\mathbf{K}}^{\dagger}\epsilon \right\}$, $\widetilde{\mathbf{B}}_4 = \mathbb{E}\left\{ \mathbf{E}^{\top} \widetilde{\mathbf{P}}_{\perp} \epsilon \right\}$, $\widetilde{\mathbf{C}}_1 = \mathbb{E}\left\{ \mathbf{E}\widehat{\mathbf{x}}\widehat{\mathbf{x}}^{\top}\mathbf{E}^{\top} \right\}$, $\widetilde{\mathbf{C}}_2 = \mathbb{E}\left\{ \mathbf{E}\widehat{\mathbf{x}}\epsilon^{\top} \right\}$, $\widetilde{\mathbf{C}} = \widetilde{\mathbf{K}}^{\top}\widetilde{\mathbf{K}}$, $\widetilde{\mathbf{P}} = \widetilde{\mathbf{K}}\widetilde{\mathbf{K}}^{\dagger}$, and $\widetilde{\mathbf{P}}_{\perp} = \mathbf{I} - \widetilde{\mathbf{P}}$.

4.2.3. Cramér-Rao lower bound of the structured errors-in-variables problem

The Cramér-Rao lower bound (CRLB) provides the lower limit on the variance of the estimate

$$\text{CRLB}(\mathbf{x}) = \left(\mathbf{I} + \frac{\partial \mathbf{b}(\widehat{\mathbf{x}})}{\partial(\widehat{\mathbf{x}})} \right)^{\top} \mathbf{Fi}^{-1}(\mathbf{x}) \left(\mathbf{I} + \frac{\partial \mathbf{b}(\widehat{\mathbf{x}})}{\partial(\widehat{\mathbf{x}})} \right), \tag{4.16}$$

where $\mathbf{b}(\widehat{\mathbf{x}})$ is the bias of the estimate and $\mathbf{Fi}(\widehat{\mathbf{x}})$ is the Fisher information matrix [Pintelon and Schoukens, 2012]. The Fisher information matrix is defined as the expected value of the Hessian of the negative likelihood function

$$\mathbf{Fi}(x) = -\mathbb{E}\left\{ \frac{\partial^2 l(\widehat{\mathbf{x}})}{\partial \widehat{\mathbf{x}}^2} \right\}, \tag{4.17}$$

where the partial derivatives are evaluated in $\widehat{\mathbf{x}} = \mathbf{x}$.

The minimization problem (**??**) is equivalent to a structured EIV problem that can be expressed as a linear in the measurements problem [Pintelon and Schoukens, 2012]

$$e(\widehat{\mathbf{x}}, \widetilde{\mathbf{z}}) = \mathbf{M}_1(\widehat{\mathbf{x}})\, \widetilde{\mathbf{z}} = \begin{bmatrix} \mathbf{I}_{T-n} & -\widehat{\mathbf{x}}^T \otimes \mathbf{I}_{T-n} \end{bmatrix} \begin{bmatrix} \widetilde{\mathbf{y}} \\ \text{vec}(\widetilde{\mathbf{K}}) \end{bmatrix} = 0. \tag{4.18}$$

where $\widetilde{\mathbf{z}} = \mathbf{z} + \varepsilon_{\mathbf{z}}$. The CRB requires that the true model $\mathbf{M}_1(\mathbf{x})\, \mathbf{z} = 0$ exists. Under the assumption of the measurement perturbation $\varepsilon_{\mathbf{z}}$ being normally distributed with covariance matrix $\mathbf{C}_{\mathbf{z}}$, the loglikelihood function of the structured EIV problem is

$$\ln l(\widetilde{\mathbf{z}}, \widehat{\mathbf{z}}, \widehat{\mathbf{x}}) = -\frac{1}{2} (\widetilde{\mathbf{z}} - \widehat{\mathbf{z}})^{\top} \mathbf{C}_{\mathbf{z}}^{-1} (\widetilde{\mathbf{z}} - \widehat{\mathbf{z}}) + \text{constant}, \tag{4.19}$$

where $\widehat{\mathbf{z}}$ are parameters of the measurements $\widetilde{\mathbf{z}}$ that have to be estimated and satisfy $\mathbf{M}_1(\widehat{\mathbf{x}})\,\widehat{\mathbf{z}} = 0$. The size of the Fisher information matrix $\mathbf{Fi}(\mathbf{x},\mathbf{z})$ depends on the number of unknowns in $\widehat{\mathbf{z}}$ and grows with the sample size. Moreover, in Chapter 19 of [Pintelon and Schoukens, 2012] it is shown that the Fisher information matrix $\mathbf{Fi}(\mathbf{x})$ can be obtained from $\mathbf{Fi}(\mathbf{x},\mathbf{z})$ after doing inversion by parts, giving

$$\mathbf{Fi}(\mathbf{x}) = \left(\frac{\partial e(\widehat{\mathbf{x}},\mathbf{z})}{\partial \mathbf{x}}\right)^{\top} \left(\mathbf{M}_1(\mathbf{x})\,\mathbf{C}_{\mathbf{z}}\,\mathbf{M}_1^{\top}(\mathbf{x})\right)^{-1} \left(\frac{\partial e(\widehat{\mathbf{x}},\mathbf{z})}{\partial \mathbf{x}}\right), \qquad (4.20)$$

where the partial derivatives are evaluated at the true values $\mathbf{x}$, and the covariance matrix of the measurements is

$$\mathbf{C}_{\mathbf{z}} = \sigma_\varepsilon^2 \begin{bmatrix} \mathbf{I}_{T-n} & \mathbf{0}_{T-n} & \mathbf{D}_{T-n\times T-n}^{1,n} & \mathbf{D}_{T-n\times T-n}^{1,n-1} & \cdots & \mathbf{D}_{T-n\times T-n}^{1,1} \\ \mathbf{0}_{T-n} & \mathbf{0}_{T-n} & \mathbf{0}_{T-n} & \mathbf{0}_{T-n} & \cdots & \mathbf{0}_{T-n} \\ \left(\mathbf{D}_{T-n\times T-n}^{1,n}\right)^{\top} & \mathbf{0}_{T-n} & \mathbf{D}_{T-n\times T-n}^{2,1} & \mathbf{D}_{T-n\times T-n}^{2,0} & \cdots & \mathbf{D}_{T-n\times T-n}^{2,2-n} \\ \left(\mathbf{D}_{T-n\times T-n}^{1,n-1}\right)^{\top} & \mathbf{0}_{T-n} & \mathbf{D}_{T-n\times T-n}^{2,2} & \mathbf{D}_{T-n\times T-n}^{2,1} & \cdots & \mathbf{D}_{T-n\times T-n}^{2,3-n} \\ \vdots & \vdots & \vdots & \vdots & & \vdots \\ \left(\mathbf{D}_{T-n\times T-n}^{1,1}\right)^{\top} & \mathbf{0}_{T-n} & \mathbf{D}_{T-n\times T-n}^{2,n} & \mathbf{D}_{T-n\times T-n}^{2,n-1} & \cdots & \mathbf{D}_{T-n\times T-n}^{2,1} \end{bmatrix}. \tag{4.21}$$

The Cramér-Rao lower bound for an biased estimator of the minimization problem (??) is given by

$$\mathrm{CRB}_{b}(\mathbf{x}) = \left(\mathbf{I}_{n+1} + \frac{\partial \mathbf{b}\,(\widehat{\mathbf{x}})}{\partial \mathbf{x}}\right)^{\top} \mathbf{Fi}^{-1}(\mathbf{x}) \left(\mathbf{I}_{n+1} + \frac{\partial \mathbf{b}\,(\widehat{\mathbf{x}})}{\partial \mathbf{x}}\right), \qquad (4.22)$$

and for an unbiased estimator it is $\mathrm{CRB}_{\mathrm{ub}}(\mathbf{x}) = \mathbf{Fi}^{-1}(\mathbf{x})$.

4.3. Simulation results

Two Monte Carlo (MC) simulation studies were conducted to test the obtained bias and variance formulas. One MC simulation was devoted to the unstructured EIV problem and the other to the structured EIV problem that corresponds to the step input estimation method (??). The MC simulations performed $N_{MC} = 10^6$ runs of the LS estimator with different realizations of the perturbation $[\mathbf{E}\quad \epsilon]$. In the structured EIV problem the perturbation $\mathbf{E}$ is correlated with ϵ. The perturbations variance was selected to have a signal-to-noise ratio (SNR) in the interval [30 dB, 80 dB], according to

$$\mathrm{SNR} = 20\log_{10} \frac{\sqrt{\dfrac{1}{T}\sum_{t=1}^{T} y(t)^2}}{\sigma_\epsilon}. \qquad (4.23)$$

For high enough SNR, the constraint $\|\mathbf{M}\| < 1$ is valid and the Taylor series expansion (4.4) holds. In this case, the derived expressions predict the LS estimate bias and variance. Thus, it is relevant to monitor the evolution of the largest $\mathbf{M}$ eigenvalue to detect the lower limit of the SNR that allows the validity of the predictions.

The MC simulations provide empirical values of the bias and variance, through the sample mean and sample variance of the LS estimate $\widehat{\mathbf{x}}$. The results presented in this Section focus the interest in the first element of $\widehat{\mathbf{x}}$, because in the structured EIV problem, the step input estimate is $\widehat{u} = \widehat{\mathbf{x}}_{[1]}$.

4.3.1. Monte Carlo simulation results for an unstructured EIV problem with uncorrelated perturbations

The MC simulation of the unstructured EIV problem solution was conducted using the following settings. The exact data elements in the matrix $\mathbf{K} \in \mathbb{R}^{(T-n)\times(n+1)}$ are normally distributed with zero mean and variance one, for $T = 200$ and $n = 2$. The to-be-estimated exact data is the vector $x = \begin{bmatrix} 1 & 2 & 3 \end{bmatrix}^{\top}$. The perturbations $\mathbf{E}$ and ϵ are normally distributed with zero mean and variances subject to $\sigma_{\mathbf{E}}^2 = 2\sigma_{\epsilon}^2$. These settings are similar to those of the structured case, aiming to have comparable situations.

The difference between the sample mean of the estimate $\widehat{\mathbf{x}}_{[1]}$ and its true value $\mathbf{x}_{[1]}$ is the empirical bias b_{e}.

$$b_{\mathrm{e}} = \frac{1}{N_{\mathrm{MC}}} \sum_{i=1}^{N_{\mathrm{MC}}} \left(\widehat{\mathbf{x}}_{[1]}\right)_i - \mathbf{x}_{[1]} \approx \mu\left(\widehat{\mathbf{x}}_{[1]}\right) - \mathbf{x}_{[1]}. \tag{4.24}$$

The standard deviation of the estimate $\widehat{\mathbf{x}}_{[1]}$ is used to obtain the standard error σ_{e} of the MC simulation, which decreases with respect to the square root of the number of MC runs N_{MC} [Hammersley and Handscomb, 1975]:

$$\sigma_{\mathrm{e}} = \frac{\sigma\left(\widehat{\mathbf{x}}_{[1]}\right)}{\sqrt{N_{\mathrm{MC}}}}, \quad \text{where} \quad \sigma^2\left(\widehat{\mathbf{x}}_{[1]}\right) = \frac{1}{N_{\mathrm{MC}}-1} \sum_{i=1}^{N_{\mathrm{MC}}} \left(\left(\widehat{\mathbf{x}}_{[1]}\right)_i - \mu\left(\widehat{\mathbf{x}}_{[1]}\right)\right)^2. \tag{4.25}$$

In each of the N_{MC} runs we also obtain the aproximations of the estimation bias $\mathbf{b}_{\widetilde{\mathrm{p}}[1]}$ and variance $\mathbf{C}_{\widetilde{\mathrm{p}}[1,1]}$ from observed data, using Equations (4.10), and (4.11). Similarly as before, we get the sample mean of the aproximations to have bias and variance predictions from observed data

$$b_{\widetilde{\mathrm{p}}} = \frac{1}{N_{\mathrm{MC}}} \sum_{i=1}^{N_{\mathrm{MC}}} \left(\mathbf{b}_{\widetilde{\mathrm{p}}[1]}\right)_i, \quad \text{and} \quad v_{\widetilde{\mathrm{p}}} = \frac{1}{N_{\mathrm{MC}}} \sum_{i=1}^{N_{\mathrm{MC}}} \left(\mathbf{C}_{\widetilde{\mathrm{p}}[1,1]}\right)_i. \tag{4.26}$$

The standard error of the bias prediction $b_{\widetilde{p}}$ is given by

$$\sigma_{\widetilde{p}} = \sqrt{\frac{1}{N_{\mathrm{MC}}\left(N_{\mathrm{MC}} - 1\right)} \sum_{i=1}^{N_{\mathrm{MC}}} \left(\left(\mathbf{b}_{\widetilde{p}[1]}\right)_i - b_{\widetilde{p}}\left(\widehat{\mathbf{x}}_{[1]}\right)\right)^2}. \tag{4.27}$$

The predicted bias $b_{\mathrm{p}} = \mathbf{b}_{\mathrm{p}[1]}$ and variance $v_{\mathrm{p}} = \mathbf{C}_{\mathrm{p}[1,1]}$ from exact data are obtained with one evaluation of the expressions (4.8) and (4.9).

Figure 4.1 shows the empirical bias and the bias predictions, with their corresponding standard errors, for the unstructured (plots in the top) and structured (plots in the bottom) EIV problems. The simulation settings for the structured and correlated EIV problem are described in the following subsection. In the figure, it can be observed that the empirical bias b_{e} is proportional to the perturbation noise variance while the standard error σ_{e} is proportional to the perturbation noise standard deviation. The bias predictions b_{p} and $b_{\widetilde{p}}$ are accurate since they coincide with the empirical bias b_{e} in all the SNR interval for unstructured EIV problems, In both unstructured and structured EIV cases, the standard errors of the MC estimates σ_{e} and $\sigma_{\widetilde{p}}$ are smaller than the bias estimates b_{e} and $b_{\widetilde{p}}$. The bias estimates are spread near their sample means. The uncertainty is smaller than the bias, therefore, the MC simulation is meaningful.

The absolute and relative errors between the predicted and the empirical bias are shown in Figure 4.2. The absolute errors decrease with respect to the perturbation variance. The relative errors are lower than 5% for SNR between 30 dB and 70 dB. There is an increment in the relative errors for SNR above 55 dB. As the SNR increases, the empirical and the predicted bias decrease, as well as the bias error between them. In order to reveal the bias error, more Monte Carlo runs are needed to reduce the uncertainty of the Monte Carlo simulation that depends on the square root of N_{MC}, see Equation (4.25). If N_{MC} is insufficient, the uncertainty of the Monte Carlo simulation hides the bias error and we see this increasing effect of the relative errors.

The errors between the predicted and the empirical variance are shown in Figure 4.3. The absolute and relative errors decrease with respect to the perturbation variance. The relative errors are lower than 5% for SNR above 40 dB.

Figure 4.4 shows the absolute and the relative errors between the predictions computed from observed data and those computed from exact data. The absolute errors between both predictions are proportional to the perturbation noise variance. The bias and variance predictions, from either exact data or observed data, are equivalent for SNR above 35 dB since the relative errors are lower than 5%. The substitution of observed data on the prediction formulas is a valid procedure that allows the prediction of the estimate statistics.
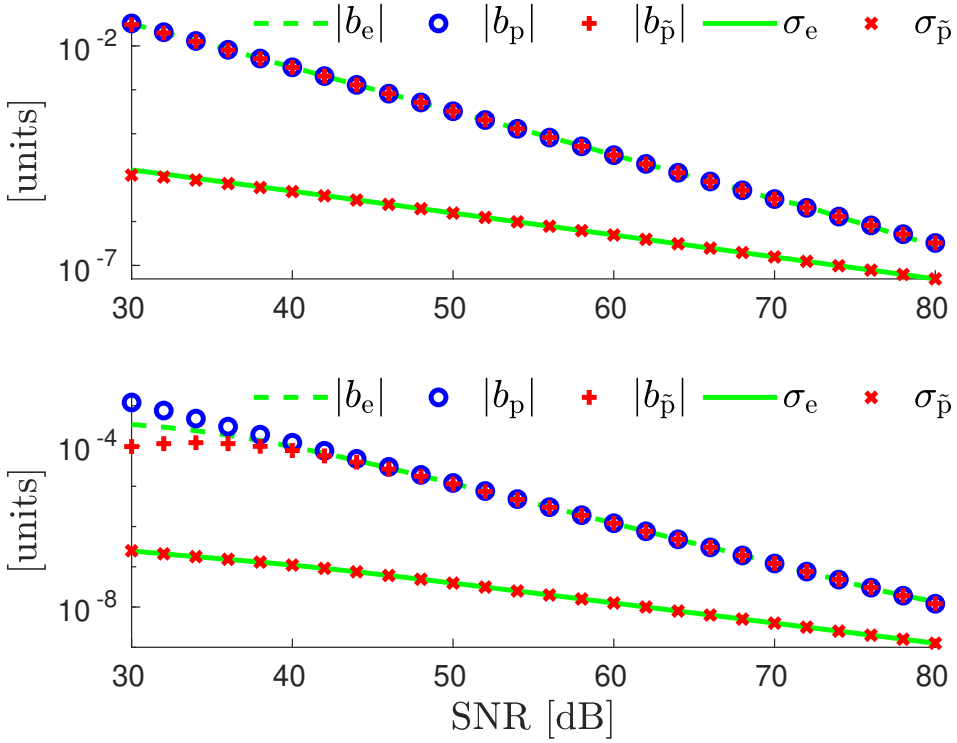
Figure 4.1.: We observe the results of the LS solutions for the unstructured (top) and the structured (bottom) EIV problems. These results are the empirical bias b_e, the predicted bias from exact data b_p, the predicted bias from observed data $b_{\tilde{p}}$, the empirical standard error σ_e, and the standard error from the estimations using observed data $\sigma_{\tilde{p}}$. The estimation biases are proportional to the perturbation variance and the estimation standard errors are proportional to the perturbation standard deviation. Since the standard errors are smaller than the biases, the MC simulation is meaningful.

4.3.2. Monte Carlo simulation results for a structured EIV problem with correlated perturbations

The MC simulation of the structured EIV problem (??) solution was conducted processing $T = 200$ samples of the transient response $\tilde{y}$ generated by a linear time invariant system of order $n = 2$, after a step input excitation with $u = 1$ units, where the units represent any physical quantity. The processed step response is
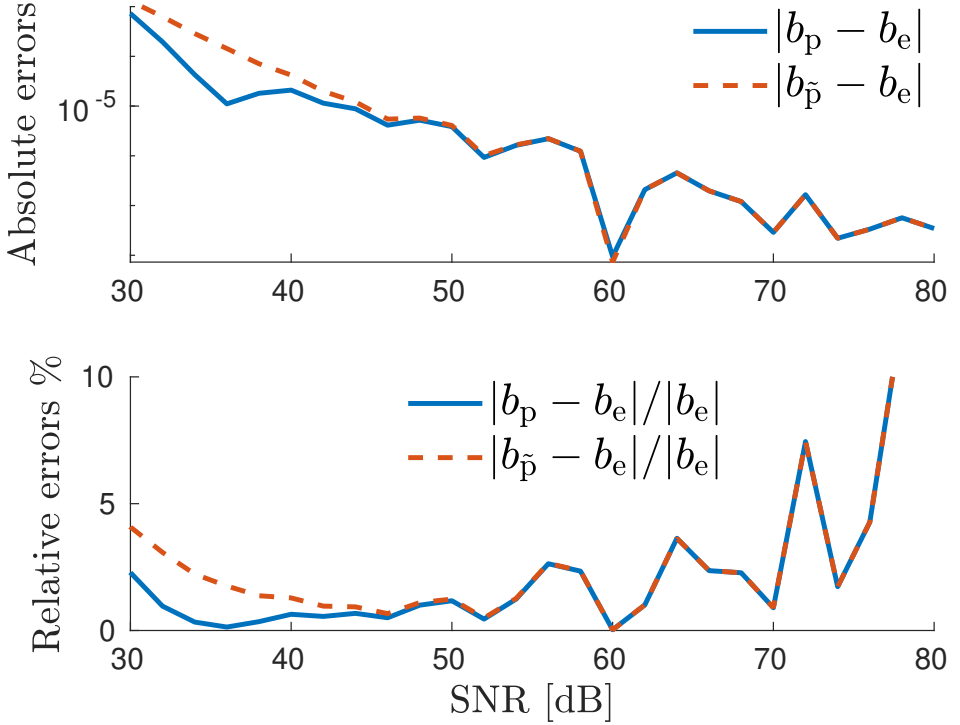
Figure 4.2.: The MC simulation shows that when we solve an unstructured EIV problem with LS, the absolute errors (top) between the predicted bias and the empirical bias are proportional to the perturbation noise variance as it is expected, and the relative errors (bottom) are smaller than 5% for SNR below 70 dB. The bias prediction computed from exact data b_{p} is very similar to that computed using observed data $b_{\tilde{\mathrm{p}}}$.

shown in Figure 4.5. The steady state response of the system is reached after 400 samples because from there on the relative error between the instantaneous values of the transient response and the steady-state response value is smaller than 2%. Processing 200 samples ensures that the step input estimation is computed from transient data only.

The empirical bias is the sample mean of the N_{MC} estimates minus the true value

$$b_{\mathrm{e}} = \frac{1}{N_{\mathrm{MC}}} \sum_{i=1}^{N_{\mathrm{MC}}} \widehat{u}_i - u \approx \mu\left(\widehat{u}\right) - u. \tag{4.28}$$
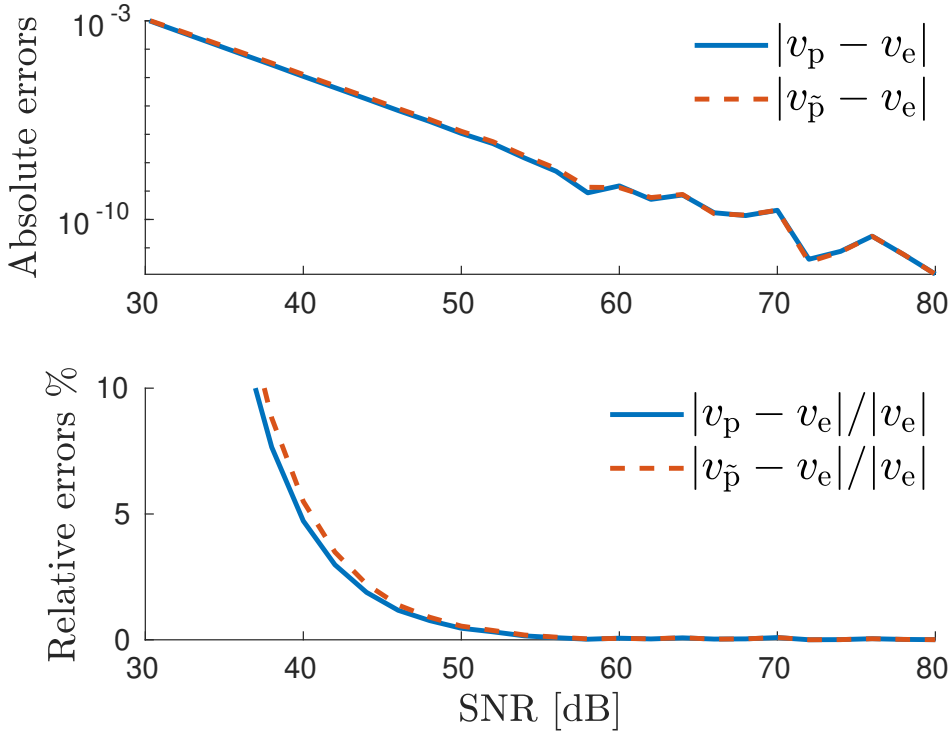
Figure 4.3.: The MC simulation shows that when we solve an unstructured EIV problem with LS, the absolute errors (top) between the predicted variances and the empirical variance are proportional to the perturbation noise variance, and the relative errors (bottom) are smaller than 5% for SNR higher that 40 dB. The variance prediction computed using exact data v_p is very similar to that computed from observed data $v_{\tilde{\mathrm{p}}}$.

The standard error associated to this empirical bias estimation [Hammersley and Handscomb, 1975] is defined as

$$\sigma_\mathrm{e} = \frac{\sigma(\hat{u})}{\sqrt{N_\mathrm{MC}}}, \quad \text{where} \quad \sigma^2(\hat{u}) = \frac{1}{N_\mathrm{MC}-1} \sum_{i=1}^{N_\mathrm{MC}} (\hat{u}_i - \mu(\hat{u}))^2. \tag{4.29}$$

The plots on the right side of Figure 4.1 show the empirical bias, the bias predictions (4.12) and (4.14), and their corresponding standard errors, for the structured EIV problem. The empirical bias b_e is proportional to the perturbation noise variance, and the bias predictions b_p and $b_{\tilde{\mathrm{p}}}$ coincide with the empirical bias b_e only for SNR above 40 dB. This indicates that the SNR drops to a point where the
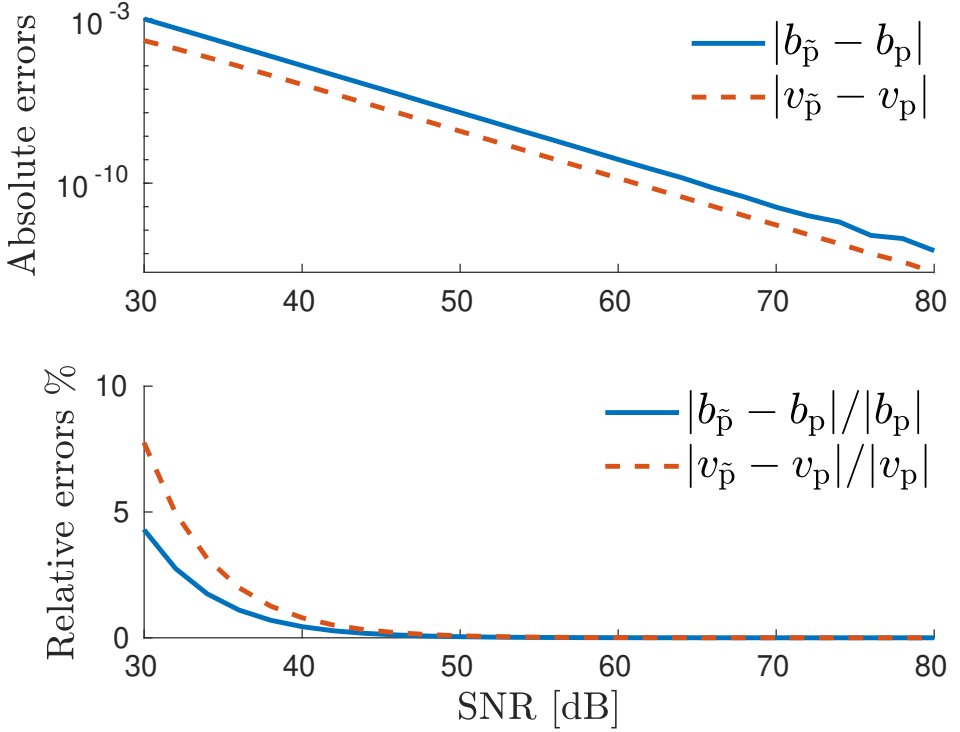
Figure 4.4.: The MC simulation shows that when we solve an unstructured EIV problem with LS, the absolute errors (top) between the prediction with observed data and the prediction with exact data are proportional to the perturbation noise variance. The use of observed data instead of exact data in the prediction formulas is valid when the SNR is above 35 dB since the relative errors (bottom) are smaller than 5%.

constraint $\|\mathbf{M}\| < 1$ is no longer satisfied. At an SNR of 30 dB the perturbation noise affects the bias prediction from observed data and it is three times smaller than the empirical bias.

The absolute and relative errors between the predicted and the empirical bias are shown in Figure 4.6. It can be seen that the absolute errors are proportional to the perturbation variance, and the relative errors are lower than 5% for SNR higher than 40 dB.

The absolute and relative errors between the empirical and the predicted variance, equations (4.13) and (4.15), are shown in Figure 4.7. These absolute errors are
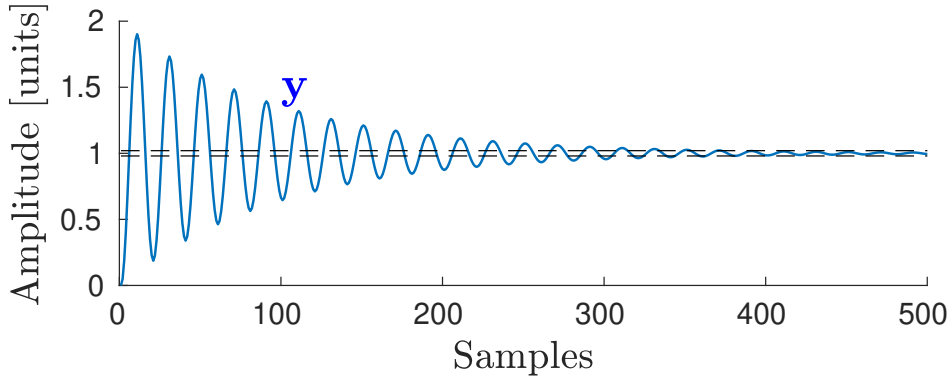
Figure 4.5.: The structured EIV problem is constructed with 200 samples of the step response to ensure that only transient data is used. The relative errors between the values of **y** and the steady state value are smaller than 2% after 400 samples, as it is indicated with dashed lines.

proportional to the perturbation noise variance, whereas the relative errors are lower than 5% for SNR higher than 45 dB.

The absolute and relative errors between the two predictions from observed data and from exact data, are shown in Figure 4.8. These absolute errors are also proportional to the perturbation noise variance, and the relative errors show that the bias and variance predictions from either of the two alternatives are equivalent for SNR higher than 45 dB.

The simulation results show that the LS solution of the structured and correlated EIV problem is more sensitive to the perturbation. This represents a low limit in the SNR interval imposed by the noise level. In practical applications it is common to have SNRs of 40 dB and the user needs to be aware of the prediction error that the method has. We measure this prediction error with the mean squared error (MSE), defined as

$$\text{MSE} = \sigma^2 + b^2. \tag{4.30}$$

By comparing the different MSEs to the CRLB of the structured EIV problem, Figure 4.9 shows that the MSEs has the same proportionality as the CRLB with respect to the disturbing noise variance. The MSEs are three times larger than the CRLB. Since the difference between $\text{MSE}_{\widehat{p}}$ and the CRLB is lower than one order of magnitude, the LS estimation of the structured EIV problem produces results that are comparable to the ML estimation. The $\text{MSE}_{\widehat{p}}$ computed from observed data approaches the CRLB for SNR below 40 dB. This is due to the constraint violation of the Taylor series expansion.
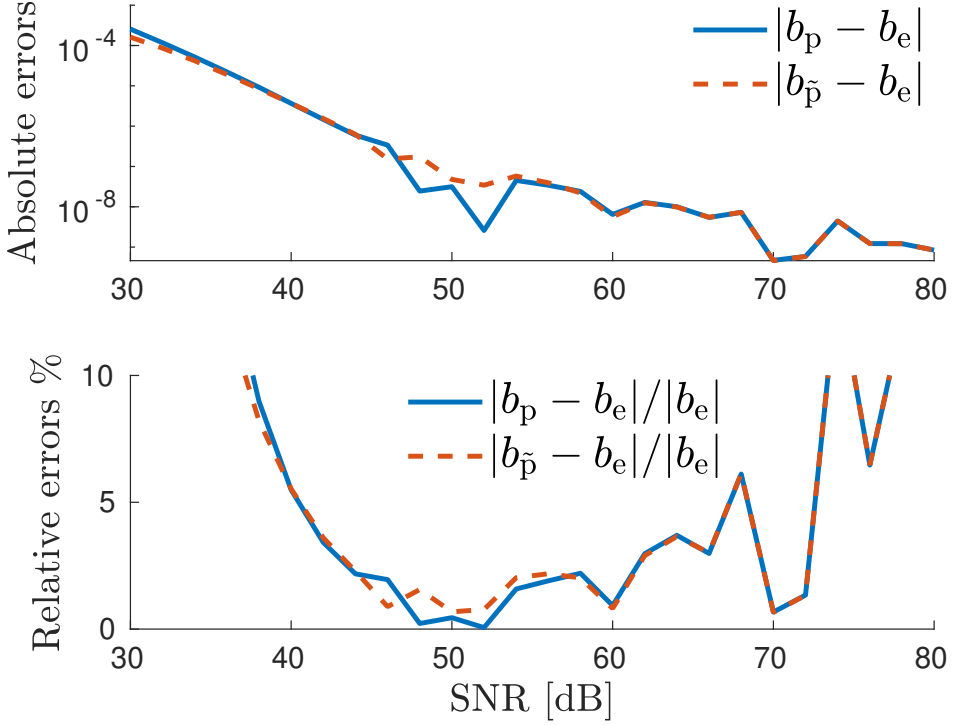
Figure 4.6.: The MC simulation shows that when we solve a structured EIV problem with LS, the absolute errors (top) between the predicted bias and the empirical bias b_e are proportional to the perturbation noise variance, and the relative errors (bottom) are smaller than 5% only for SNR above 40 dB.
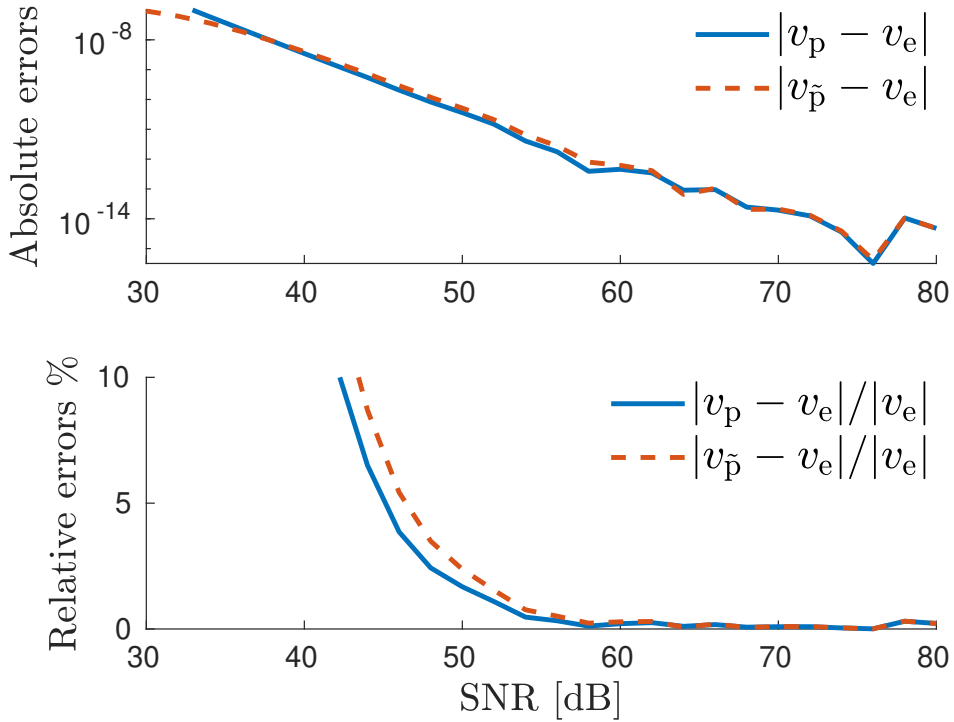
Figure 4.7.: The MC simulation shows that when we solve a structured EIV problem with LS, the absolute errors (top) between the predicted and the empirical variance are proportional to the perturbation variance, and the relative errors (bottom) between the predicted and the empirical variance are smaller than 5% for SNR above 45 dB.
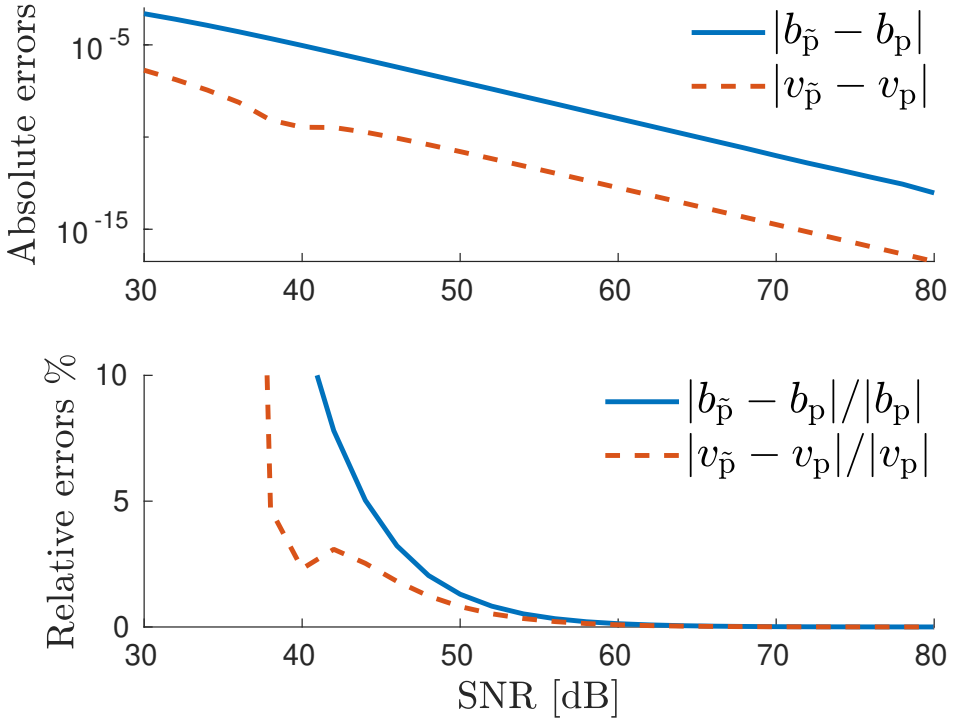
Figure 4.8.: The MC simulation shows that when we solve a structured EIV problem with LS, the absolute errors (top) between the predictions computed from observed data and those from exact data are proportional to the perturbation noise variance. According to the relative errors (bottom), the substitution is valid for SNR higher than 45 dB.
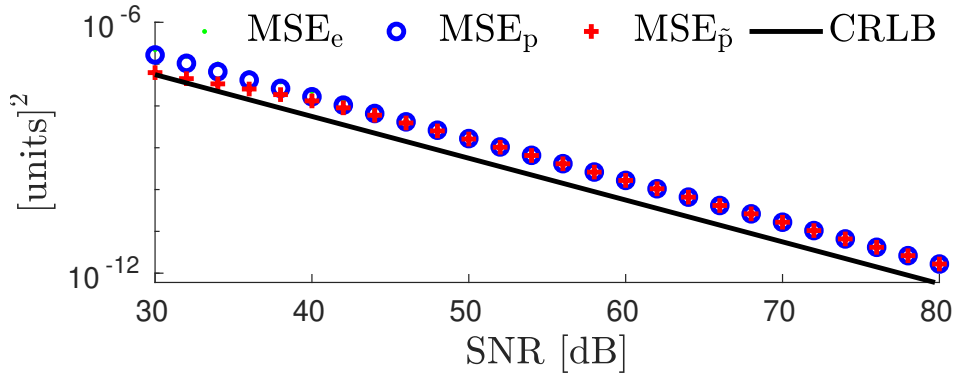
Figure 4.9.: The mean squared errors of the LS estimate are close to the Cramér-Rao lower bound. This is a positive indication of the goodness of the LS estimator for the structured EIV problem. The mean squared error of the empirical estimates is represented by MSE_e, and those of the predictions are MSE_p and $MSE_{\tilde{p}}$. The $MSE_{\tilde{p}}$ is smaller than CRLB below 40 dB of SNR because of the introduced bias error, but the difference between $MSE_{\tilde{p}}$ and the CRLB is lower than one order of magnitude.

4.4. Conclusions

We conducted a statistical analysis of a structured errors-in-variables (EIV) estimation problem with correlation to find the first and second moments of its least-squares solution. This estimation problem occurs in metrology when we estimate the value of a measurand directly from the sensor transient response. The data-driven estimation of the physical quantity is formulated as a structured EIV problem with correlation that uses the observed transient response to construct both the regression matrix and the regressor. The real-time implementation of the method uses a recursive least squares algorithm that is simple and has low computational complexity. The assessment of the uncertainty is done using the estimate bias and variance.

The conducted statistical analysis produced expressions that predict the estimate bias and variance for given sample size and perturbation level of the observed response. The Monte Carlo simulation validated the predictions. We compared the results of solving an unstructured and uncorrelated EIV problem with a structured and correlated EIV problem to understand how the structure and the correlation impacts in the estimation. We found that the predictions in the structured case are more susceptible to perturbations. This is due to the two approximations involved, a second-order Taylor series expansion of the estimate, and the substitution of perturbed data on the prediction expressions. The relative error results indicate that the estimate bias, and variance are predicted using the derived expressions, and the observed data. The mean squared error of the estimate is close to the results of the maximum likelihood estimate given by the Cramér-Rao lower bound.

The bias and variance can be accurately predicted, provided that the Taylor series expansion is valid. This constraint has to be taken into account to ensure the effectiveness of the method in practical applications. In the example, it was observed that when the SNR lies outside the validity region, the bias and variance estimation was at most three times larger than the empirical values.

The methodology presented in this paper can be applied to estimate the uncertainty of the solutions to other structured EIV problems. The bias and variance expressions obtained after the statistical analysis depend on each specific structure.

5. Experimental validation of the step input estimation method

The results of this chapter ...

5.1. Introduction

A measurement is a dynamic process. The sensor is a dynamic system that experiments changes after an input excitation. The sensor output is first a transient state response and followed by a steady state response.

The influence of the input is observed in the sensor output, and thus it makes sense to estimate the input using the sensor response. When the sensor reaches its steady-state, the input is a straightforwardly estimated from the sensor output making use of the sensor static gain. To obtain a fast estimation, the sensor transient response must be considered instead of the steady state response.

A common approach is to filter the sensor transient response with another dynamic system to reduce the sensor transient time by inverting the sensor dynamics. To design such a compensator system it is necessary a sensor model. A different approach uses digital signal processing methods that are independent of the sensor model. One of these methods is the data-driven method that estimates the unknown level of step inputs by processing the sensor step response. To assess the uncertainty of the data-driven step input estimation method, a experimental validation of this method was conducted in a real-life metrology application. This chapter describes the measurement experiments with a weighing sensor system and discuss the results observed. The results are put in perspective to simulations and consider the measurement noise that is additive to the response of the sensor.

The experimental results validate the data-driven step input estimation method, and indicate in which intervals of SNR and sample size the effectiveness of the method is guaranteed.

5.2. Simulation results

A Monte Carlo (MC) simulation was conducted to test the bias and covariance expressions (4.14) and (4.15). The MC simulation performed $N_{MC} = 10^4$ runs of the data-driven step input estimation with different realizations of the measurement noise ϵ. We are interested in the first element of $\widehat{\mathbf{x}}$, which is the input estimate $\widehat{u}$. The measurement noise variance was selected to have a signal-to-noise ratio (SNR) in the interval [30 dB, 80 dB], according to

$$\text{SNR} = 20\log_{10}\frac{\sqrt{\dfrac{1}{T}\int\limits_{0}^{T}y(\tau)^2\mathrm{d}\tau}}{\sigma_{\varepsilon}} \tag{5.1}$$

The MC simulation was conducted processing $T = 5000$ samples of a simulated transient step response $\widehat{\mathbf{y}}$ generated by a stable LTI system of order $n = 5$, with a sampling frequency of $f_s = 4$ kHz. This system is a state space model obtained with the System Identification Toolbox using the measured step response of the actual sensor described in the Practical Implementation Section. The steady state response of the system is practically reached after 500 samples because from there on the relative error between the transient response and the steady-state response is smaller than 0.2%, see Fig. 5.1.

A sensor is a dynamic system, therefore, a fast measurement process must necessarily cope with the systemâs transient response. In that respect we must distinguish between the transient response of the system under test, and the transient phase of the measurement process (i.e. before the process has settled on a final measurement outcome). Notice that the transient phase of the measurement process is considerably smaller than the settling time of the system under test, and this is a major advantage of the step input estimation method.

The difference between the sample mean $\widehat{\mu}_u$ of the step input estimates and the true value u is the empirical bias b_{e}.

$$b_{\mathrm{e}} = \frac{1}{N_{MC}} \sum_{i=1}^{N_{MC}} \widehat{u}_i - u = \widehat{\mu}_u - u. \tag{5.2}$$

The sample variance $\widehat{\sigma}_u^2$ of the step input estimates is used to obtain the standard error of the MC simulation σ_{e}, which decreases with respect to the square root of the number of MC runs N_{MC}.

$$\sigma_{\mathrm{e}} = \frac{\widehat{\sigma}_u}{\sqrt{N_{MC}}}, \text{ where } \widehat{\sigma}_u^2 = \frac{1}{N_{MC} - 1} \sum_{i=1}^{N_{MC}} \left(\widehat{u}_i - \widehat{\mu}_u\right)^2. \tag{5.3}$$

In each of the N_{MC} runs, we compute the predictions of the step input estimation bias and variance from measured data using Equations (4.14) and (4.15). The step input bias and variance predictions from observed data $b_{\widetilde{\mathrm{p}}}$ and $v_{\widetilde{\mathrm{p}}}$, and the associated standard error $\sigma_{\widetilde{\mathrm{p}}}$, are obtained from

$$b_{\widetilde{\mathrm{p}}} = \frac{1}{N_{MC}} \sum_{i=1}^{N_{MC}} \mathbf{b}_{\widetilde{\mathrm{p}}}^i \left(\widehat{\mathbf{x}}\right) \big|_{[1]}, \; v_{\widetilde{\mathrm{p}}} = \frac{1}{N_{MC}} \sum_{i=1}^{N_{MC}} \mathbf{C}_{\widetilde{\mathrm{p}}}^i \left(\widehat{\mathbf{x}}\right) \big|_{[1,1]},$$

$$\text{and} \quad \sigma_{\widetilde{\mathrm{p}}} = \sqrt{\frac{\sum_{i=1}^{N_{MC}} \left(\mathbf{b}_{\widetilde{\mathrm{p}}}^i \left(\widehat{\mathbf{x}}\right) \big|_{[1]} - b_{\widetilde{\mathrm{p}}}\right)^2}{N_{MC} \left(N_{MC} - 1\right)}}, \tag{5.4}$$

where $\widetilde{\mathbf{b}}_{\mathrm{p}}^i \left(\widehat{\mathbf{x}}\right) \big|_{[1]}$ is the first element in the bias vector and $\widetilde{\mathbf{C}}_{\mathrm{p}}^i \left(\widehat{\mathbf{x}}\right) \big|_{[1,1]}$ is the first element in the covariance matrix obtained in the $i-$th approximations. The
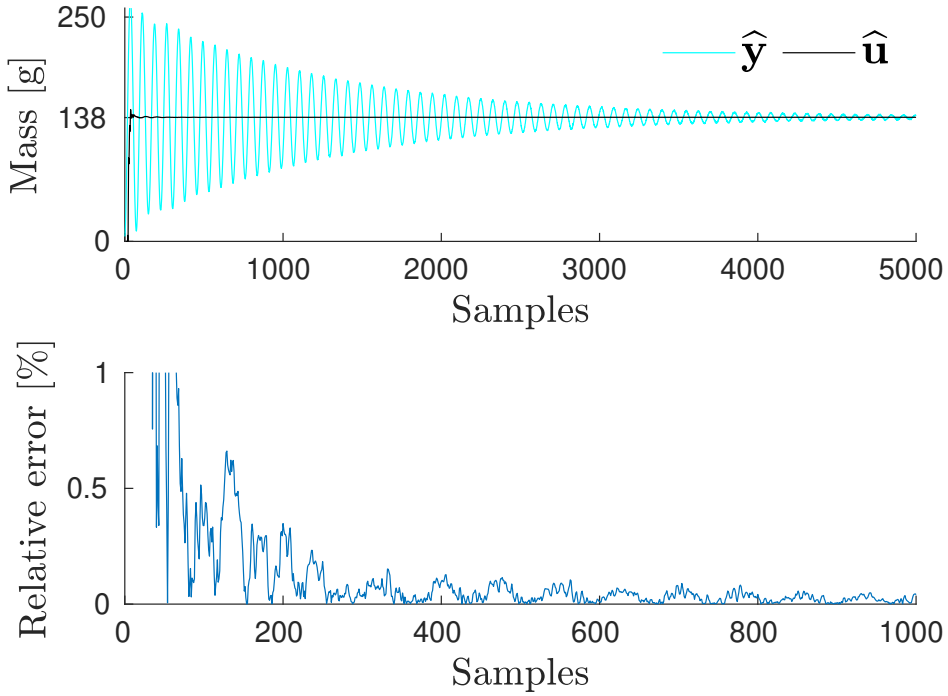
Figure 5.1.: Above: example of a simulated response $\widehat{\mathbf{y}}$ and its step input estimation $\widehat{u}$ assuming measurement Gaussian noise with 50 dB of SNR. Below: the relative error $|\widehat{u} - u|/u$ is below 1% after 100 samples. We take the estimate at 500 samples because there the relative error is smaller than 0.2%.

predicted bias and variance from exact data are obtained with one evaluation of the expressions (4.12) and (4.13)

$$b_{\text{p}} = \frac{1}{N_{MC}} \sum_{i=1}^{N_{MC}} \mathbf{b}_{\text{p}}(\widehat{\mathbf{x}})\big|_{[1]}, \text{ and } v_{\text{p}} = \frac{1}{N_{MC}} \sum_{i=1}^{N_{MC}} \mathbf{C}_{\text{p}}(\widehat{\mathbf{x}})\big|_{[1,1]}. \tag{5.5}$$

The uncertainty of the step input estimate is defined as the spread of the estimates that is given by the predicted variance v_{p}.

Fig. 5.2 shows the empirical bias, the bias predictions and the standard errors of the MC simulation. It can be seen that the empirical bias b_{e} and the predicted bias $b_{\widetilde{\text{p}}}$ are proportional to the perturbation noise variance while the standard errors σ_{e} and $\sigma_{\widetilde{\text{p}}}$ are proportional to the perturbation noise standard deviation. For SNR below 40 dB there is a difference of a small order of magnitude between the empirical bias b_{e} and the bias prediction $b_{\widetilde{\text{p}}}$.

The standard errors of the MC simulation σ_e and $\sigma_{\tilde{p}}$ are smaller than b_e and $b_{\tilde{p}}$. The estimates are spread near the sample mean and the uncertainty is smaller than the bias. Therefore, the empirical bias of the MC simulation is meaningful.
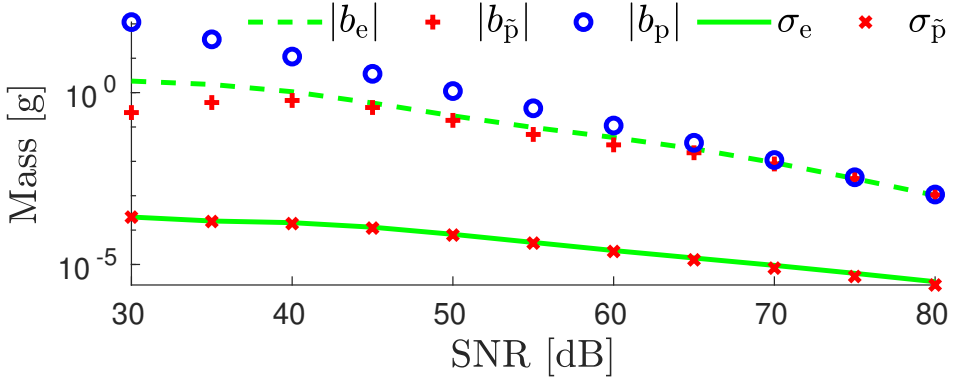

Figure 5.2.: The results of the Monte Carlo simulation of the step input estimation method are the empirical bias b_e, the predicted bias using exact data b_p, the predicted bias using measured data $b_{\tilde{p}}$, the empirical standard error σ_e, and the predicted standard error $\sigma_{\tilde{p}}$. The estimation biases are proportional to the perturbation variance and the estimation standard errors are proportional to the perturbation standard deviation. Since the standard errors are smaller than the biases, the MC simulation is meaningful.

The mean squared error (MSE) of the step input estimate, defined as

$$\text{MSE} = b^2 + v, \tag{5.6}$$

where b and v are the bias and the variance of the step input estimate, can be applied to the obtained empirical and predicted results and can be compared to the Cramér-Rao lower bound (CRB). Fig. 5.3 shows that $\text{MSE}_e = b_e^2 + v_e$ and $\text{MSE}_{\tilde{p}} = b_{\tilde{p}}^2 + v_{\tilde{p}}$ have the same proportionality with respect to the measurement noise variance as the bound for an unbiased estimator CRB_{ub}. For SNR above 35 dB, MSE_e and $\text{MSE}_{\tilde{p}}$ are equivalent, and below 35 dB the difference between them is of less than a factor of 10.

We obtained an approximation of the CRB_b for our biased estimator using the partial derivative of the bias in expression (4.14). Fig. shows that the bounds for the unbiased and biased estimators are almost equal because the partial derivatives of the bias are negligible w.r.t. 1 in Equation (4.22). By adding the square of the predicted bias to the biased estimator bound CRB_b we obtain an approximation of

the minimum MSE that the biased estimator can achieve. This minimum MSE is close to the CRBs for large SNR but the square of the bias causes an increase of the MSE around 35 dB. The differences between the CRBs and MSE_e and $MSE_{\widetilde{p}}$ are of one order of magnitude for large SNR and become small for SNR lower than 40 dB. This difference is the cost of solving a structured EIV problem with a simple LS method.
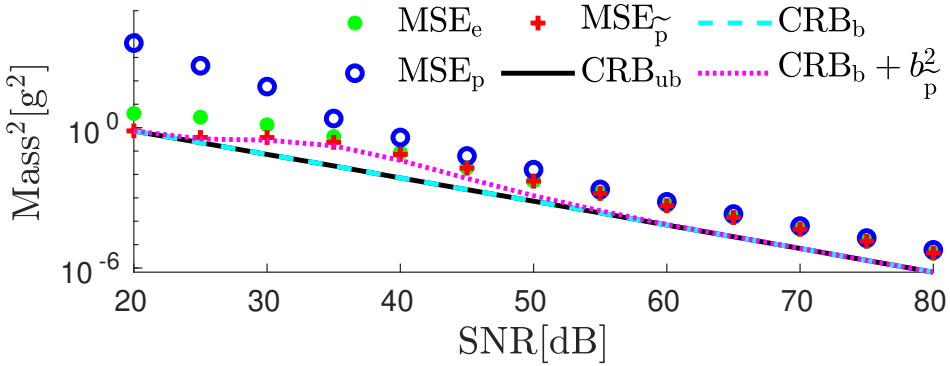

Figure 5.3.: The observation instant is fixed at 500 samples. The bias and the MSEs decrease for large SNR. The empirical MSE_e and the predicted $MSE_{\widetilde{p}}$ of the step input estimation are one order of magnitude larger than the Cramér-Rao lower bound. Adding the CRB for a biased estimator with the predicted bias squared we have the minimum MSE, that grows in the interval [25 dB, 45 dB]. Below 35 dB the difference between $MSE_{\widetilde{p}}$ and the CRB is less than a factor of 10.

There are two features of the system step response that make the CRB small. One is the measurement noise variance and the second is sample size. The estimation from step response perturbed with small noise variance has lower uncertainty. Also, using larger sample size to perform the estimation boils down to smaller estimation uncertainty.

In order to get more insight into the step input estimation method we conducted another simulation study. The step input estimation method assumes the order n is given in (**??**). In this simulation, the step input estimation method processed the step response generated by a $5 - th$ order system using different values of n in the interval from 2 to 100.

The step response is perturbed with Gaussian white noise with SNR values in the interval [20 dB, 80 dB]. For each order n and SNR value, 100 step input estimations are performed from independent noise realizations. Fig. 5.4 shows the average of

the squared biases and the variances, and the MSEs of the input estimate using the first 500 samples. It is evident that the estimation variance and MSE depend on the SNR.

Increasing the order n is equivalent to adding more regressors in the regression problem. It is well known that increasing the order n causes a monotonic decrement of the estimation bias and increment of the variance. This is the asymptotic behavior of the estimation statistical moments with respect to the number of regressors. Nevertheless, the simulation results presented in Fig. 5.4 show that the variance first increases for small values of n, followed by a decrement and finally after $n \approx 40$ the variances exhibit a slow and steady increment. This apparent contradiction does not prove the invalidity of the estimation method since the results presented correspond to a finite sample size and the asymptotic results cannot be applied. The theoretical explanation of the estimation statistics for finite sample sizes is out of the scope of this paper.

There is a bias-variance tradeoff and the MSEs exhibit local minima with respect to n. The principal contribution to the MSE is the squared bias for the smaller values of n and the variance for the larger values of n. However, the higher orders do not produce overfitting since the MSEs do not grow fast and remain close to the minimum values.

The optimum value of n is not necessarily equal to the order of the generating system and varies for each SNR. According to the plots in Fig. 5.4, there are orders that provide local minima of the step input estimation MSEs. From the right hand side of Fig. 5.4, the orders that give the first two MSE minima were identified and those values are listed in Table 5.1. For each SNR, there is a first minimum at a low order and a second minimum at a high order. For SNR of 30 and 40 dB, it is recommended to use the order that gives the first minimum since the MSE at the second minimum is less than one order of magnitude smaller than at the first minimum. Depending on the requirements, the user can choose between the simplicity of an estimation with a low order or an estimation with higher computational complexity and a smaller MSE. In a calibration stage, during the setup of the estimation method, the user can search and set the order that enables the estimation method to provide a required MSE.
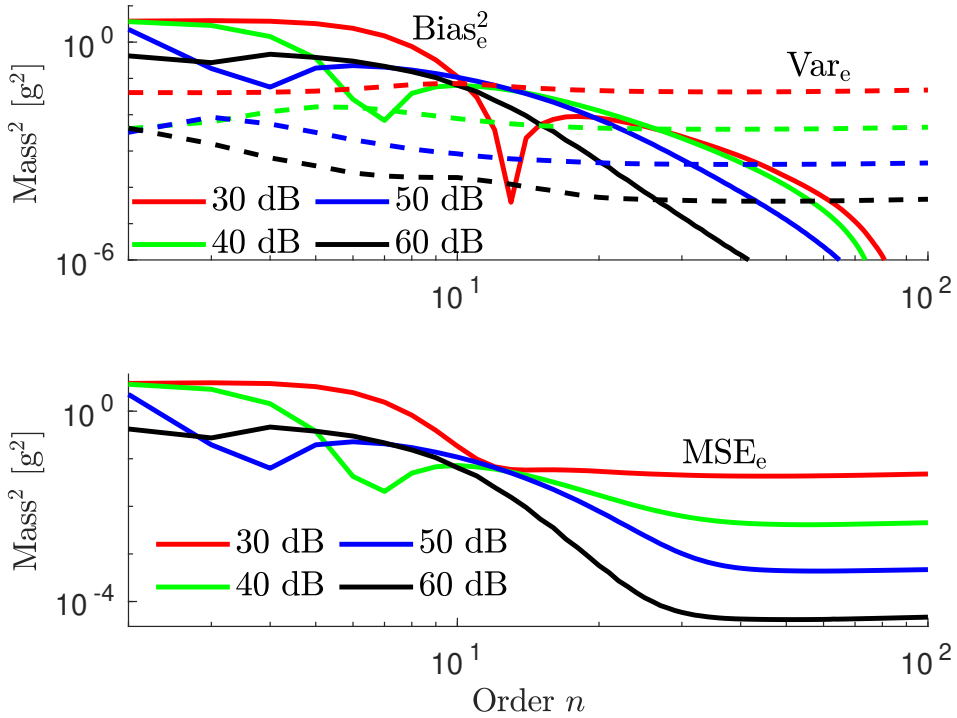
Figure 5.4.: The simulated step responses of a $5-th$ order system are processed by the step input estimation method using different orders *n* and independent noise realizations. The perturbation of the step responses is Gaussian white noise with SNRs of 30, 40, 50, and 60 dB. The square of the empirical bias (solid) and the empirical variance (dashed) are shown on the left hand side and the MSE is shown on the right hand side, for *n* between 2 and 100. These results suggest that, during the setup of the estimation method, we have to search the order that gives the minimum MSE without increasing unnecessarily the complexity of the estimation method.

Table 5.1.: Orders *n* that provide local minima for the MSE of the step input estimate. It is recommended to use the order that gives the first minimum when there is a difference of small order of magnitude with respect to the MSE at the second minimum.

SNR [dB]	30	40	50	60
order at first minimum	11	7	4	3
order at second minimum	40	35	40	31

5.3. Practical implementation

An experimental setup was constructed to test the step input estimation method. The implementation is a weighing system that uses a load cell Tedea Huntleigh 1004 [Tedea-Huntleigh, 2015]. The maximum rating of the load cell is 600 g. A cylindrical aluminium object of 138.32 g of mass was used to excite the load cell. This value was found by calibration using a balance KERN PCB 200-2 that has an uncertainty of 0.01 g. The step input excitation was provided by a magnet that holds and releases a mass from above the load cell. The magnet is located sufficiently far from the load cell to avoid magnetic interference in the sensor response.
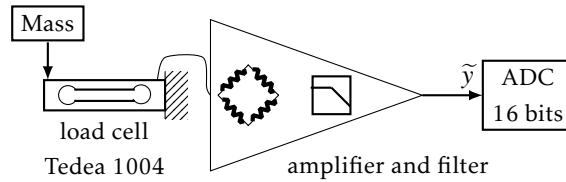

Figure 5.5.: Diagram of the load cell and the conditioning amplifier that provide the sensor response.

A two-stage linear conditioning amplifier performs amplification and filtering of the load cell signal. The first stage is a precision instrumentation amplifier INA114 that has high common mode rejection ratio. The second stage is a third-order low-pass Butterworth filter with cut-off frequency of 100 Hz. The low-pass filter prevents the aliasing noise in the measured transient response. The signal obtained from the conditioning amplifier is considered to be the response of the sensor. The sensor responses to step excitations were sampled with a frequency of $f_s = 4$ kHz, and therefore the Nyquist frequency is 2 kHz. The step responses were collected and stored as datasets for further analysis. The number of samples

collected for each step response is $N = 20000$. For practical purposes, we consider that the last 10000 samples correspond to the steady state response.
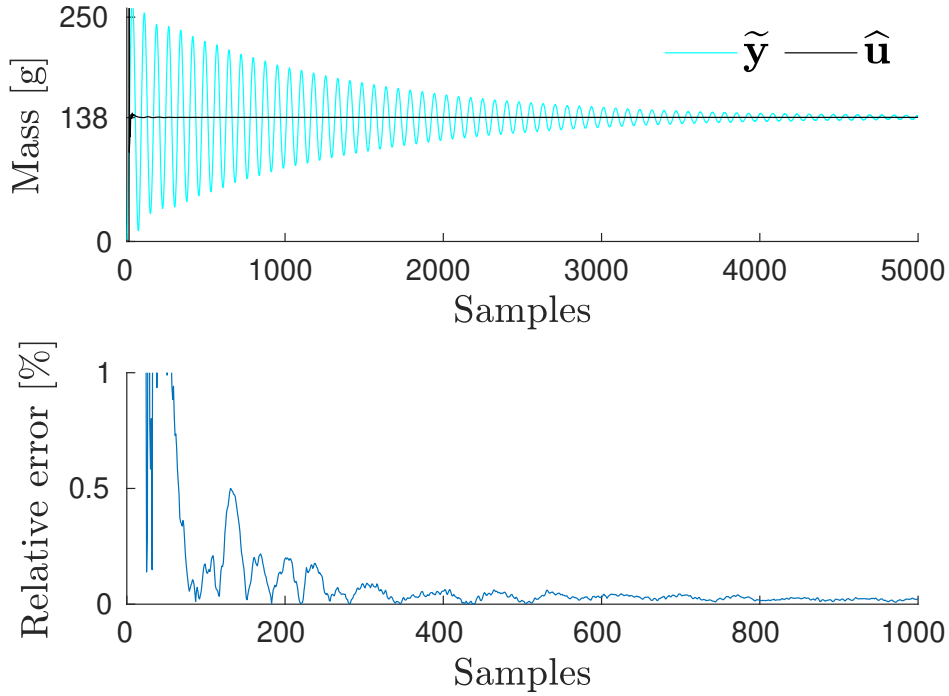

Figure 5.6.: Above: a typical measured sensor transient response $\widetilde{y}$ takes more than 1.25 s (5000 samples, $f_s = 4$ kHz) to converge to the steady state response. Below: the relative error of the input estimate $\widehat{u}$ is smaller than 0.2% from 300 samples. We consider that at 500 samples the relative error of the estimate $\widehat{u}$ is small enough to consider that $\widehat{u}$ is close to its expected value u.

The step input estimation method processed 100 measured sensor step responses, assuming the sensor is of $7-th$ order. Fig. 5.6 shows a typical measured transient response $\widetilde{y}$ and an example of the estimated input $\widehat{u}$.

The empirical bias b_e is the difference between the average of the 100 estimates $\widehat{u}$ and the mass calibration value $u = 138.32$ g, at each instant of time, and the standard error σ_e is the standard

deviation of the mean estimate of the responses processed, i.e.,

$$\widehat{\mu}_e = \frac{1}{100} \sum_{i=1}^{100} \widehat{u}_i, \quad b_e = \widehat{\mu}_e - u, \quad \text{and}$$

$$\sigma_e = \frac{\widehat{\sigma}}{\sqrt{100}}, \quad \text{where } \widehat{\sigma}^2 = \frac{1}{99} \sum_{i=1}^{100} (\widehat{u}_i - \widehat{\mu}_e)^2. \tag{5.7}$$

The bias $\widetilde{b}_{\mathrm{p}}$ and variance $\widetilde{v}_{\mathrm{p}}$ predictions from the measured data were obtained by processing off-line the 100 measured sensor transient step responses with expressions (4.14) and (4.15). These expressions require the measurement noise variance σ_{ε}^2 to obtain the bias and variance prediction. One way to estimate the measurement noise variance is computing the variance of each sensor steady state response, see Fig. 5.7. Later in this section we will explore another way to estimate the measurement noise variance. Computing the noise variance from the steady state response we observed that the SNR of the measured step responses is 55 dB in average.
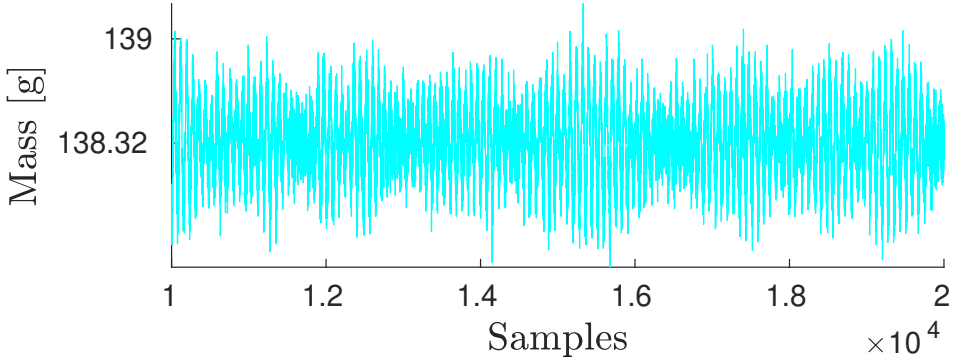
Figure 5.7.: From the sensor steady-state response an estimation of the measurement noise variance is obtained.

Fig. 5.8 shows the empirical bias b_e and the standard error σ_e that result after processing the first $T = 500$ samples of the 100 measured step responses $\widetilde{\mathbf{y}}$. The standard error is smaller than the bias. As it was observed in the MC simulation, this is the uncertainty of the estimation method. The oscillations observed in the bias are mainly due to the transient response and not to the measurement noise. The measurement noise effects are partially removed since we averaged the 100 transient responses, which is a small number compared with the N_{MC} runs averaged in the simulation section.

It is expected that the empirical bias is large when a small number of samples is processed. The data-driven input estimation method is recursive and it is implemented in real-time. The estimation errors decrease as more data is processed.
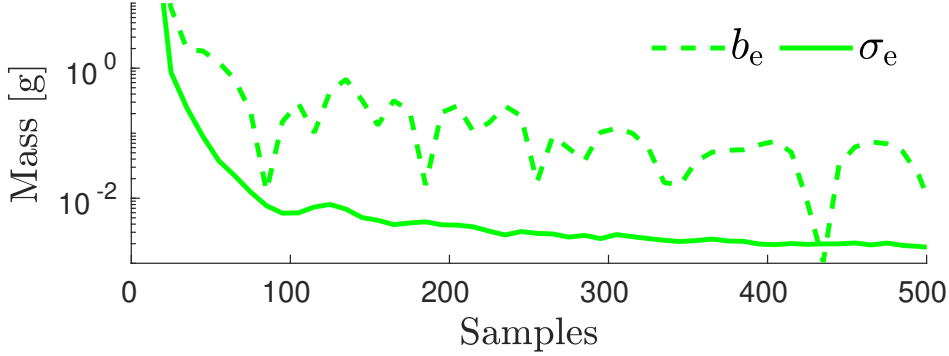

Figure 5.8.: The results of estimating the step input level after processing 100 measured step responses are the empirical bias b_e and the empirical standard error σ_e. The estimation bias and the estimation standard error decrease as more samples are processed. The estimation bias is affected by the transient effects of the sensor response. The values of b_e and σ_e provide the estimate accuracy and uncertainty for a given sample size.

The measurement noise is not white since there is evidence of frequency components in the sensor steady state response that are observed as oscillations in Fig 5.7. To get insight into the properties of the measured sensor response $\widetilde{\mathbf{y}}$, a $7-th$ order model was identified from input-output data assuming that the input is a step of level u. A response $\widehat{\mathbf{y}}$ was simulated from the identified model and the residual $\mathbf{r} = \widetilde{\mathbf{y}} - \widehat{\mathbf{y}}$ was obtained. We can observe these signals in the frequency domain using the discrete Fourier transform, that for the signal $\widetilde{\mathbf{y}}$ is defined as

$$\widetilde{Y}(f) = \frac{1}{\sqrt{N}} \sum_{k=0}^{N-1} \widetilde{y}(k) e^{-j2\pi kf/N} \tag{5.8}$$

where $f = 1, \ldots, N/2$ are the frequency lines and N is the total number of samples. The power spectrum of the signal $\widetilde{\mathbf{y}}$ is given in decibels by $\widetilde{\mathbf{Y}}_{dB} = 20\log_{10}|\widetilde{\mathbf{Y}}|$. Figure 5.9 shows the corresponding power spectra of the sensor response $\mathbf{Y}_{dB}$, the simulated response $\widehat{\mathbf{Y}}_{dB}$, and the residual $\mathbf{R}_{dB}$. There are frequency components near the main resonance peak in the magnitude spectrum of the residual. The presence of frequency components near the main resonance peak is commonly

found in mechanical devices. The vibrations captured from the environment explain the accumulation of energy near the main resonance modes.
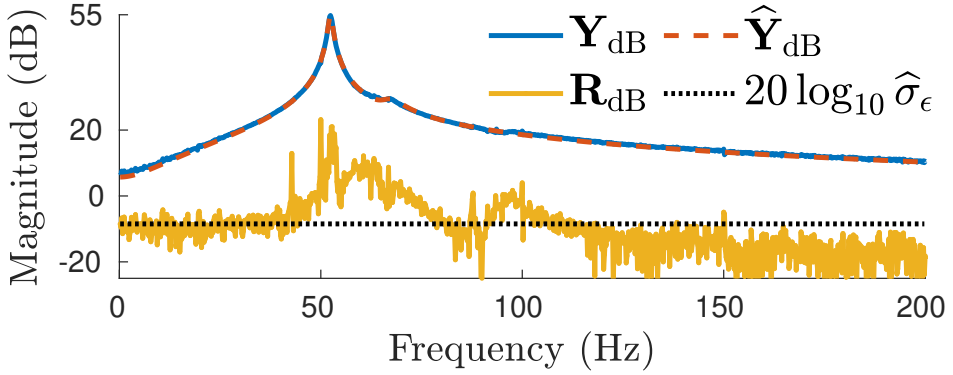

Figure 5.9.: The power spectra of a measured response $\widetilde{\mathbf{Y}}_{\mathrm{dB}}$, a simulated response $\widehat{\mathbf{Y}}_{\mathrm{dB}}$, and the residual $\mathbf{R}_{\mathrm{dB}}$ is not flat and then the measurement noise is not white. The average of the residual power spectrum provides a conservative estimate of the measurement noise variance $\widehat{\sigma}_\varepsilon^2$, represented with the dotted line.

Even when the residual $\mathbf{r}$ is not white, it provides an alternative way to estimate the measurement noise variance. The average of the residual power spectrum approximates the measurement noise variance as follows

$$\widehat{\sigma}_\varepsilon^2 \approx \frac{2}{N} \sum_{f=1}^{N/2} |R(f)|^2. \tag{5.9}$$

The dotted line in Figure 5.9 indicates the $10\log_{10}\left(\widehat{\sigma}_\varepsilon^2\right)$ level of the measurement noise variance estimated from the residual. This level is higher than the mean value of the residual power spectrum $\mathbf{R}_{\mathrm{dB}}$ in the frequencies above 120 Hz.

Using the residual power spectra that correspond to the measured step responses, we obtained the measurement noise variance and the SNR for each experiment. Figure 5.10 shows the estimated SNRs from the residual power spectra. The SNR mean value is 50 dB. Therefore, we assume that the SNR of the measured transient responses is 50 dB instead of 55 dB, as it was estimated from the steady state response.

The 5 dB difference provides a conservative bound since the bias and variance computed from 50 dB of SNR are higher than those obtained using the variance estimation from the steady-state response. Fig. 5.11 shows a comparison of
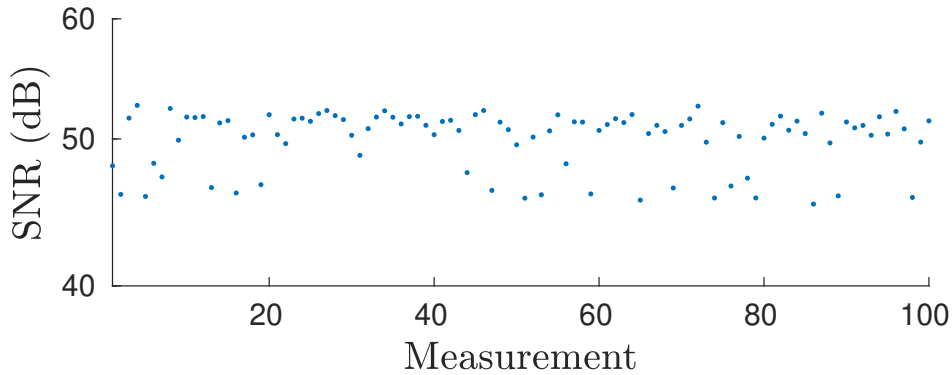
Figure 5.10.: The mean value of the signal-to-noise ratios estimated from the residual power spectra is 50 dB. We consider that this is the estimated SNR of the measured step responses.

the results obtained with both measurement noise variance estimations after processing the first $T = 500$ samples of the step response $\mathbf{y}$. Using expression (4.14), the bias prediction $b_{\tilde{p}2}$ obtained using an SNR of 50 dB approximates more closely the empirical bias than $b_{\tilde{p}1}$ obtained using an SNR of 55dB. In accordance, the standard error of the bias predictions $\sigma_{\tilde{p}2}$ is larger than $\sigma_{\tilde{p}1}$ and is a conservative measure of the input estimation uncertainty. In conclusion, using the noise variance estimated from the residual prevents underestimating the step input estimation uncertainty.

We investigated another aspect of the step input estimation method performance when processing measured step responses. The step input estimation method requires an assumption of the generating system order in the formulation of the estimation problem (??). The estimation method performance is assessed under different assumptions of the values of n in the interval from 2 to 10. For each value of n, 100 step input estimations are computed from measured transient responses and the empirical MSEs are compared. Fig. 5.12 shows that, similar to the observations made in the simulation study, the MSEs have two local minima at $n = 7$ and $n = 48$. It is recommended to use $n = 7$ in the estimation method to provide a small estimation MSE without the higher computational complexity that $n = 48$ implies.
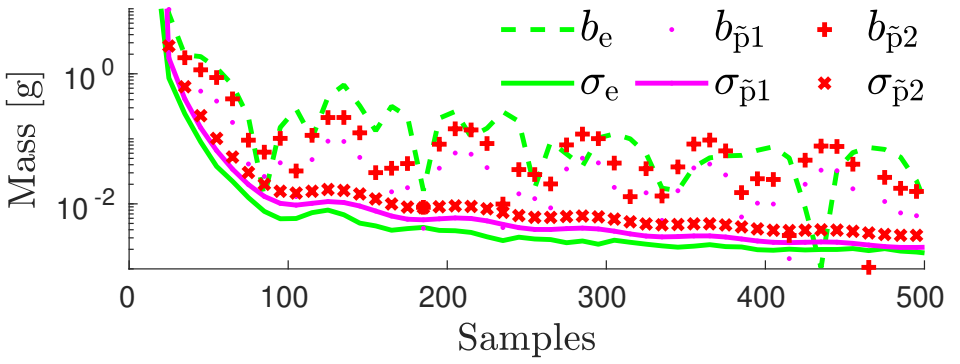
Figure 5.11.: Comparative view of the bias prediction using two different noise variance estimations. Estimating the variance from the step response residual gives a bias prediction $b_{\tilde{p}2}$ and a standard error $\sigma_{\tilde{p}2}$ that are slightly higher than using the noise variance estimated from the steady state response $\sigma_{\tilde{p}1}$ and $\sigma_{\tilde{p}1}$. The bias prediction $b_{\tilde{p}2}$ approximates better the empirical bias. The standard error $\sigma_{\tilde{p}2}$ provides a conservative value of the input estimation uncertainty.
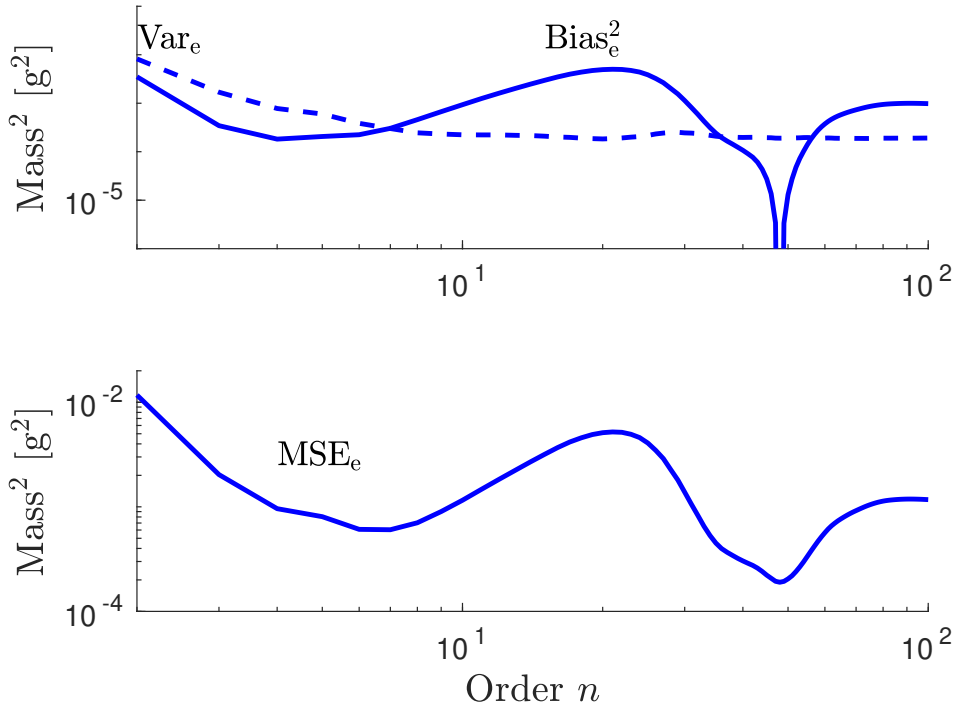
Figure 5.12.: The hundred measured sensor step responses are processed by the step input estimation method for different values of the order n. The empirical squared bias (solid) and the empirical variance (dashed) are shown on the left and the empirical MSE on the right. The MSE has a local minimum at $n = 7$ and another at $n = 48$. It is recommended to use the estimation method with $n = 7$ because at $n = 48$ the decrement of the MSE is not significant.

5.4. Conclusions

In this paper we investigated the statistical properties of a data-driven step input estimation method in a real-life application. The step input estimation method is a structured and correlated errors-in-variables problem that is solved with recursive least squares. A statistical analysis was conducted using the ordinary least squares condensed notation. This statistical analysis of the input estimate provides expressions that approximate the estimation bias and variance assuming that the measurement noise is Gaussian white noise. The variance approximation is useful to assess the uncertainty of the input estimate. In simulation we observed that the mean squared error of the input estimate is close to the theoretical minimum that uses the Cramér-Rao lower bound for biased estimators. Since the data-driven step input estimation method is not statistically efficient, there is room for improvement. This is a topic for future research. In the practical experiments, the measurement noise is not white. The noise variance obtained from the sensor steady state response underestimates the measurement noise variance, that was observed 5 dB larger in the power spectrum due to nonlinearities of the sensor. Considering this difference in the measurement noise variance, we introduced a conservative bound of the measurement noise variance so that the first and second moments of the input estimate are more accurately predicted. Using the variance approximation, we can assess the uncertainty of the input estimate with respect to the number of samples processed by the data-driven step input estimation method. The step input estimation method is useful in practical applications where the whiteness assumption of the measurement noise is not fulfilled.

6. Ramp input estimation method

The results of this chapter ...

6.1. Introduction

The goal of a measurement is to accurately estimate the input value using the sensor transient response. The input might vary during the measurement being the simplest case the input that changes with a constant rate, described with an affine function. The inputs that vary at a constant rate activate the sensor gradually. An affine input estimation method is needed to estimate the slope and the interception parameters of the affine function.

This chapter describes two signal processing methods for the estimation of affine input parameters. These methods are a data-driven subspace method and a maximum-likelihood (ML) estimation method based on local-optimization. The subspace is a recursive method independent of the sensor model, and the ML method iteratively minimizes a cost function using a simulated sensor response in a receding time horizon.

In this chapter, the dynamic weighing is chosen as an implementation example. The dynamic weighing of an affine input is an interesting metrology application because the affine input turns a linear time invariant sensor model into a time-varying sensor model. The affine input estimation methods provide an insight on the properties of the dynamic measurement of time-varying inputs.

The effectiveness and the uncertainty of the methods are evaluated with simulation studies. The uncertainty is assessed, for the subspace method, using a Taylor expansion of the exponentially weighted recursive least squares estimate, and for the ML method, using the derivatives of the residual error obtained from the to-be-minimized cost function.

6.1.1. Affine input estimation problem

The affine input is modeled as a straight line $u = at + b$ with parameters the slope a and the interception b. The affine input estimation problem is formulated as a signal processing problem as follows.

Problem   Given the sequence of measured output observations $\mathbf{y} = (y(1), \ldots, y(T)), y(t) \in \mathbb{R}$, of a stable linear time-invariant system of order n, and static gain γ, generated by an affine input $u = at + b$, estimate the parameters of the affine input, *i.e.*, find the values of the parameters $\widehat{a}, \widehat{b} \in \mathbb{R}$ such that $\widehat{u} = \widehat{a}t + \widehat{b}$ approximates u. The measured observations $\mathbf{y} = \mathbf{y} + \boldsymbol{\epsilon}$ are exact sensor responses $\mathbf{y}$ perturbed by additive noise $\boldsymbol{\epsilon}$ assumed to be independent and normally distributed of zero mean and given variance σ_ε^2.

Motivating example   Dynamic weighing is an application example where the affine input can be observed. The weighing of objects in a conveyor belt gives the sensor input an ideal straight line profile when the conveyor belt moves at a constant speed. The straight line represents the mass coming gradually into the weighing scale sensor in the conveyor belt. The mass can be estimated from the slope a of the straight line model. The mechanical vibrations of the conveyor belt perturb the input and the sensor response is affected by measurement noise. The interest is to estimate the mass of the object using the sensor response observations.

Consider the weighing scale modeled as a second order mass-spring-damper system, such as the one shown in the diagram of Figure 6.1. The application of an affine input turns the linear time-invariant system into a linear time-varying system, whose dynamics depends on the input $u(t) = at + b$, as it is described by the differential equation:

$$\frac{d}{dt}\left((at+b+m)\frac{dy}{dt}\right) + k_d\frac{dy}{dt} + k_sy = (at+b+m)g \tag{6.1}$$

where m is the mass of the scale, k_d is the damping constant, k_s is the elasticity constant, and $g = 9.81 \text{ m/s}^2$ is the gravitational acceleration.

The weighing system admits a state space representation where the states $x_1 = y$ and $x_2 = \dot{y}$ are the position and the speed of the weighing scale:

$$\dot{\mathbf{x}} = \begin{bmatrix} 0 & 1 \\ \dfrac{-k_s}{at+b+m} & \dfrac{-(k_d+a)}{at+b+m} \end{bmatrix} \mathbf{x} + \begin{bmatrix} 0 \\ g \end{bmatrix}, \quad y = \begin{bmatrix} 1 & 0 \end{bmatrix} \mathbf{x}.$$
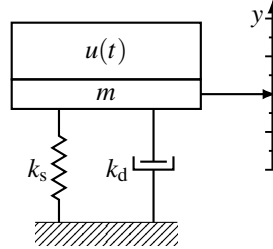

Figure 6.1.: A second order mass-spring-damper model represents the dynamic weighing system. The dynamics of the system depend on the affine input. The weighing system is time-varying when the applied input changes with respect to time.

In this paper we use the dynamic weighing example to illustrate the implementation of the affine input estimation methods.

6.2. Solution methods

In this section we describe the proposed subspace method to solve the affine input estimation problem. The method is motivated by the step input estimation method that is formulated as a structured errors-in-variables (EIV) problem and is solved using recursive least squares (RLS). The exponentially weighted recursive least squares (EWRLS) is a generalization of RLS that allows the extension of the estimation method to reconstruct the affine input.

A maximum-likelihood (ML) method that performs simultaneous system identification and input estimation is described and its results are used as reference to compare the subspace method results.

An example of the subspace method is illustrated with a weighing system. An existing time-varying (TV) compensation filter that was designed for weighing applications is described briefly. This TV filter is also used to compare the results of the proposed subspace method.

6.2.1. Subspace method

RLS is a special case of the EWRLS that can solve the minimization problem (**??**). The minimization problem is a structured EIV problem and its EWRLS solution is equivalent to

$$\widehat{\mathbf{x}} = \operatorname*{argmin}_{\mathbf{x}} \left\| \mathbf{W}^{1/2} \left(\mathbf{y} - \mathbf{K}\mathbf{x} \right) \right\|_2^2. \tag{6.2}$$

where $\mathbf{y}$, $\widehat{\mathbf{x}}$, and $\mathbf{K}$ are defined in (**??**) and (**??**) and $\mathbf{W} \in \mathbb{R}^{(T-n)\times(T-n)}$ is a diagonal matrix of descending powers of the weight $\lambda \in [0,1)$, *i.e.*, $W = \operatorname{diag}\left(\lambda^{T-n}, \dots, \lambda^2, \lambda^1\right)$. The weight λ is a data selection forgetting factor since it enables to apply different weights to the residuals $\mathbf{y} - \mathbf{K}\mathbf{x}$. When $\lambda = 1$, we have the same solution as RLS. When $\lambda < 1$, the older residuals are weighted with lower values than the residuals of recent observations. In this way, the solution of the minimization problem depends more on new data.

The profile of an affine input excitation can be reconstructed by solving the structured errors-in-variables problem (6.2) where y is the corresponding response of a stable dynamic system, $\mathbf{K}$ is constructed from the output observations, and $\lambda < 1$.

After the affine input $\widehat{u}$ has been estimated, the affine input parameters a and b are estimated by fitting $\widehat{u}$ to the straight line $\widehat{u} = at + b$ using linear regression, as

follows

$$\begin{bmatrix} 1 & 1 \\ \vdots & \vdots \\ T-\tau+1 & 1 \end{bmatrix} \begin{bmatrix} \widehat{a} \\ \widehat{b} \end{bmatrix} = \begin{bmatrix} \widehat{u}(\tau) \\ \vdots \\ \widehat{u}(T) \end{bmatrix} \tag{6.3}$$

where τ is a number of samples used as a tuning parameter that counteracts the time delay that exists when a LTI system is excited with an affine input u. The subspace method can process online the sensor response to the affine excitation. For each new observation $y(t)$, the estimation $\widehat{u}$ is updated followed by the update of the slope $\widehat{a}$ and the interception $\widehat{b}$. The values of the tuning parameters λ and τ can be obtained in the calibration of the method using the response of the sensor.

The subspace method estimates the input applied to a dynamic system directly from the caused transient response. This is a recursive method that can be implemented in real time to estimate the input using low cost digital signal processors. The method is a model-free approach and can be used in a variety of physical measurements. The method tracks any arbitrary time-varying input and can estimate the parameters of the input when it is associated to a particular input model.

6.2.2. Maximum-likelihood method

Using a model of the sensor, the ML method estimates the sensor initial conditions and the parameters of the applied affine input. The affine input parameters a and b are the slope and the interception of the straight line model $u = at + b$.

Algorithm 6.2.2 lists the steps of the proposed ML method. This is an iterative minimization method that uses the Jacobian of the residual error function $\mathbf{r} = \widehat{\mathbf{y}} - \mathbf{y}$ to search the direction that minimizes the difference between the measured sensor response $\mathbf{y}$ and the simulated response $\widehat{\mathbf{y}}$.

ML Affine input estimation. $\mathbf{y}$, and sensor model parameters Initialize $\theta = (a, b, \mathbf{x}_{\mathrm{ini}})$ each N observations of $\mathbf{y}$ Simulate model response $\widehat{\mathbf{y}}(\theta)$ Compute error $\mathbf{r}(\theta) = \mathbf{y} - \widehat{\mathbf{y}}(\theta)$ Minimize $\mathbf{r}^\top \mathbf{r}$ over θ using analytic Jacobian $\partial\mathbf{r}/\partial\theta$ Update θ Optimized parameters $\widehat{a}, \widehat{b}$, and $\widehat{\mathbf{x}}_{\mathrm{ini}}$

To initialize the optimization variables a, b, and $\mathbf{x}_{\mathrm{ini}}$, we use the subspace estimation method using at least the first $2n+2$ samples. With the initial affine input parameters we simulate a sensor excitation and, since we are using few samples, we have an approximation of the initial conditions. The optimization variables updates are computed every N new observations. The minimization can be done using the Levenberg-Marquardt algorithm Nocedal and Wright [2006].

Covariance of the ML method estimates

The ML method simulates a dynamic system, and computes the Jacobian of the residual error in each iteration. The analytic formulation of the Jacobian benefits the estimation method in two ways: it speeds up the minimization and gives direct access to the variance of the estimates. The covariance matrix of the ML estimates can be expressed as Pintelon and Schoukens [2012]

$$\mathbf{Cov}\left(\widehat{x}\right) = \left(\left(\frac{\partial \mathbf{r}}{\partial \boldsymbol{\theta}}\right)^{\top}\left(\frac{\partial \mathbf{r}}{\partial \boldsymbol{\theta}}\right)\right)^{-1}. \tag{6.4}$$

ML affine input estimation example

We use the previously described dynamic weighing system to illustrate the ML method. In this case, the formulation of the problem is:

$$\text{Minimize} \quad \text{over } a, b, \mathbf{x}_{\text{ini}} \quad \mathbf{r}^{T}\mathbf{r}, \text{ subject to:}$$

$$\dot{\mathbf{x}} = \begin{bmatrix} 0 & 1 \\ \frac{-k_{\text{s}}}{at+b+m} & \frac{-(a+k_{\text{d}})}{at+b+m} \end{bmatrix}\mathbf{x} + \begin{bmatrix} 0 & \frac{x_{\text{ini},1}}{at+b+m} \\ g & \frac{x_{\text{ini},2}}{at+b+m} \end{bmatrix}\begin{bmatrix} 1 \\ \delta(t) \end{bmatrix}, \tag{6.5}$$

$$\widehat{y} = \begin{bmatrix} 1 & 0 \end{bmatrix}\mathbf{x}.$$

where a, b are the affine input parameters, m, k_{d}, and k_{s} are the model parameters, the model states $\mathbf{x}$ are the position and the speed of the weighing scale, the difference between the sensor response $\mathbf{y}$ and the simulated response $\widehat{\mathbf{y}}$ is the residual $\mathbf{r} = \widehat{\mathbf{y}} - \mathbf{y}$. The model initial conditions $\mathbf{x}_{\text{ini}}$ are considered optimization variables and appear in the augmented column of the input matrix.

The analytic Jacobian for the weighing system example is described in the appendix.

6.2.3. Time-varying compensation filter

The time-varying (TV) filter described in Pietrzak et al. [2014] was designed to compensate the measured responses of a conveyor weighing system, considering they are modeled as a saturated ramp. The TV filter consists of three low-pass infinite impulse response (IIR) filters in cascade, where the $i-$th IIR filter is given by

$$\widehat{y}_i(t) + k_1(t)\widehat{y}_i(t-1) = k_2(t)\left(\widehat{y}_{i-1}(t) + \widehat{y}_{i-1}(t-1)\right) \tag{6.6}$$

for $i = 1, \ldots, 3$ and $t = 0, \ldots, T$. The sensor response is fed to the filter, then $\widehat{y}_0(t) = y(t)$, and the output of the TV filter $\widehat{u}_{\text{ltv}}(t) = \widehat{y}_3(t)$ is an estimation of the affine input. Since in our case we are processing only the ramp without the saturation, the estimates $\widehat{a}_{\text{ltv}}$ and $\widehat{b}_{\text{ltv}}$ of the input parameters are obtained by fitting a straight line to the estimated input $\widehat{u}_{\text{ltv}}$ using linear regression.

The time-varying coefficients $k_1(t)$ and $k_2(t)$ are computed from

$$k_1(t) = \frac{f_c(t) - \frac{k_3}{\pi T_s}}{f_c(t) + \frac{k_3}{\pi T_s}}, \quad k_2(t) = \frac{1 + k_1(t)}{2}, \quad k_3 = \sqrt{\sqrt[3]{2} - 1} \qquad (6.7)$$

where T_s is the sampling time and $f_c(t)$ is a heuristic "cutoff" frequency

$$f_c(t) = f_u + (f_l - f_u)\beta^{(t-1)/\alpha(T-1)} \qquad (6.8)$$

that changes between the lower f_l and upper f_u limits, where the coefficient β is lower than one, and α is the decay rate. The lower frequency value f_l and the coefficient β are fixed and the variables f_u and α are optimized off-line by solving the minimization problem

$$\text{minimize} \quad \text{over } f_u, \alpha \quad \max\left(\frac{\mu_{\widetilde{a}_{\text{ltv}}}}{\mu_{\text{spec}}}, \frac{\mu_{\widetilde{b}_{\text{ltv}}}}{\mu_{\text{spec}}}, \frac{\sigma_{\widetilde{a}_{\text{ltv}}}}{\sigma_{\text{spec}}}, \frac{\sigma_{\widetilde{b}_{\text{ltv}}}}{\sigma_{\text{spec}}}\right) + \max\left(\frac{\eta_i}{T}\right) \qquad (6.9)$$

where $\mu_{\widetilde{a}_{\text{ltv}}}$, $\mu_{\widetilde{b}_{\text{ltv}}}$, $\sigma_{\widetilde{a}_{\text{ltv}}}$ and $\sigma_{\widetilde{b}_{\text{ltv}}}$ are the mean values and the standard deviations of the estimation errors $\widetilde{a}_{\text{ltv}} = \widehat{a}_{\text{ltv}} - a$, and $\widetilde{a}_{\text{ltv}} = \widehat{b}_{\text{ltv}} - b$, and where a and b are the true values of the input parameters. The values μ_{spec} and σ_{spec} are specified in the OIML recommendation R51 International Recommendation OIML R 51 1 [2006] for mass measurements that use a conveyor belt.

6.3. Simulation results

The results of the affine input parameters estimation are discussed in this section. We performed a simulation study using the weighing system presented as an example. We compared the performance of the proposed subspace method to a conventional time-varying (TV) filter, that was conceived for weighing applications, and to the maximum-likelihood (ML) method.

A second order weighing system was excited with an affine input to get the transient response. The parameters of the weighing system are $m = 15$ g, $d = 5.5$ Ns/m and $k = 10250$ N/m. The applied affine input $u = 100t + 10$ represents a mass that changes from 10 g to 110 g, at a constant rate, in a time interval of 0.1 s.

This change of mass represents one example of the weighing input in a conveyor weighing system when an object of 100 g is measured while it is moving at constant speed. The sensor response is acquired using sampling time $T_s = 0.1$ ms. In Figure 6.2 the input u is represented with the dotted line, the oscillatory curve is the corresponding sensor ramp response y, and $\widehat{u}$ is a typical input estimate obtained with the subspace method.
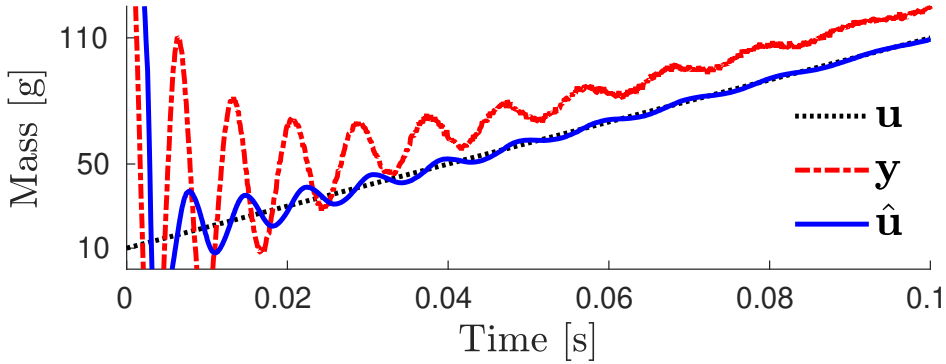

Figure 6.2.: The sensor transient response y to an affine input excitation $u = at + b$ is processed by the estimation methods to estimate the parameters a and b. In the figure we observe an example of the input estimate $\widehat{u}$ obtained with the subspace method. The input parameters are calculated from $\widehat{u}$ using linear regression.

In each simulation, the sensor response was perturbed with an independent realization of additive normally distributed measurement noise. The added perturbation noise has signal-to-noise ratios (SNR) in the interval [20 dB, 60 dB], values that are realistic in practical applications. The SNR is defined as the ratio of signal power to the noise power, that is equivalent to the root-mean-square value of the true signal to the variance of the perturbation noise, and in dB is given as

$$\text{SNR} = 20\log_{10} \frac{\frac{1}{T}\int_0^T y(t)^2 dt}{\sigma_\epsilon} \tag{6.10}$$

6.3.1. Results of the subspace method

The subspace method processed online the sensor transient response. The first estimation was obtained with $2n + 1$ samples. The method updated recursively

the value of the estimated parameters for each new collected sample, using the forgetting factor λ listed in Table 6.1. In Figure 6.3 we observe the relative errors of the estimates $\widehat{a}$ and $\widehat{b}$ obtained when SNR = 40 dB. The relative errors are smaller than 5 % after 400 and 500 samples are processed, i.e., 0.04 s and 0.05 s, respectively. As more samples are collected, the parameter estimation improves. Figure 6.4 shows the final value of the relative errors, found at $t = 0.1$ s, for the different SNR values considered. The relative errors are smaller than 2 % regardless of the measurement noise level.

Table 6.1.: The values of the forgetting factor λ and the samples shift τ that config-
ure the subspace method for the different values of SNR. These values
were obtained after calibration of the method and fixed during the
simulation study.

SNR [dB]	20	30	40	50	60
λ	0.939	0.940	0.955	0.959	0.959
τ	15	15	17	14	20
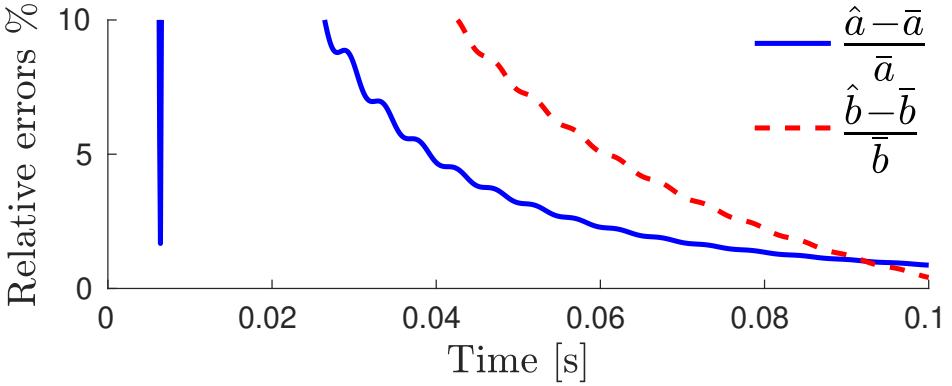
Figure 6.3.: The relative errors of the affine input parameters estimation decrease
as the subspace method processes more samples. The relative errors of
the estimates $\widehat{a}$ and $\widehat{b}$ are smaller than 5 % after 400 and 500 samples,
respectively ($T_s = 0.1$ ms).

The Cramér-Rao lower bound (CRLB) of the errors-in-variables problem formu-
lated by the subspace method was numerically computed for different sample
size using Equation (4.20). The CRLB is the minimum variance that the estimates
$\widehat{a}$ and $\widehat{b}$ can have. The average of 10^4 runs with independent noise realizations

Figure 6.4.: The minimum value of the estimation relative errors obtained with the subspace method is less than 2 % regardless of the SNR between 20 dB and 60 dB.

allows to find the empirical mean squared error (MSE) of the estimates, defined as
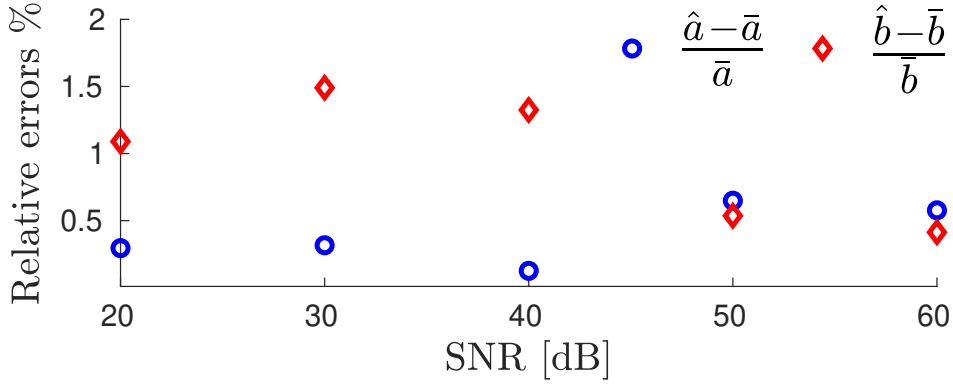
$$\mathrm{MSE}_{\widehat{a}} = \big(b_{\mathrm{p}}\,(\widehat{a})\big)^2 + v_{\mathrm{p}}\,(\widehat{a})\,, \quad \text{and} \quad \mathrm{MSE}_{\widehat{b}} = (b_{\mathrm{p}}(\widehat{b}))^2 + v_{\mathrm{p}}(\widehat{b}), \qquad (6.11)$$

where $b_{\mathrm{p}}\,(\widehat{a})$ and $b_{\mathrm{p}}(\widehat{b})$ are the bias, and $v_{\mathrm{p}}\,(\widehat{a})$ and $v_{\mathrm{p}}(\widehat{b})$ are the variances of the input parameters. Figure 6.5 shows that the mean squared errors $\mathrm{MSE}_{\widehat{a}}$ and $\mathrm{MSE}_{\widehat{b}}$ are near to their theoretical minimum CRLB_a and CRLB_b within two orders of magnitude, when SNR = 40 dB. Figure 6.6 shows the final value of the Cramér-Rao lower bounds and the empirical mean-squared errors, found at $t = 0.1$ s, for the different SNR values considered. Both $\mathrm{MSE}_{\widehat{a}}$ and $\mathrm{MSE}_{\widehat{b}}$ are less than one order of magnitude near to CRLB_a and CRLB_b, respectively, for SNR ≤ 30 dB. The difference increases for larger SNR but the maximum is two orders of magnitude for SNR = 60 dB.

Table 6.2 shows a comparative view of the estimation mean-squared-errors maximum values when the ramp that excites the sensor corresponds to different masses and time durations. For each mass and duration, the sensor responses were perturbed with measurement noise of SNR in the interval [20 dB, 60 dB]. The sensor parameters and sampling frequency are fixed and are the same described in the first paragraph of this section. The maximum values of the MSE are mainly found at low SNR values between 20 and 40 dB. The higher levels of noise increase the uncertainty of the estimation defined in terms of the MSE. For fast ramp excitations, the MSE's increase considerably. The used sampling frequency constrains the estimation method effectiveness for the ramp input duration of 0.05

s or shorter and there it is recommended to use a higher sampling frequency that
will reduce the estimation MSE.
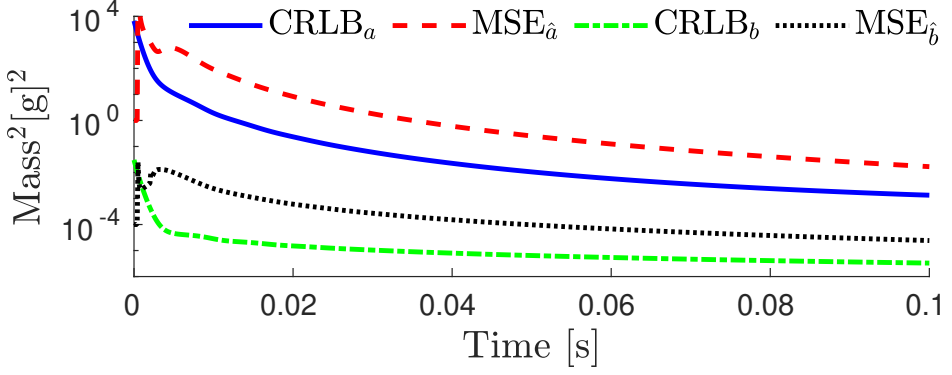
Figure 6.5.: When the SNR of the sensor response is 40 dB, the mean squared
errors of the slope estimate $\widehat{a}$ and the interception estimate $\widehat{b}$, ob-
tained by the subspace method, are two orders of magnitude above
the theoretical minimum variance given by the Cramér-Rao lower
bound.
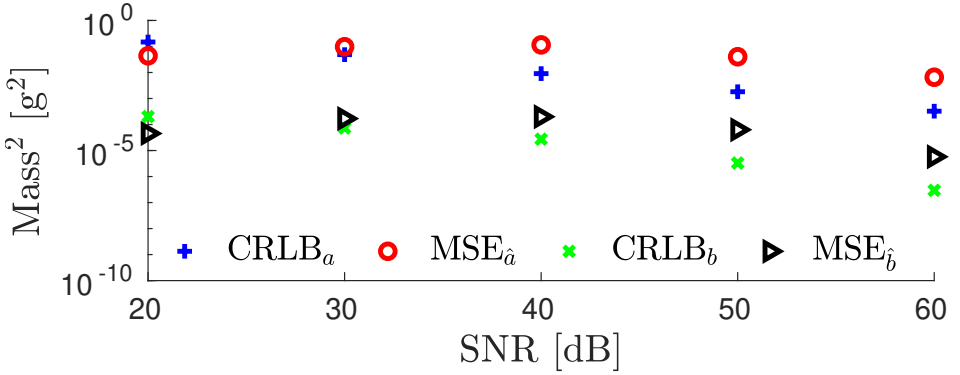
Figure 6.6.: The Cramér-Rao lower bounds of the estimates CRLB_a and CRLB_b de-
termine the minimum uncertainty that can be achieved and increases
with the measurement noise. The empirical mean squared errors
$\text{MSE}_{\widehat{a}}$ and $\text{MSE}_{\widehat{b}}$ are near to the Cramér-Rao lower bounds within one
order of magnitude for SNR smaller than 30 dB, and within two orders
of magnitude for SNR between 40 dB and 60 dB.

Table 6.2.: The maximum values of the estimation mean squared errors observed when the subspace method processed the sensor transient responses caused by ramp excitations of masses 0.1, 0.3, 0.5, and 1.0 kg, that last 0.05, 0.1 and 0.5 s, with signal to noise ratios in the interval [20 dB, 60 dB] occur mainly at 40 dB and for lower SNR. There is an increment in the MSE values when the ramp excitation is faster.

Time	Mass			
	0.1 kg	0.3 kg	0.5 kg	1.0 kg
0.05 s				
$\mathrm{MSE}_{\hat{a}}\ [g^2]$	$3.5\mathrm{x}10^0_{(@40\ \mathrm{dB})}$	$13.5\mathrm{x}10^0_{(@50\ \mathrm{dB})}$	$3.8\mathrm{x}10^0_{(@20\ \mathrm{dB})}$	$8.3\mathrm{x}10^0_{(@50\ \mathrm{dB})}$
$\mathrm{MSE}_{\hat{b}}\ [g^2]$	$3.1\mathrm{x}10^{-3}_{(@40\ \mathrm{dB})}$	$1.1\mathrm{x}10^{-2}_{(@40\ \mathrm{dB})}$	$1.1\mathrm{x}10^{-2}_{(@40\ \mathrm{dB})}$	$1.9\mathrm{x}10^{-2}_{(@60\ \mathrm{dB})}$
0.1 s				
$\mathrm{MSE}_{\hat{a}}\ [g^2]$	$3.1\mathrm{x}10^{-2}_{(@30\ \mathrm{dB})}$	$1.1\mathrm{x}10^0_{(@40\ \mathrm{dB})}$	$8.3\mathrm{x}10^{-1}_{(@60\ \mathrm{dB})}$	$1.3\mathrm{x}10^0_{(@50\ \mathrm{dB})}$
$\mathrm{MSE}_{\hat{b}}\ [g^2]$	$6.0\mathrm{x}10^{-5}_{(@30\ \mathrm{dB})}$	$1.2\mathrm{x}10^{-1}_{(@50\ \mathrm{dB})}$	$2.1\mathrm{x}10^{-2}_{(@40\ \mathrm{dB})}$	$3.7\mathrm{x}10^{-2}_{(@40\ \mathrm{dB})}$
0.5 s				
$\mathrm{MSE}_{\hat{a}}\ [g^2]$	$3.0\mathrm{x}10^{-2}_{(@20\ \mathrm{dB})}$	$3.0\mathrm{x}10^{-1}_{(@20\ \mathrm{dB})}$	$3.2\mathrm{x}10^0_{(@20\ \mathrm{dB})}$	$8.6\mathrm{x}10^{-2}_{(@20\ \mathrm{dB})}$
$\mathrm{MSE}_{\hat{b}}\ [g^2]$	$3.1\mathrm{x}10^{-5}_{(@50\ \mathrm{dB})}$	$9.8\mathrm{x}10^{-4}_{(@40\ \mathrm{dB})}$	$2.0\mathrm{x}10^{-5}_{(@50\ \mathrm{dB})}$	$1.7\mathrm{x}10^{-5}_{(@20\ \mathrm{dB})}$

A numerical sensitivity analysis of the subspace method was conducted by adding uncertainty to ramp input generation and looking into the estimation results. The uncertainty σ_s of the speed in which the ramp increases, and the uncertainties of the input parameters, represented by $\sigma_{a,b}$, were selected to be 0%, 5% and 10% of their true values. A Monte Carlo simulation with 10^4 runs was performed for each SNR and the maximum values of the estimation uncertainty are shown in Table 6.3. According to these results, the input parameters uncertainties $\sigma_{a,b}$ affect more the uncertainty of the estimation than the speed uncertainty σ_s. The parameter that is more affected by the input parameters uncertainty is the interception $\hat{b}$, since the uncertainty of the slope $\hat{a}$ is smaller.

6.3.2. Results of the maximum-likelihood method

The maximum-likelihood (ML) method processed off-line the sensor transient response. The ML method used the first 50 samples to initialize the optimization variables and updated the variables every $N = 1$ sample. In Figure 6.3 are shown the relative errors of the estimates $\hat{a}$, $\hat{b}$, $\hat{x}_{\mathrm{ini},1}$, and $\hat{x}_{\mathrm{ini},2}$. The convergence of the ML estimates gives relative errors below 5 % after three iterations. The largest relative

Table 6.3.: A sensitivity analysis of the subspace method was conducted by adding uncertainty to the ramp input. The speed σ_s, and the input parameters σ_s uncertainties are 0%, 5%, and 10% of their true values. The table shows the maximum values of the estimates uncertainty. The speed uncertainty causes a smaller spread of the estimates than the input parameters uncertainty.

$\sigma_{a,b}$	σ_s		
	0%	5%	10%
0%			
$\widehat{a}$ [kg/s]	$1.0 \pm 9.6\%_{(@50\ dB)}$	$1.0 \pm 8.2\%_{(@20\ dB)}$	$1.0 \pm 8.2\%_{(@50\ dB)}$
$\widehat{b}$ [g]	$10.0 \pm 10.3\%_{(@20\ dB)}$	$9.9 \pm 14.2\%_{(@30\ dB)}$	$10.0 \pm 21.7\%_{(@60\ dB)}$
5%			
$\widehat{a}$ [kg/s]	$1.0 \pm 9.7\%_{(@50\ dB)}$	$1.0 \pm 11.3\%_{(@20\ dB)}$	$1.0 \pm 8.0\%_{(@50\ dB)}$
$\widehat{b}$ [g]	$10.0 \pm 22.4\%_{(@50\ dB)}$	$10.0 \pm 33.2\%_{(@30\ dB)}$	$9.9 \pm 16.6\%_{(@50\ dB)}$
10%			
$\widehat{a}$ [kg/s]	$1.0 \pm 20.3\%_{(@40\ dB)}$	$1.0 \pm 22.0\%_{(@50\ dB)}$	$1.0 \pm 17.7\%_{(@40\ dB)}$
$\widehat{b}$ [g]	$9.9 \pm 46.8\%_{(@40\ dB)}$	$9.8 \pm 58.8\%_{(@50\ dB)}$	$9.9 \pm 41.6\%_{(@40\ dB)}$

error observed is in the scale velocity $\widehat{x}_{ini,2}$ estimate, which is more sensitive than the other optimization variables.
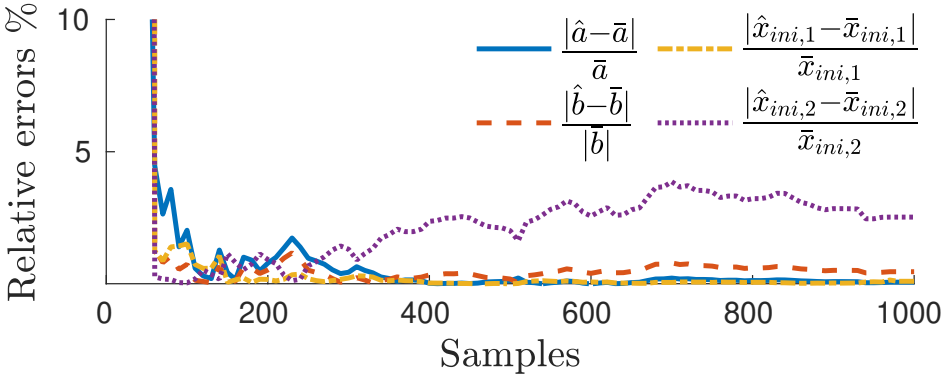

Figure 6.7.: The affine input parameters and the sensor initial conditions are estimated with the ML method. After three iterations the relative errors of the estimates are smaller than 5 %.

Using the analytic Jacobian and Equation (6.4), we computed the covariance of the estimate. In Figure 6.8 are shown the variances of the optimization variables

taken from the diagonal of the covariance matrix. We can see that the variances of $\widehat{a}$ and $\widehat{b}$ decrease faster than the variances of $\widehat{x}_{\text{ini},1}$ and $\widehat{x}_{\text{ini},2}$ as more samples are processed.
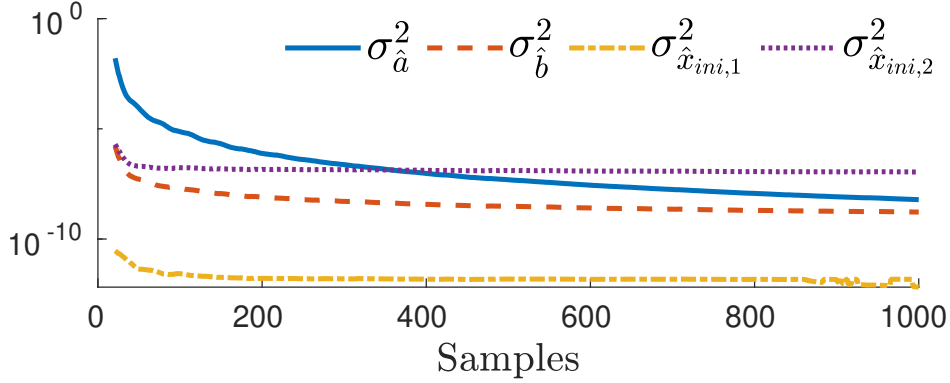

Figure 6.8.: The variances of the ML estimates are calculated using the information provided by the analytic Jacobian. The variances of the affine input parameters estimates decrease faster than the variances of the initial conditions estimates.

The ML method is computationally more expensive than the subspace method because the ML method simulates the response of a sensor model to optimize the input parameters and the sensor initial conditions.

A typical run of the ML method takes 30 s to complete. With this execution time, the ML estimation can only be performed offline. Nevertheless, the ML method objectives are to give the best estimation possible and to serve as a reference to assess the results of the other methods. An efficient implementation of the ML method to make it feasible for real-time implementation is not trivial and requires additional research that is considered a topic for future research.

A numerical sensitivity analysis of the ML method was conducted by adding uncertainty to the ramp input, and to the parameters of the time-varying model. The ramp input was perturbed with uncertainty of the speed in which the ramp increases σ_s, and with uncertainty on the input parameters $\sigma_{a,b}$. The perturbation uncertainty of the model parameters m, d, and k is represented by $\sigma_{m,d,k}$. The perturbation uncertainty was simulated by adding normally distributed random noise with standard deviation equal to 0%, 5% and 10% of the corresponding true values of the perturbed parameters. A Monte Carlo simulation with 10^3 runs was conducted for each SNR in the SNR inntervall of interest, and in Table ?? are shown the maximum values of the observed estimation uncertainties. The results show

that the speed uncertainty σ_s has a small impact on the estimation uncertainty. On the contrary, the input parameters uncertainties $\sigma_{a,b}$, and the uncertainties of the model parameters $\sigma_{m,d,k}$ cause a large increment in the uncertainty of the estimation.

6.3.3. Results of the time-varying filter

We fixed the frequency lower value $f_l = 0.01$ Hz and the base $\beta = 0.01$. The upper value f_u and the decay rate α were found using optimization (6.9). We chose the values $\mu_{\text{spec}} = 0.5$ and $\sigma_{\text{spec}} = 0.24$ as they are specified in the OIML recommendation International Recommendation OIML R 51 1 [2006] for a mass of 100 g measured in a conveyor belt. The optimized values of the frequency upper value and the decay rate, using a dataset of 100 transient responses, were $f_u = 26.94$ Hz and $\alpha = 5.71$.

Figure 6.9 shows the relative errors of the estimates $\hat{a}$ and $\hat{b}$ computed with the TV filter after processing the sensor transient response. The relative error of the slope estimate is below 5 % after 300 samples but the relative error of the interception estimate is near 10 %. The convergence rate of the estimate $\hat{a}$ was similar to that of the subspace method.
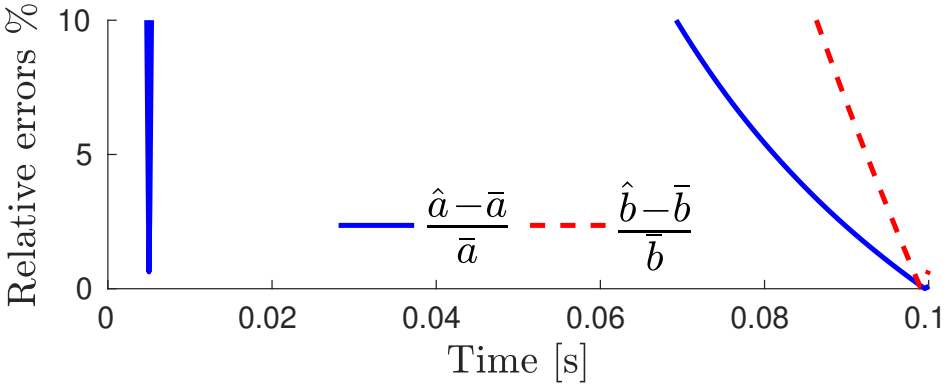

Figure 6.9.: The relative errors of the time-varying filter estimation converge slower than with the subspace method. The relative errors of $\hat{a}$ and $\hat{b}$ are smaller than 5 % only after 800 and 950 samples, respectively. With the subspace method the relative errors are below 5 % after 400 and 500 samples.

6.3.4. Discussion of the observed results

The subspace method obtains an estimation of the affine input parameters with a recursive least squares solution of a structured errors-in-variables problem. Updating the parameter estimates without matrix inversion simplifies the method implementation on digital signal processors of low cost. The price we pay by computing the least squares solution of an errors-in-variables problem is an increase in the bias of the estimates. Nevertheless, the empirical mean squared errors of the estimates are at most two orders of magnitude larger than the Cramér-Rao lower bound, meaning that the estimates uncertainty is low, even when the SNR is lower than 40 dB.

The proposed subspace method is a general method that can be used in different applications, with realistic signal-to-noise ratios. It is suitable not only for mass measurements. The weighing example shows that the subspace method can be used even when the measurement system is linear time-varying.

It was shown that the time-varying (TV) compensation filter can be modified to estimate the mass only from the increasing section of the saturated ramp, without the need of processing the saturation part. The modified TV filter can be implemented in real-time as the subspace method after a previous off-line coefficients optimization stage with sensor measured data. Nevertheless, the estimation results of the subspace method are better than the TV filter since they are twice as fast and one order of magnitude more acurate.

The subspace method can estimate the affine input parameters from the sensor response using few parameters, the sensor order n, the sensor static gain γ, and the RLS forgetting factor λ. The subspace method does not necessarily requires optimization of λ using a dataset of measured sensor responses. It is required to tune λ online during the calibration of the system and later λ remains fixed during the measurements.

The results of the sensitivity analysis show how the uncertainty of the subspace method estimates is affected when the ramp input is subject to perturbation. The impact on the uncertainty on the slope $\widehat{a}$ and the interception $\widehat{b}$ parameters is different. The ramp speed uncertainty σ_s is added to the uncertainty of the parameter $\widehat{b}$, but does not contribute to the uncertainty of the parameter $\widehat{a}$. On the other hand, the ramp parameters uncertainty ramp speed uncertainty $\sigma_{a,b}$ is added to the uncertainty of the estimates of both parameters $\widehat{a}$ and $\widehat{b}$. This is not surprising since the estimation parameters are linked to the ramp input parameters.

The maximum-likelihood (ML) method is an approach that requires larger computational resources. This is an iterative method and in each iteration computes a simulation of a dynamic system followed by the evaluation of the residual error Jacobian matrix. The advantage of the ML method is that we can estimate simultaneously sensor parameters and the initial conditions of the sensor. In the weighing case presented as an illustrative example it was not possible to incorporate other parameters of the sensor because they are not identifiable. According to the estimation relative errors, that are lower than 0.01 after 100 samples, from there on the ML method estimates are near to the true values and we may not require to run the method along all the measurement period. With only the first 100 samples we have an accurate parameter estimation and variance assessment.

However, the main drawback of the ML method that prevents online implementations is the required computational power to iteratively simulate the response of a sensor model. It takes an average of 30 s to complete an estimation with the ML method, and this time is too large for fast changing inputs. The development of an efficient ML method, suitable for real-time implementation, is not straightforward, and is proposed for future research.

The results of the sensitivity analysis of the ML method show that the uncertainty of the ramp input speed σ_s does not have an impact on the estimates uncertainty. Similar to the subspace case, the uncertainty of the ramp input parameters $\sigma_{a,b}$ is additive to the uncertainty of the estimated parameters $\widehat{a}$ and $\widehat{b}$, but does not contribute to the uncertainty of the first element of the initial conditions. On the other hand, the estimates uncertainty is affected by the perturbation on the model parameters $\sigma_{m,d,k}$. It is observed that the uncertainty of the estimated parameters $\widehat{a}$ and $\widehat{b}$ increases two and three times the uncertainty of the model parameters. This implies that we need to have an accurate model of the dynamic system to have a small uncertainty on the estimated input parameters. Unfortunately, the uncertainty of the second element of the inital conditions is always very high and this is not because of the perturbation of the ramp speed or the model parameters. This issue requires more investigation to see if it is due the identifiability of the parameter in the particular example we have.

6.4. Conclusions

An adaptive subspace method was proposed for the estimation of affine input parameters given the measurement of the caused sensor transient response. The subspace estimation method is a recursive method that allows online implementation. This method tracks the input of a system, using exponential forgetting, to

process the system response. The subspace method is model-free and estimates directly the input parameters without identifying a sensor model. Therefore, it can be applied to the measurement of different physical magnitudes. In the specific weighing example described in the manuscript, the input is an affine function. The method is also applicable when the sensor is time-varying. The subspace method is computationally cheap, simple and suitable for implementation on digital signal processor of low computational power.

A maximum-likelihood estimator based on local optimization was designed to obtain a comparative reference for the other methods. The maximum-likelihood method estimates the affine input parameters and also model parameters and the sensor's initial conditions. This method simulates, in a receding horizon scheme, the response of a sensor model to estimate the input and minimizes the sum of the squares of the residual between the measured and the estimated responses. The main drawback of the maximum-likelihood method is its computational cost and efficient implementation of the method is left for future work.

A linear time-invariant weighing system is used as an test example for the estimation methods. The weighing system becomes time-varying when an affine input excites the system. The estimation methods are compared in a simulation study where the time-varying sensor response is perturbed by measurement noise, that is assumed white of zero mean and known variance. The subspace method results are also compared to those of an existing digital time-varying filter. The coefficients of the time-varying filter require offline optimization. The estimation results obtained with the subspace method converges two times faster and is one order of magnitude smaller than those obtained with the time-varying filter. The empirical mean squared errors of the subspace method estimation is two orders of magnitude larger than the theoretical minimum given by the Cramér-Rao Lower bound.

Future work of this research is the practical implementation of the subspace method for real-time measurements.

7. Conclusions and future work

In this final chapter, we first summarize the contributions made to both parts of the thesis: **Part ??** and **Part ??**. Then, we propose some possible further improvements to extend this work in future research.

Conclusions

Conclusions - Statistical analysis

We conducted a statistical analysis of a structured errors-in-variables (EIV) estimation problem with correlation to find the first and second moments of its least-squares solution. This estimation problem occurs in metrology when we estimate the value of a measurand directly from the sensor transient response. The data-driven estimation of the physical quantity is formulated as a structured EIV problem with correlation that uses the observed transient response to construct both the regression matrix and the regressor. The real-time implementation of the method uses a recursive least squares algorithm that is simple and has low computational complexity. The assessment of the uncertainty is done using the estimate bias and variance.

The conducted statistical analysis produced expressions that predict the estimate bias and variance for given sample size and perturbation level of the observed response. The Monte Carlo simulation validated the predictions. We compared the results of solving an unstructured and uncorrelated EIV problem with a structured and correlated EIV problem to understand how the structure and the correlation impacts in the estimation. We found that the predictions in the structured case are more susceptible to perturbations. This is due to the two approximations involved, a second-order Taylor series expansion of the estimate, and the substitution of perturbed data on the prediction expressions. The relative error results indicate that the estimate bias, and variance are predicted using the derived expressions, and the observed data. The mean squared error of the estimate is close to the results of the maximum likelihood estimate given by the Cramér-Rao lower bound.

The bias and variance can be accurately predicted, provided that the Taylor series expansion is valid. This constraint has to be taken into account to ensure the effectiveness of the method in practical applications. In the example, it was observed that when the SNR lies outside the validity region, the bias and variance estimation was at most three times larger than the empirical values.

The methodology presented in this paper can be applied to estimate the uncertainty of the solutions to other structured EIV problems. The bias and variance expressions obtained after the statistical analysis depend on each specific structure.

Conclusions - Experimental validation

In this paper we investigated the statistical properties of a data-driven step input estimation method in a real-life application. The step input estimation method

is a structured and correlated errors-in-variables problem that is solved with recursive least squares. A statistical analysis was conducted using the ordinary least squares condensed notation. This statistical analysis of the input estimate provides expressions that approximate the estimation bias and variance assuming that the measurement noise is Gaussian white noise. The variance approximation is useful to assess the uncertainty of the input estimate. In simulation we observed that the mean squared error of the input estimate is close to the theoretical minimum that uses the Cramér-Rao lower bound for biased estimators. Since the data-driven step input estimation method is not statistically efficient, there is room for improvement. This is a topic for future research. In the practical experiments, the measurement noise is not white. The noise variance obtained from the sensor steady state response underestimates the measurement noise variance, that was observed 5 dB larger in the power spectrum due to nonlinearities of the sensor. Considering this difference in the measurement noise variance, we introduced a conservative bound of the measurement noise variance so that the first and second moments of the input estimate are more accurately predicted. Using the variance approximation, we can assess the uncertainty of the input estimate with respect to the number of samples processed by the data-driven step input estimation method. The step input estimation method is useful in practical applications where the whiteness assumption of the measurement noise is not fulfilled.

Conclusions - Ramp input

An adaptive subspace method was proposed for the estimation of affine input parameters given the measurement of the caused sensor transient response. The subspace estimation method is a recursive method that allows online implementation. This method tracks the input of a system, using exponential forgetting, to process the system response. The subspace method is model-free and estimates directly the input parameters without identifying a sensor model. Therefore, it can be applied to the measurement of different physical magnitudes. In the specific weighing example described in the manuscript, the input is an affine function. The method is also applicable when the sensor is time-varying. The subspace method is computationally cheap, simple and suitable for implementation on digital signal processor of low computational power.

A maximum-likelihood estimator based on local optimization was designed to obtain a comparative reference for the other methods. The maximum-likelihood method estimates the affine input parameters and also model parameters and the sensor's initial conditions. This method simulates, in a receding horizon scheme, the response of a sensor model to estimate the input and minimizes the sum of the squares of the residual between the measured and the estimated responses.

The main drawback of the maximum-likelihood method is its computational cost and efficient implementation of the method is left for future work.

A linear time-invariant weighing system is used as an test example for the estimation methods. The weighing system becomes time-varying when an affine input excites the system. The estimation methods are compared in a simulation study where the time-varying sensor response is perturbed by measurement noise, that is assumed white of zero mean and known variance. The subspace method results are also compared to those of an existing digital time-varying filter. The coefficients of the time-varying filter require offline optimization. The estimation results obtained with the subspace method converges two times faster and is one order of magnitude smaller than those obtained with the time-varying filter. The empirical mean squared errors of the subspace method estimation is two orders of magnitude larger than the theoretical minimum given by the Cramér-Rao Lower bound.

Future work of this research is the practical implementation of the subspace method for real-time measurements.

text

A. Appendices

A.1. Appendix - Derivation of bias and covariance expressions.

The bias and covariance of the least-squares (LS) estimate (4.5) are obtained using the mathematical expectation in the definitions (4.6) and (4.7). For an unstructured and uncorrelated EIV problem, the expected value, and the covariance of $\widehat{\mathbf{x}}$ are approximated by

$$
\mathbb{E}\left\{\widehat{\mathbf{x}}\right\} \approx \mathbf{x} + \mathbf{Q}^{-1}\mathbb{E}\left\{\mathbf{K}^{\top}\mathbf{E}\mathbf{Q}^{-1}\mathbf{K}^{\top}\mathbf{E} + \mathbf{E}^{\top}\mathbf{K}\mathbf{Q}^{-1}\mathbf{K}^{\top}\mathbf{E} - \mathbf{E}^{\top}\mathbf{E}\right\}\mathbf{x}, \quad \text{and}
$$

$$
\begin{aligned}
\mathbf{C}\left(\widehat{\mathbf{x}}\right) \approx \mathbf{x}\mathbf{x}^{\top} &+ \mathbf{Q}^{-1}\mathbb{E}\left\{\mathbf{K}^{\top}\boldsymbol{\epsilon}\boldsymbol{\epsilon}^{\top}\mathbf{K} + \mathbf{K}^{\top}\mathbf{E}\mathbf{x}\mathbf{x}^{\top}\mathbf{E}^{\top}\mathbf{K}\right\}\mathbf{Q}^{-1} \\
&+ \mathbf{Q}^{-1}\mathbb{E}\left\{\mathbf{K}^{\top}\mathbf{E}\mathbf{Q}^{-1}\mathbf{K}^{\top}\mathbf{E} + \mathbf{E}^{\top}\mathbf{K}\mathbf{Q}^{-1}\mathbf{K}^{\top}\mathbf{E} - \mathbf{E}^{\top}\mathbf{E}\right\}\mathbf{x}\mathbf{x}^{\top} \\
&+ \mathbf{x}\mathbf{x}^{\top}\mathbb{E}\left\{\mathbf{E}^{\top}\mathbf{K}\mathbf{Q}^{-1}\mathbf{E}^{\top}\mathbf{K} + \mathbf{E}^{\top}\mathbf{K}\mathbf{Q}^{-1}\mathbf{K}^{\top}\mathbf{E} - \mathbf{E}^{\top}\mathbf{E}\right\}\mathbf{Q}^{-1} - \mathbb{E}\left\{\widehat{\mathbf{x}}\right\}\mathbb{E}\left\{\widehat{\mathbf{x}}\right\}^{\top},
\end{aligned}
\tag{A.1}
$$

where we have considered the second order Taylor series approximation (4.4), and we have removed the terms of zero expected value, and the terms of order higher than 2. After an elementwise evaluation of the corresponding expected values in (A.1), the expressions result in

$$
\begin{aligned}
\mathbb{E}\left\{\widehat{\mathbf{x}}\right\} &\approx \mathbf{x} + \mathbf{b}_{\mathrm{p}}\left(\widehat{\mathbf{x}}\right) = \mathbf{x} + \sigma_{\mathbf{E}}^{2}\mathbf{Q}^{-1}\left(2\mathbf{I} + 2n\mathbf{I} - T\mathbf{I}\right)\mathbf{x}, \quad \text{and} \\
\mathbf{C}_{\mathrm{p}}\left(\widehat{\mathbf{x}}\right) &\approx \sigma_{\boldsymbol{\epsilon}}^{2}\,\mathbf{Q}^{-1} + \sigma_{\mathbf{E}}^{2}\,\mathrm{trace}\left(\mathbf{x}\mathbf{x}^{\top}\right)\mathbf{Q}^{-1} - \sigma_{\mathbf{E}}^{4}\left(2 + 2n - T\right)^{2}\,\mathbf{Q}^{-1}\mathbf{x}\mathbf{x}^{\top}\mathbf{Q}^{-1},
\end{aligned}
\tag{A.2}
$$

from where equations (4.8) and (4.9) are obtained.

On the other hand, due to the correlation, the expressions that approximate the expected value of the LS estimate of the structured and EIV problem (**??**) have a different form:

$$\mathbb{E}\left\{\widehat{\mathbf{x}}\right\} \approx \mathbf{x} + \mathbf{Q}^{-1}\mathbb{E}\left\{\mathbf{K}^\top\mathbf{E}\mathbf{Q}^{-1}\mathbf{K}^\top\mathbf{E} + \mathbf{E}^\top\mathbf{K}\mathbf{Q}^{-1}\mathbf{K}^\top\mathbf{E} - \mathbf{E}^\top\mathbf{E}\right\}\mathbf{x}$$

$$+ \mathbf{Q}^{-1}\mathbb{E}\left\{\mathbf{E}^\top\boldsymbol{\epsilon} - \mathbf{K}^\top\mathbf{E}\mathbf{Q}^{-1}\mathbf{K}^\top\boldsymbol{\epsilon} - \mathbf{E}^\top\mathbf{K}\mathbf{Q}^{-1}\mathbf{K}^\top\boldsymbol{\epsilon}\right\}, \quad \text{and}$$

$$\mathbf{C}\left(\widehat{\mathbf{x}}\right) \approx \mathbf{x}\mathbf{x}^\top + \mathbf{Q}^{-1}\mathbb{E}\left\{\mathbf{K}^\top\boldsymbol{\epsilon}\boldsymbol{\epsilon}^\top\mathbf{K} + \mathbf{K}^\top\mathbf{E}\mathbf{x}\mathbf{x}^\top\mathbf{E}^\top\mathbf{K} - \mathbf{K}^\top\mathbf{E}\mathbf{x}\boldsymbol{\epsilon}^\top\mathbf{K} - \mathbf{K}^\top\boldsymbol{\epsilon}\mathbf{x}^\top\mathbf{E}^\top\mathbf{K}\right\}\mathbf{Q}^{-1}$$

$$+ \mathbf{Q}^{-1}\mathbb{E}\left\{\mathbf{K}^\top\mathbf{E}\mathbf{Q}^{-1}\mathbf{K}^\top\mathbf{E} + \mathbf{E}^\top\mathbf{K}\mathbf{Q}^{-1}\mathbf{K}^\top\mathbf{E} - \mathbf{E}^\top\mathbf{E}\right\}\mathbf{x}\mathbf{x}^\top$$

$$+ \mathbf{x}\mathbf{x}^\top\mathbb{E}\left\{\mathbf{E}^\top\mathbf{K}\mathbf{Q}^{-1}\mathbf{E}^\top\mathbf{K} + \mathbf{E}^\top\mathbf{K}\mathbf{Q}^{-1}\mathbf{K}^\top\mathbf{E} - \mathbf{E}^\top\mathbf{E}\right\}\mathbf{Q}^{-1} - \mathbb{E}\left\{\widehat{\mathbf{x}}\right\}\mathbb{E}\left\{\widehat{\mathbf{x}}\right\}^\top$$

$$+ \mathbf{Q}^{-1}\mathbb{E}\left\{\mathbf{E}^\top\boldsymbol{\epsilon} - \mathbf{K}^\top\mathbf{E}\mathbf{Q}^{-1}\mathbf{K}^\top\boldsymbol{\epsilon} - \mathbf{E}^\top\mathbf{K}\mathbf{Q}^{-1}\mathbf{K}^\top\boldsymbol{\epsilon}\right\}\mathbf{x}^\top$$

$$+ \mathbf{x}\mathbb{E}\left\{\boldsymbol{\epsilon}^\top\mathbf{E} - \boldsymbol{\epsilon}^\top\mathbf{K}\mathbf{Q}^{-1}\mathbf{E}^\top\mathbf{K} - \boldsymbol{\epsilon}^\top\mathbf{K}\mathbf{Q}^{-1}\mathbf{K}^\top\mathbf{E}\right\}\mathbf{Q}^{-1}.$$

$$\text{(A.3)}$$

These expressions have the non zero expected value terms, up to the second order. We have then

$$\mathbb{E}\left\{\widehat{\mathbf{x}}\right\} = \mathbf{x} + \mathbf{b}_\text{p}\left(\widehat{\mathbf{x}}\right) \approx \mathbf{x} + \mathbf{Q}^{-1}\mathbf{K}^\top\underbrace{\mathbb{E}\left\{\mathbf{E}\mathbf{Q}^{-1}\mathbf{K}^\top\mathbf{E}\right\}}_{\mathbf{B}_1} - \mathbf{Q}^{-1}\underbrace{\mathbb{E}\left\{\mathbf{E}^\top\left(\mathbf{I} - \mathbf{K}\mathbf{Q}^{-1}\mathbf{K}^\top\right)\mathbf{E}\right\}}_{\mathbf{B}_2}\mathbf{x}$$

$$- \mathbf{Q}^{-1}\mathbf{K}^\top\underbrace{\mathbb{E}\left\{\mathbf{E}\mathbf{Q}^{-1}\mathbf{K}^\top\boldsymbol{\epsilon}\right\}}_{\mathbf{B}_3} + \mathbf{Q}^{-1}\underbrace{\mathbb{E}\left\{\mathbf{E}^\top\left(\mathbf{I} - \mathbf{K}\mathbf{Q}^{-1}\mathbf{K}^\top\right)\boldsymbol{\epsilon}\right\}}_{\mathbf{B}_4}, \quad \text{and}$$

$$\mathbf{C}\left(\widehat{\mathbf{x}}\right) \approx \mathbf{Q}^{-1}\mathbf{K}^\top\left(\underbrace{\mathbb{E}\left\{\boldsymbol{\epsilon}\boldsymbol{\epsilon}^\top\right\}}_{\sigma_\epsilon^2\mathbf{I}_{T-n}} + \underbrace{\mathbb{E}\left\{\mathbf{E}\mathbf{x}\mathbf{x}^\top\mathbf{E}^\top\right\}}_{\mathbf{C}_1} - \underbrace{\mathbb{E}\left\{\mathbf{E}\mathbf{x}\boldsymbol{\epsilon}^\top\right\}}_{\mathbf{C}_2} - \underbrace{\mathbb{E}\left\{\boldsymbol{\epsilon}\mathbf{x}^\top\mathbf{E}^\top\right\}}_{\mathbf{C}_2^\top}\right)\mathbf{K}\mathbf{Q}^{-1} - \mathbf{b}_\text{p}\left(\widehat{\mathbf{x}}\right)\mathbf{b}_\text{p}^\top\left(\widehat{\mathbf{x}}\right).$$

$$\text{(A.4)}$$

from where the expressions (4.12) and (4.13) are obtained.

A.2. Appendix - Proof of Lemma 1

Proof In the first case considered in the lemma, the elements of the expected value $\mathbf{Z} = \mathbb{E}\left\{\mathbf{E}\mathbf{A}\mathbf{E}\right\}$ are

$$z_{ij} = \mathbb{E}\left\{\mathbf{E}\mathbf{A}\mathbf{E}\right\}_{ij} = \mathbb{E}\left\{\mathbf{e}_i\mathbf{A}\mathbf{E}_j\right\} = \text{tr}\left(\mathbf{A}\,\mathbb{E}\left\{\mathbf{E}_j\mathbf{e}_i\right\}\right), \quad\quad\quad \text{(A.5)}$$

where $\mathbf{e}_i$, and $\mathbf{E}_j$ are the i-th row, and the j-th column of $\mathbf{E}$, for $i = 1, \ldots, T - n$, and $j = 2, \ldots, n + 1$. The matrix $\mathbb{E}\left\{\mathbf{E}_j\mathbf{e}_i\right\}$ is the product of σ_ϵ^2 times a matrix whose

elements are 0 in the first column, 2 in the $(j-i-1)$-th diagonal, and -1 in the $(j-i-2)$-th, and $(j-i)$-th diagonals, with zeros elsewhere. By using the definition of the second differential operator, we express

$$\mathbb{E}\left\{\mathbf{E}_j\mathbf{e}_i\right\} = \sigma_\epsilon^2 \begin{bmatrix} \mathbf{0}_{T-n} & \mathbf{D}_{T-n\times n}^{2,j-i} \end{bmatrix}. \tag{A.6}$$

The proof of the other cases in the Lemma is similar. For the second case, the elements of the expected value $\mathbf{Z} = \mathbb{E}\left\{\mathbf{E}^\top\mathbf{A}\mathbf{E}\right\}$ are

$$z_{ij} = \mathbb{E}\left\{\mathbf{E}^\top\mathbf{A}\mathbf{E}\right\}_{ij} = \mathbb{E}\left\{\mathbf{e}_i\mathbf{A}\mathbf{E}_j\right\} = \mathrm{tr}\left(\mathbf{A}\,\mathbb{E}\left\{\mathbf{E}_j\mathbf{e}_i\right\}\right), \tag{A.7}$$

where now $\mathbf{e}_i$ is the i-th row of $\mathbf{E}^\top$, and $\mathbf{E}_j$ is the j-th column of $\mathbf{E}$, for $i=2,\ldots,n+1$, and $j=2,\ldots,n+1$. The matrix $\mathbb{E}\left\{\mathbf{E}_j\mathbf{e}_i\right\}$ is σ_ϵ^2 times a matrix whose elements are 2 in the $(j-i)$-th diagonal, and -1 in the $(j-i-1)$-th and $(j-i+1)$-th diagonals, with zeros elsewhere. Therefore we have

$$\mathbb{E}\left\{\mathbf{E}_j\mathbf{e}_i\right\} = \sigma_\epsilon^2\mathbf{D}_{T-n\times T-n}^{2,j-i+1}. \tag{A.8}$$

The expected values that involve the vector ϵ are especial cases of the previous cases. The vector ϵ in the expected values $\mathbb{E}\left\{\mathbf{E}\mathbf{A}\epsilon\right\}$, $\mathbb{E}\left\{\mathbf{E}^\top\mathbf{A}\epsilon\right\}$, and $\mathbb{E}\left\{\mathbf{E}\mathbf{A}\epsilon^\top\right\}$ is

$$\epsilon = \begin{bmatrix} \varepsilon(n+1) & \varepsilon(n+2) & \cdots & \varepsilon(T) \end{bmatrix}^\top, \tag{A.9}$$

as it is imposed by the input estimation method formulation. $\qquad\square$

A.3. Appendix - Jacobians in Ramp input ML estimation

The entries of the Jacobian matrix are the first order partial derivatives of the residual error $\mathbf{r}$ with respect to the optimization variables. The state space representation of the weighing model allows to find the analytical expression of the Jacobian. The partial derivative of the residual error $\mathbf{r}$ with respect to the optimization variable a is

$$\mathbf{J}_a = \frac{\partial\mathbf{r}}{\partial a} = \frac{\partial\widehat{y}}{\partial a} = \begin{bmatrix} 1 & 0 \end{bmatrix}\frac{\partial\mathbf{x}}{\partial a} = \begin{bmatrix} 1 & 0 \end{bmatrix}\mathbf{x}_a \tag{A.10}$$

where we use $\mathbf{x}_a = \partial\mathbf{x}/\partial a$ to simplify the notation. Now, from the derivative of the state equation, we have

$$\dot{\mathbf{x}}_a = \begin{bmatrix} 0 & 1 \\ \frac{-k_s}{at+b+m} & \frac{-(a+k_d)}{at+b+m} \end{bmatrix}\mathbf{x}_a + \begin{bmatrix} 0 & 0 \\ \frac{k_st}{(at+b+m)^2} & \frac{k_dt-b-m}{(at+b+m)^2} \end{bmatrix}\mathbf{x} - \frac{t\,\delta(t)}{(at+b+m)^2}\mathbf{x}_{\mathrm{ini}}. \tag{A.11}$$

Then, the partial derivative of the error $\mathbf{r}$ with respect to the optimization variable a results in an additional dynamic system.

By repeating the procedure, we obtain the partial derivatives with respect to b as follows:

$$\dot{\mathbf{x}}_b = \begin{bmatrix} 0 & 1 \\ \frac{-k_s}{at+b+m} & \frac{-(a+k_d)}{at+b+m} \end{bmatrix} \mathbf{x}_b + \begin{bmatrix} 0 & 0 \\ \frac{k_s}{(at+b+m)^2} & \frac{a+k_d}{(at+b+m)^2} \end{bmatrix} \mathbf{x} - \frac{\delta(t)}{(at+b+m)^2} \mathbf{x}_{\text{ini}},$$
$$\mathbf{J}_b = \begin{bmatrix} 1 & 0 \end{bmatrix} \mathbf{x}_b. \tag{A.12}$$

The partial derivatives of the error $\mathbf{r}$ with respect to the initial conditions yield the following two Jacobians

$$\dot{\mathbf{x}}_{\mathbf{x}_{\text{ini},1}} = \begin{bmatrix} 0 & 1 \\ \frac{-k_s}{at+b+m} & \frac{-(a+k_d)}{at+b+m} \end{bmatrix} \mathbf{x}_{\mathbf{x}_{\text{ini},1}} + \begin{bmatrix} \frac{\delta(t)}{at+b+m} \\ 0 \end{bmatrix},$$
$$\mathbf{J}_{\mathbf{x}_{\text{ini},1}} = \begin{bmatrix} 1 & 0 \end{bmatrix} \mathbf{x}_{\mathbf{x}_{\text{ini},1}}. \tag{A.13}$$

and

$$\dot{\mathbf{x}}_{\mathbf{x}_{\text{ini},2}} = \begin{bmatrix} 0 & 1 \\ \frac{-k_s}{at+b+m} & \frac{-(a+k_d)}{at+b+m} \end{bmatrix} \mathbf{x}_{\mathbf{x}_{\text{ini},2}} + \begin{bmatrix} 0 \\ \frac{\delta(t)}{at+b+m} \end{bmatrix},$$
$$\mathbf{J}_{\mathbf{x}_{\text{ini},2}} = \begin{bmatrix} 1 & 0 \end{bmatrix} \mathbf{x}_{\mathbf{x}_{\text{ini},2}}. \tag{A.14}$$

The Jacobian matrix is constructed using the responses of the additional dynamic systems

$$\mathbf{J} = \begin{bmatrix} \mathbf{J}_a & \mathbf{J}_b & \mathbf{J}_{\mathbf{x}_{\text{ini},1}} & \mathbf{J}_{\mathbf{x}_{\text{ini},2}} \end{bmatrix} \tag{A.15}$$

List of Publications

Journal publications

G. Quintana-Carapia, I. Markovsky, R. Pintelon, P. Z. Csurcsia and D. Verbeke, "Bias and covariance of the least squares estimate in a structured errors-in-variables problem," *Computational Statistics Data Analysis*, Vol. 144, No. 106893, 2020, ISSN 0167-9473, doi: 10.1016/j.csda.2019.106893.

G. Quintana-Carapia, I. Markovsky, R. Pintelon, P. Z. Csurcsia and D. Verbeke, "Experimental validation of a data-driven step input estimation method for dynamic measurements," *IEEE Transactions on Instrumentation and Measurement*, Vol. x, No. x, pp. xx-xx, 2019, doi: 10.1109/TIM.2019.2951865

G. Quintana-Carapia, I. Markovsky, "Input parameters estimation from time-varying measurements," *Measurement*, Vol. 153, No. 1, pp. 107418, 2020, ISSN 0263-2241, doi: 10.1016/j.measurement.2019.107418.

Conference publications

G. Quintana-Carapia, I. Markovsky, "Data driven dynamic measurements", In: *9th International Workshop on the Analysis of Dynamic Measurements*", Berlin, Germany, 2016.

G. Quintana-Carapia, I. Markovsky, "Data driven dynamic measurements", In: *35th Benelux Meeting on Systems and Control*", Soesterberg, The Netherlands, 2016.

Bibliography

L. Angrisani and A. Napolitano. Modulation quality measurement in wimax systems through a fully digital signal processing approach. *IEEE Transactions on Instrumentation and Measurement*, 59(9):2286–2302, 2010. ISSN 0018-9456. doi: 10.1109/TIM.2009.2034577.

S.E. Azam, E. Chatzi, and C. Papadimitriou. A dual kalman filter approach for state estimation via output-only acceleration measurements. *Mechanical Systems and Signal Processing*, 60-61:866–886, 2015. ISSN 0888-3270. doi: 10.1016/j.ymssp.2015.02.001.

F. Ballo, M. Gobbi, G. Mastinu, and G. Previati. A six axis load cell for the analysis of the dynamic impact response of a hybrid III dummy. *Measurement*, 90: 309–317, 2016. ISSN 0263-2241. doi: 10.1016/j.measurement.2016.04.047.

BIPM, IEC, IFCC, ILAC, ISO, IUPAC, IUPAP, and OIML. *Evaluation of measurement data - Guide to the expression of uncertainty in measurement*. (Geneva: International Organization for Standardization) (Joint Committee for Guides in Metrology, JCGM 101:2008.), 2008.

G. Boschetti, R. Caracciolo, D. Richiedei, and A. Trevisani. Model-based dynamic compensation of load cell response in weighing machines affected by environmental vibrations. *Mechanical Systems and Signal Processing*, 34(1–2):116–130, 2013. ISSN 0888-3270. doi: 10.1016/j.ymssp.2012.07.010.

J. Cai, X. Qu, W. Xu, and G. Ye. Robust recovery of complex exponential signals from random Gaussian projections via low rank Hankel matrix reconstruction. *Applied and Computational Harmonic Analysis*, 41(2):470–490, 2016. ISSN 1063-5203. doi: 10.1016/j.acha.2016.02.003.

O. Casas, R. Dalazen, and A. Balbinot. 3D load cell for measure force in a bicycle crank. *Measurement*, 93:189–201, 2016. ISSN 0263-2241. doi: 10.1016/j.measurement.2016.07.031.

M.G. Cox and B.R. Siebert. The use of a Monte Carlo method for evaluating uncertainty and expanded uncertainty. *Metrologia*, 43(4):S178, 2006. URL `http://stacks.iop.org/0026-1394/43/i=4/a=S03`.

B.A. de Castro, F.G. Baptista, and F. Ciampa. New signal processing approach for structural health monitoring in noisy environments based on impedance measurements. *Measurement*, 137:155–167, 2019. ISSN 0263-2241. doi: 10.1016/j.measurement.2019.01.054.

G. D'Emilia, A. Gaspari, and E. Natale. Evaluation of aspects affecting measurement of three-axis accelerometers. *Measurement*, 77:95–104, 2016. ISSN 0263-2241. doi: 10.1016/j.measurement.2015.08.031.

A. Dienstfrey and Hale P.D. Analysis for dynamic metrology. *Measurement Science and Technology*, 25(3):1–12, 2014.

A. Diniz, M. de Almeida, J. Vianna, A. Oliveira, and A. Fabro. Methodology for estimating measurement uncertainty in the dynamic calibration of industrial temperature sensors. *Journal of the Brazilian Society of Mechanical Sciences and Engineering*, 39(3):1053–1060, 2017. ISSN 1678-5878.

S. Eichstädt, C. Elster, Esward T.J., and Hessling J.P. Deconvolution filters for the analysis of dynamic measurement processes: a tutorial. *Metrologia*, 47(5):522–533, 2010. doi: 10.1088/0026-1394/47/5/003.

S. Eichstädt, N. Makarava, and C. Elster. On the evaluation of uncertainties for state estimation with the Kalman filter. *Measurement Science and Technology*, 27(12):125009, 2016.

C. Elster and A. Link. Uncertainty evaluation for dynamic measurements modelled by a linear time-invariant system. *Metrologia*, 45(4):464, 2008.

C. Elster, A. Link, and T. Bruns. Analysis of dynamic measurements and determination of time-dependent measurement uncertainty using a second-order model. *Measurements science and technology*, 18(12):3682–3687, 2007. ISSN 0957-0233. doi: 10.1088/0957-0233/18/12/002.

T.J. Esward. Investigating dynamic measurement applications through modelling and simulation, 2016. ISSN 01718096. URL `https://www.degruyter.com/view/j/teme.2016.83.issue-10/teme-2015-0128/teme-2015-0128.xml`.

T.J. Esward, C. Elster, and Hessling J.P. Analysis of dynamic measurements: New challenges require new solutions. In *In Proceedings of XIX IMEKO World Congress*, 2009.

R. Feiz and M. Rezghi. A splitting method for total least squares color image restoration problem. *Journal of Visual Communication and Image Representation*, 46:48–57, 2017. ISSN 1047-3203. doi: 10.1016/j.jvcir.2017.03.001.

A. Ferrero and S. Salicone. Measurement uncertainty. *IEEE Instrumentation Measurement Magazine*, 9(3):44–51, 2006. ISSN 1094-6969. doi: 10.1109/MIM. 2006.1637979.

P. da Silva Hack and C.S. ten Caten. Measurement Uncertainty: Literature Review and Research Trends. *IEEE Transactions on Instrumentation and Measurement*, 61 (8):2116–2124, 2012. ISSN 0018-9456. doi: 10.1109/TIM.2012.2193694.

P.D. Hale, A. Dienstfrey, J.C.M. Wang, D.F. Williams, A. Lewandowski, D.A. Keenan, and T.S. Clement. Traceable Waveform Calibration With a Covariance-Based Uncertainty Analysis. *IEEE Transactions on Instrumentation and Measurement*, 58(10):3554–3568, 2009. ISSN 0018-9456. doi: 10.1109/TIM.2009. 2018012.

J.M. Hammersley and D.C. Handscomb. *Monte Carlo Methods*. Methuen's monographs on applied probability and statistics. Methuen, 1975. ISBN 9780416523409.

W. Hernandez. Improving the Response of a Load Cell by Using Optimal Filtering. *Sensors*, 6(7):697–711, 2006. ISSN 1424-8220. doi: 10.3390/s6070697.

J.P. Hessling. A novel method of dynamic correction in the time domain. *Measurement Science and Technology*, 19(7):1–10, 2008. doi: 10.1088/0957-0233/19/7/ 075101.

J.P. Hessling. Metrology for non-stationary dynamic measurements. In M. Sharma, editor, *Advances in Measurement Systems*, chapter 9, pages 221–256. InTech, 2010. ISBN 978-3-319-05353-0. doi: 10.5772/8730.

J.P. Hessling. Propagation of dynamic measurement uncertainty. *Measurement Science and Technology*, 22(10):105105, 2011. URL http://stacks.iop.org/ 0957-0233/22/i=10/a=105105.

Q. Huang, Z. Teng, X. Tang, H. Lin, and H. Wen. Mass Measurement Method for the Electronic Balance Based on Continuous-Time Sigma-Delta Modulator. *IEEE Transactions on Instrumentation and Measurement*, 65(6):1300–1309, 2016. ISSN 0018-9456. doi: 10.1109/TIM.2015.2490358.

International Recommendation OIML R 51 1. *Automatic catchweighing instruments Part 1: Metrological and technical requirements - Tests*. International Organization for Legal Metrology, 2006.

M. Jafaripanah, Al-Hashimi B.M., and White N.M. Application of analog adaptive filters for dynamic sensor compensation. *IEEE Transactions on Instrumentation and Measurement*, 54(1):245–251, 2005. ISSN 0018-9456. doi: 10.1109/TIM. 2004.839763.

T. Jia, H. Wang, X. Shen, Z. Jiang, and K. He. Target localization based on structured total least squares with hybrid TDOA-AOA measurements. *Signal Processing*, 143:211–221, 2018. ISSN 0165-1684. doi: 10.1016/j.sigpro.2017.09.011.

Y.Q. Jing, Q.H. Meng, P.F. Qi, M. Zeng, and Y.J. Liu. Signal processing inspired from the olfactory bulb for electronic noses. *Measurement Science and Technology*, 28(1):015105, 2016. doi: 10.1088/1361-6501/28/1/015105.

J. Kiviet and G. Phillips. Higher-order asymptotic expansions of the least-squares estimation bias in first-order dynamic regression models. *Computational Statistics & Data Analysis*, 56(11):3705–3729, 2012. ISSN 0167-9473. doi: 10.1016/j.csda.2010.07.013.

J. Kiviet and G. Phillips. Improved variance estimation of maximum likelihood estimators in stable first-order dynamic regression models. *Computational Statistics & Data Analysis*, 76:424–448, 2014. ISSN 0167-9473. doi: 10.1016/j. csda.2013.09.021.

S. Kueppers, H. Cetinkaya, and N. Pohl. A compact 120 ghz sige:c based 2Ã8 fmcw mimo radar sensor for robot navigation in low visibility environments. In *2017 European Radar Conference (EURAD)*, pages 122–125, 2017.

W. Lee, H. Yoon, C. Han, K. Joo, and K. Park. Physiological signal monitoring bed for infants based on load-cell sensors. *Sensors*, 16(3), 2016. ISSN 1424-8220. doi: 10.3390/s16030409.

A. Link and C. Elster. Uncertainty evaluation for IIR (infinite impulse response) filtering using a state-space approach. *Measurement Science and Technology*, 20 (5):1–5, 2009. URL http://stacks.iop.org/0957-0233/20/i=5/a=055104.

A. Link, A. Täubner, W. Wabinski, T. Bruns, and C. Elster. Modelling accelerometers for transient signals using calibration measurements upon sinusoidal excitation. *Measurement*, 40(9–10):928–935, 2007. ISSN 0263-2241. doi: 10.1016/j.measurement.2006.10.011.

I. Markovsky. An application of system identification in metrology. *Control Engineering Practice*, 43:85–93, 2015a. doi: 10.1016/j.conengprac.2015.07.001.

I. Markovsky. Comparison of adaptive and model-free methods for dynamic measurement. *IEEE Signal Proc. Letters*, 22:1094–1097, 2015b. doi: 10.1109/LSP.2014.2388369.

I. Markovsky and S. Van Huffel. Overview of total least-squares methods. *Signal Processing*, 87(10):2283–2302, 2007. ISSN 0165-1684. doi: 10.1016/j.sigpro.2007.04.004.

N. Mastronardi and D. O'Leary. Fast robust regression algorithms for problems with Toeplitz structure. *Computational Statistics & Data Analysis*, 52(2):1119–1131, 2007. ISSN 0167-9473. doi: 10.1016/j.csda.2007.05.008.

C. Matthews, F. Pennecchi, S. Eichstädt, A. Malengo, T.J. Esward, I. Smith, C. Elster, A. Knott, F. Arrhén, and A. Lakka. Mathematical modelling to support traceable dynamic calibration of pressure sensors. *Metrologia*, 51(3):326–338, 2014. doi: 10.1088/0026-1394/51/3/326.

D.Q. Mayne. Model predictive control: Recent developments and future promise. *Automatica*, 50(12):2967–2986, 2014. ISSN 0005-1098. doi: 10.1016/j.automatica.2014.10.128.

M. Munther, D.I. Moon, B. Kim, J.W. Han, K. Davami, and M. Meyyappan. Array of chemiresistors for single input multiple output (simo) variation-tolerant all printed gas sensor. *Sensors and Actuators B: Chemical*, 299:126971, 2019. ISSN 0925-4005. doi: 10.1016/j.snb.2019.126971.

M. Niedźwiecki and P. Pietrzak. High-Precision FIR-Model-Based Dynamic Weighing System. *IEEE Transactions on Instrumentation and Measurement*, 65(10): 2349–2359, 2016. ISSN 0018-9456. doi: 10.1109/TIM.2016.2575180.

M. Niedźwiecki, M. Meller, and P. Pietrzak. System identification based approach to dynamic weighing revisited. *Mechanical Systems and Signal Processing*, 80: 582–599, 2016. ISSN 0888-3270. doi: 10.1016/j.ymssp.2016.04.007. URL `http://www.sciencedirect.com/science/article/pii/S0888327016300450`.

J. Nocedal and S. Wright. *Numerical Optimization*. Springer Verlag, New York, 2 edition, 2006. ISBN 978-0-387-30303-1.

J. Ogorevc, J. Bojkovski, I. Pušnik, and J. Drnovšek. Dynamic measurements and uncertainty estimation of clinical thermometers using Monte Carlo method. *Measurement Science and Technology*, 27(9):1–14, 2016. doi: 10.1088/0957-0233/27/9/095001.

G. Olmi. Load Cell Training for the Students of Experimental Stress Analysis. *Experimental Techniques*, 40(3):1147–1161, 2016. ISSN 1747-1567. doi: 10.1007/s40799-016-0115-8.

H. Palanthandalam-Madapusi, T. Van Pelt, and D. Bernstein. Parameter consistency and quadratically constrained errors-in-variables least-squares identification. *International Journal of Control*, 83(4):862–877, 2010. ISSN 1366–5820. doi: 10.1080/00207170903470666.

Y. Pan, G.Q. Luo, H. Jin, and W. Cao. Direction-of-Arrival Estimation With ULA: A Spatial Annihilating Filter Reconstruction Perspective. *IEEE Access*, 6:23172–23179, 2018. ISSN 2169-3536. doi: 10.1109/ACCESS.2018.2828799.

P. Pietrzak, M. Meller, and M. Niedźwiecki. Dynamic mass measurement in checkweighers using a discrete time-variant low-pass filter. *Mechanical Systems and Signal Processing*, 48(1–2):67–76, 2014. ISSN 0888-3270. doi: 10.1016/j.ymssp. 2014.02.013. URL http://www.sciencedirect.com/science/article/pii/ S0888327014000715.

R. Pintelon and J. Schoukens. *System Identification: A Frequency Domain Approach*. IEEE Press, Piscataway, NJ, 2 edition, 2012. ISBN 978-0470640371.

R. Pintelon, Y. Rolain, M. V. Bossche, and J. Schoukens. Towards an ideal data acquisition channel. *IEEE Transactions on Instrumentation and Measurement*, 39 (1):116–120, 1990. ISSN 0018-9456. doi: 10.1109/19.50428.

G. Quintana-Carapia, I. Markovsky, R. Pintelon, P. Zoltán, and D. Verbeke. Bias and covariance of the least squares estimate of a structured errors-in-variables problem. *Computational Statistics and Data Analysis*, 144(106893):1–2, 2019. ISSN 0167-9473. doi: 10.1016/j.csda.2019.106893.

S. Rhode, K. Usevich, I. Markovsky, and F. Gauterin. A recursive restricted total least-squares algorithm. *IEEE Transactions on Signal Processing*, 62(21):5652–5662, 2014. ISSN 1053-587X. doi: 10.1109/TSP.2014.2350959.

M. Rossander, E. Dyachuk, S. Apelfršojd, K. Trolin, A. Goude, H. Bernhoff, and S. Eriksson. Evaluation of a blade force measurement system for a vertical axis wind turbine using load cells. *Energies*, 8(6):5973–5996, 2015. ISSN 1996-1073. doi: 10.3390/en8065973.

B. Saggin, S. Debei, and M. Zaccariotto. Dynamic error correction of a thermometer for atmospheric measurements. *Measurement*, 30(3):223–230, 2001. ISSN 0263-2241.

W.Q. Shu. Dynamic weighing under nonzero initial conditions. *IEEE Transactions on Instrumentation and Measurement*, 42(4):806–811, 1993. ISSN 0018-9456. doi: 10.1109/19.234489.

T. Söderström. Errors-in-variables methods in system identification. *Automatica*, 43(6):939–958, 2007. ISSN 0005-1098. doi: 10.1016/j.automatica.2006.11.025.

G. Stewart. Stochastic Perturbation Theory. *SIAM Review*, 32(4):579–610, 1990. doi: 10.1137/1032121.

R. Tasaki, T. Yamazaki, H. Ohnishi, M. Kobayashi, and S. Kurosu. Continuous weighing on a multi-stage conveyor belt with FIR filter. *Measurement*, 40(7–8):791–796, 2007. ISSN 0263-2241. doi: 10.1016/j.measurement.2006.05.010. URL http://www.sciencedirect.com/science/article/pii/S0263224106000959. Precision Measurement of Force, Mass, and Torque.

Tedea-Huntleigh. Aluminum Single-Point Load Cell 1004, 2015. http://docs.vpgtransducers.com/?id=2831.

K. Ushiki, K. Nishimori, N. Honma, and H. Makino. Intruder detection performance of simo and mimo sensors with same number of channel responses. *IEICE Transactions*, 96-B:2499–2505, 2013.

R. Vaccaro. A Second-Order Perturbation Expansion for the SVD. *SIAM J. Matrix Anal. Appl.*, 15(2):661–671, 1994. ISSN 0895-4798. doi: 10.1137/S0895479891224245.

S. Van Huffel and J. Vandewalle. *The total least squares problem: computational aspects and analysis*. SIAM, 1991. doi: 10.1137/1.9781611971002.

S. Van Huffel, C. Cheng, N. Mastronardi, C. Paige, and A. Kukush. Total Least Squares and Errors-in-variables Modeling. *Computational Statistics & Data Analysis*, 52(2):1076–1079, 2007. ISSN 0167-9473. doi: 10.1016/j.csda.2007.07.001.

N. Vlajic and A. Chijioke. Traceable dynamic calibration of force transducers by primary means. *Metrologia*, 53(4):S136, 2016.

L. Wang, Y. Yan, Y. Hu, and X. Qian. Rotational speed measurement through electrostatic sensing and correlation signal processing. *IEEE Transactions on Instrumentation and Measurement*, 63(5):1190–1199, 2014. ISSN 0018-9456. doi: 10.1109/TIM.2013.2292283.

A. Yeredor and B. De Moor. On homogeneous least-squares problems and the inconsistency introduced by mis-constraining. *Computational Statistics & Data Analysis*, 47(3):455–465, 2004. doi: 10.1016/j.csda.2003.12.001.

N. Zahradka, I. Jeong, and P. Searson. Distinguishing positions and movements in bed from load cell signals. *Physiological Measurement*, 39(12):1–11, 2018. doi: 10.1088/1361-6579/aaeca8.